Pedro Miguel Mendonça Ferreira

Licenciado em Química Aplicada

Photochromic Supramolecular Assemblies Based on Diarylethenes

Dissertação para obtenção do Grau de Mestre em
Química Bioorgânica

Orientador: Dr. A. Jorge Parola, Professor Associado, FCT/UNL

Co-orientador: Dr. Nuno Basílio, Investigador Pos-Doc, FCT/UNL

Júri:

Presidente: Doutora Paula Cristina de Sério Branco, Professor Auxiliar, FCT-UNL

Arguente: Doutor Eurico José da Silva Cabrita, Professor Auxiliar com Agregação, FCT-UNL

Vogal: Doutor António Jorge Dias Parola, Professor Associado com Agregação, FCT-UNL

FACULDADE DE CIÊNCIAS E TECNOLOGIA
UNIVERSIDADE NOVA DE LISBOA

Setembro 2017

Pedro Miguel Mendonça Ferreira

Licenciado em Química Aplicada

Photochromic Supramolecular Assemblies Based on Diarylethenes

Dissertação para obtenção do Grau de Mestre em
Química Bioorgânica

Orientador: Dr. A. Jorge Parola, Professor Associado, FCT/UNL

Co-orientador: Dr. Nuno Basílio, Investigador Pos-Doc, FCT/UNL

Júri:

Presidente: Doutora Paula Cristina de Sério Branco, Professor Auxiliar, FCT-UNL

Arguente: Doutor Eurico José da Silva Cabrita, Professor Auxiliar com Agregação, FCT-UNL

Vogal: Doutor António Jorge Dias Parola, Professor Associado com Agregação, FCT-UNL

FACULDADE DE CIÊNCIAS E TECNOLOGIA
UNIVERSIDADE NOVA DE LISBOA

Setembro 2017

Photochromic Supramolecular Assemblies Based on Diarylethenes

ACKNOWLEDGMENTS

First, I would like to express my gratitude to the Photochemistry Laboratory from the Chemistry Department from FCT-UNL for having me and supporting my master thesis. Special thanks to my supervisors Prof. Dr Jorge Parola and Dr Nuno Basílio, for teaching me, helping me develop the necessary tools to produce the present work and for all responsibility they gave me to grow as a professional and as a person and sometimes believe in me more than myself.

Special thanks to Dr Andrea Barbieri and Dr Barbara Ventura for teaching me and having me during the time I spent in ISOF-CNR Bologna, and all remain group members that I have the opportunity to meet.

I would like to thank Dr José Paulo Silva for ESI-MS spectroscopy, and all my laboratory colleagues, especially Noémi Jordão, João Avó, Artur Moro, Sandra Gago, Andreia Forte, Ana Lúcia and Tiago Moreira for the help, patience for teaching me over this work and fun moments spent in their presence. To all thank you for the support, the advice and especially for the friendship, and to provide a pleasant workplace, and to Paula Nabais for all craziness, breakfast, coffee break times and friendship.

I would also like to thank all my friends. Special thanks to Sofia Santos, Vanessa Fadista and João Macara for being a part of my professional and personal life and the “most important” for all the time spent playing cards, lunches, dinners and moments we passed together for the last years.

Ana Delgado, Catarina Carinhas, Pedro Bichardo, Miguel Picado and Margarida Krauchuk although they don’t share the scientific interest that I have, they always support me and give me their friendship.

Finally, I want to thank my family, parents, and brother, for the support, the education, the love, the comprehension, the teaching and the money spent in my education over the years. Special thanks to my brother that takes care of my old ones when I am not around, almost all the time.

This work was supported by the Project INFUSION, H2020-MSCA-RISE-2016, Grant N. 734834.

ABSTRACT

The design and construction of functional systems from self-assembly and molecular recognition processes are topics of current interest that can lead to new classes of materials, devices, and technologies. Contrary to conventional synthetic strategies where the formation and rupture of covalent bonds often occur under kinetic control, the supramolecular approach is based on thermodynamically controlled noncovalent interactions and dynamic covalent bonds. Systems under thermodynamic equilibrium, such as supramolecular polymers, are highly reversible by their nature, once their components are continuously interconverting between them. Due to these dynamic properties, supramolecular materials are able to adapt to different environments and display special features, such as self-healing, shape-memory, and stimuli-responsiveness. To achieve supramolecular organizations with multiresponsive/multistate properties, the building blocks should combine recognition units with functional groups capable of existing in more than two forms (multistate). The multistate forms can be interconverted into more than one type of external stimulus (multifunctional). This work aims to design, synthesize and study photochromic monomers able to polymerize upon host-guest interactions with suitable receptors in aqueous media.

These supramolecular assemblies based on host-guest interactions in aqueous media with potential applications as photochromic, electrochromic and luminescent devices were developed, using diarylethene as photochromic units and cucurbit[n]urils as host macrocycles. Two compounds 4,4'-(cyclopent-1-ene-1,2-diylbis(5-methylthiophene-4,2-diyl))bis(1-(naphthalen-2-ylmethyl)pyridin-1-ium) bromide (PF7) and a model compound 4,4'-(cyclopent-1-ene-1,2-diylbis(5-methylthiophene-4,2-diyl))bis(1-methylpyridin-1-ium) iodide (PF20) were synthesized and characterized by NMR spectroscopy, ESI-MS and elemental analysis. Host-Guest studies were performed by UV-Vis absorption spectroscopy, NMR, ITC, ESI-MS, and by steady-state and time-resolved fluorescence spectroscopy. The photochromic properties were studied upon continuous irradiation and the quantum yields determined. Association constants for [11] complexes with CB7 and CB8 were in the order of magnitude of 10^4 and 10^7 M^{-1}, respectively, for both compounds, PF7 and PF20, in both opened and closed forms. Large assemblies of supramolecular polymers were obtained for PF7 with CB8 and detected by UV-Vis and ESI-MS.

Keywords: Photochromism, Supramolecular Chemistry, Host-Guest interactions, Supramolecular Polymers, Diarylethenes, Spectroscopy

RESUMO

O design e a construção de sistemas funcionais a partir de processos de "self-assembly" e reconhecimento molecular são tópicos de interesse que levam a uma nova classe de materiais, dispositivos e tecnologias. As contrario das vias sintéticas convencionais, onde a formação e a quebra das ligações é (geralmente) controlada cineticamente, a química supramolecular baseia-se no controlo termodinâmico das interações não-covalentes e ligações covalentes dinâmicas. Este tipo de sistemas, como é o caso dos polímeros supramoleculares, são reversíveis devido à natureza dos seus componentes, onde os componentes estão continuamente a converterem-se. Devido a este efeito, estes materiais supramoleculares têm a habilidade de se adaptarem a diferentes ambientes e apresentam determinadas características, tais como "self-healing", "shape-memory" e "stimuli-responsiveness". Na medida a obter estes sistemas supramoleculares com propriedades multiresposta/multiestados, as unidades químicas devem conter na sua estruturas grupos de reconhecimento e grupos funcionais que apresentem mais de dois estados. Este trabalho tem como objetivo a síntese e o estudo de monómeros com propriedades fotocrómicas capazes de polimerizar numa estratégia "host-guest".

Estes complexos supramoleculares baseados em interações host-guest, com aplicações em dispositivos fotocrómicos, electrocrómicos e luminescentes, foram desenvolvidos, usando como unidade fotocrómica o diarileteno e o cucurbiturilo como unidade recetora. Dois compostos "4,4'-(cyclopent-1-ene-1,2-diylbis(5-methylthiophene-4,2-diyl))bis(1-(naphthalen-2-ylmethyl)pyridin-1-ium) bromide" (PF7) e um outro denominado composto modelo "4,4'-(cyclopent-1-ene-1,2-diylbis(5-methylthiophene-4,2-diyl))bis(1-methylpyridin-1-ium) iodide" (PF20) foram sintetizados e caraterizados por espectroscopia RMN e análise elementar. As interações host-guest foram estudadas com recurso à espectrosocpia UV-Vis, RMN, ESI-MS, e o estado excitado foi caracterizado por técnicas de fluorescência de estado estacionário e resolvida no tempo. Constantes de asociação na ordem dos 10^4 e 10^7 M^{-1} foram determinadas para CB7 e CB8, respectivamente, para ambos os compostos sintetizados. Polímeros supramoleculares foram detectados a quando interações entre PF7 e CB8, por espectroscopia UV-Vis e ESI-MS.

Palavras-Chave: Fotocromismo, Química Supramolecular, Interações Host-Guest, Polímeros Supramoleculares, Diarileteno

TABLE OF CONTEXT

vii

FIGURE INDEX

TABLE INDEX

ABBREVIATIONS LIST

Abs	Absorbance
ap	Anti-parallel conformer
c	Closed Isomer
CBn	Cucurbit[n]uril
DAE's	Diarylethenes
DCM	Dichloromethane
EDG	Electron donating group
EWG	Electron withdrawing group
ESI-MS	Electrospray Ionisation Mass Spectrometry
EA	Elemental Analysis
EtOAc	Ethyl Acetate
λ_{ex}	Excitation wavelength
I	Intensity
ITC	Isothermal titration calorimetry
λ_{max}	Maximum wavelength
NMR	Nuclear Magnetic Resonance
o	Open Isomer
p	Parallel conformer
PSS	Photostationary state
PEG	Polyethylene glycol
DP	Polymerization degree
ϕ	Quantum Yield
T	Temperature
THF	Tetrahydrofuran
t	Time
UV-Vis	Ultraviolet-Visible spectroscopy
λ	Wavelength

1 INTRODUCTION

1.1 PHOTOCHROMISM: FROM MOLECULES TO PROPERTIES

Photochromism, from the Greek words "phos" (light) and "chroma" (colour), and the suffix "-ism" (that denotes phenomenon), is a process that induces chemical changes in a molecule upon absorption of electromagnetic radiation (UV, visible or infrared).[1] The isomer *a* is transformed into isomer *b* that shows different electronic properties, in particular, a different absorption spectrum and consequently a change in colour. The term "photochromism" was firstly introduced by Hirshberg in 1950.[2] Organic photochromic compounds have been extensively studied over the years and led to the appearance of ophthalmic lenses during the 1960s. This required the design of photochromic compounds able to respond in a wide range of wavelength in the visible spectrum.[3] Some important classes of organic photochromic compounds are illustrated in figure 1.1.

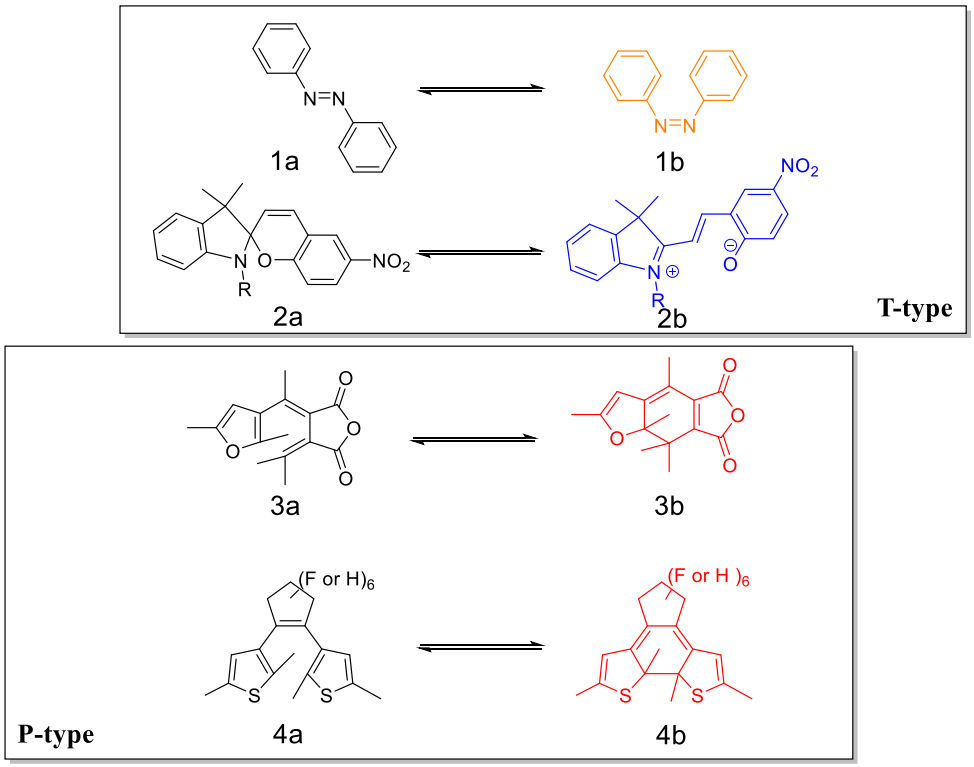

Figure 1.1 Some important classes of organic photochromic compounds: (a) before and (b) after photoirradiation .[4]

The *b* species can be reverted to form *a* either thermally or photochemically, defining T-type or P-type photochromism respectively.[3] The two upper molecules, azobenzene (1) and spiropyran (2), are T-type photochromes, while the lower ones, furylfulgide (3) and diarylethene (4), are P-type photochromes. Compounds that are classified into the T-type are thermally reversible, this means that the right-side isomers (*b*) are thermodynamically unstable, and return to the left-side isomers (*a*) in the dark, accompanied by a change of the colour, the unfavourable photochromic inverse reaction can also take place for these compounds. The P-type molecules were described later and show higher thermal stability. The photogenerated right-isomers (*b*) are thermodynamic stable and hardly return to the left-isomers (*a*)

in the dark.[5] So, the conversion of the right-isomer (*b*) to the left-isomer (*a*) occurs only by a photochemical process.

These colour changes are ascribed to photoinduced electronic and structural changes of the molecules, left (*a*) to right (*b*) isomers, as shown in figure 1.1.[5] In azobenzenes (1), the structural change is an isomerization of a double bond; in spiropyrans (2), the structural change is the opening of the pyran ring induced by the electron pair of the amine nitrogen; in furylfulgides and diarylethenes (3 and 4) the structural changes result from photoinduced electrocyclization reactions that convert the open- into closed-isomers.

A vast number of photochromic compounds have been explored towards several different applications.[6] In literature, new molecules and families of photochromic compounds with higher thermal stability (P-type) have been reported.[7] The thermal stability is an essential and indispensable property for the application of photochromic molecules in optical memories, switches and molecular machines.[8]

In the present work, diarylethene systems DAE's will be studied so their specific characteristics such as high thermal stability, fatigue resistance, and photochromic properties will be briefly described.

1.2 DIARYLETHENES

1.2.1 Brief structure-property relationships

Photochromic processes of DAE involve a photoinduced conrotatory cyclization and a 6π electron cycloreversion reaction between a 1,3,5-hexatriene (5o, Fig. 1.2) moiety and a 1,3-cyclohexadiene (5c) core, which proceeds according to the Woodward-Hoffmann rules. Diarylethene derivatives (7) are analogues of stilbene (6), where the phenyl groups were replaced by five-membered heterocyclic rings with the lower energy difference between the open- and closed-isomers.[5] The difference of energy between the open and closed forms of different heterocycle- based DAE are listed in table 1.1. A vast number of DAE's have been reported in literature using a thiophene ring as heterocycle, since it has the smallest energy difference between both isomers, facilitating the photochemical reaction.[9]

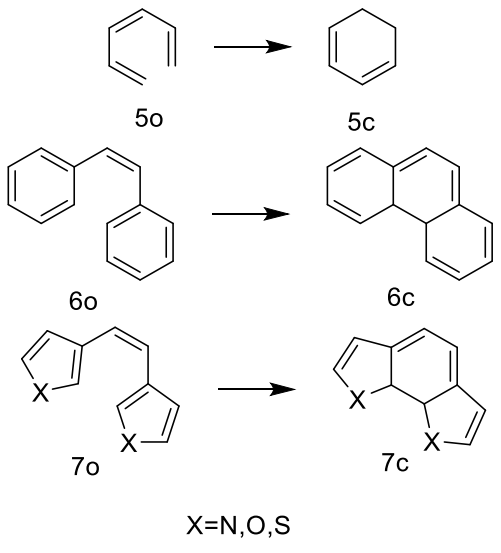

Figure 1.2 Photocyclization reaction of 6π-electron of hexatriene (5), stilbene (6) and diarylethene (7).

In DAE's the thermal 6π-electron disrotatory cyclization of the hexatriene core has an endergonic character, which means that the photochemical conrotatory pathway is preferred. Assuming a thermal equilibrium between the two conformers of the open isomer, parallel (p) and antiparallel (ap, the photoactive conformer) where the population is 1:1, only 50% of the molecules will undergo a conrotatory cyclization reaction upon irradiation, leading to a theoretical maximum quantum yield (ϕ) of 0.5.[10] This value can change if there is a significantly higher energetic preference for one of the conformers in the ground state, and consequently, a change in populations (figure 1.3).

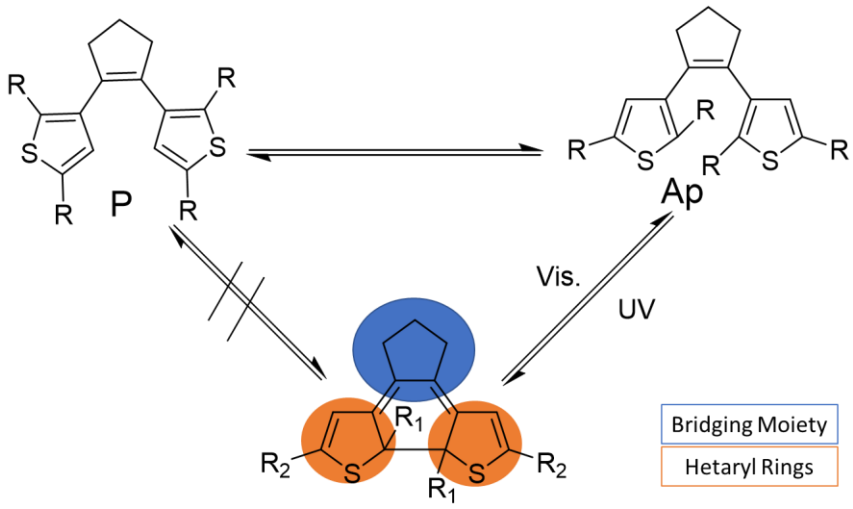

Figure 1.3 Conformations of DAE's open-isomers, which are called parallel and antiparallel conformations.

Table 1.1 Energy difference between the open and the closed forms of DAE with a different heteroatom (structures 7 in figure 1.2).[11]

Heteroatom	Energy (kcal/mol)
N	13.8
O	9.1
S	4.7

Usually, the open isomer of DAE's is colourless and shows a strong absorption in the UV region of the electromagnetic spectrum. This strong absorption is characterized by the electronic decoupling caused by the cross-conjugated (hetero)aryl moieties. So, UV light can be used to convert the open- into the closed-isomer (coloured) as illustrated in figure 1.4. Consequently, a new absorption band in the visible range appears and is responsible for the colouration of the solution. This new band is explained by the π-electrons delocalized over the entire molecular backbone in the closed isomer.

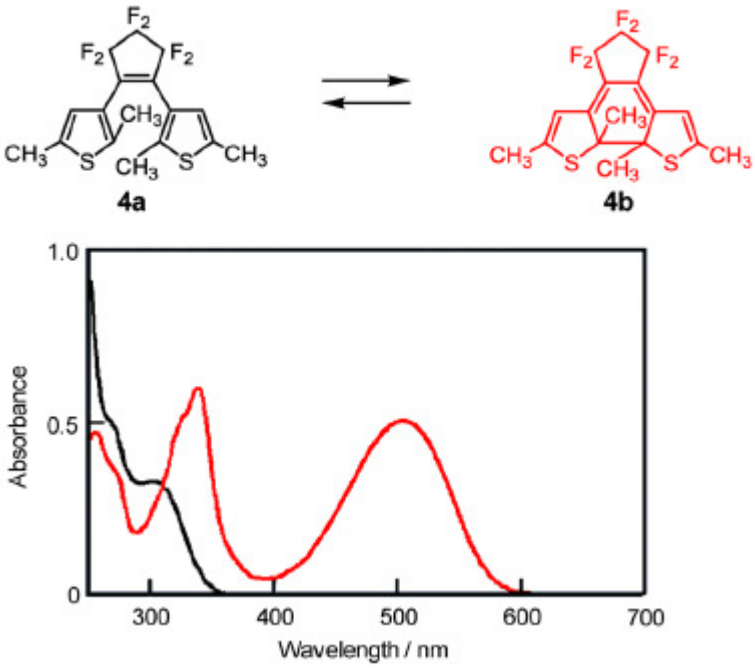

Figure 1.4 (up) Chemical structure of the open- and closed- isomer of (1,2-bis(2,5-dimethyl-3-thienyl)perfluorocyclopentene (bottom) absorption spectra of the open- (black line) and the closed-isomer (red line).[4]

As both isomers generally absorb in the UV region, when the open form is irradiated the closed species that forms also starts to absorb at the irradiation wavelength forming back the open form. In this way, a photostationary state (PSS) evolves, which composition is highly dependent on the quantum yields of the direct and inverse photochemical reactions. When visible light is used to irradiate the molecules only the closed form absorbs and a quantitative photochemical conversion is achieved upon excitation of the closed-isomer.[12]

In the open-isomer, a free rotation between the ethylene moiety and the aryl groups occurs. The consequence of this rotation is the existence of two conformations, as introduced above. One with a non-planar geometry, where the π-system is localized in the two aryl groups (p conformation), and the other where the π-system is delocalized over the full molecular backbone (ap conformation). Different π-systems lead to differences between both conformations, parallel where heterocyclic rings are in mirror symmetry (photo-inactive conformer), or anti-parallel with a C_2 symmetry (photo-active conformer).

In the 1980s, Irie and co-workers recognized the potential of 1,2-dihetarylethenes as thermally stable photochromic switches and systematically developed their basic design principles.[5] For the past 30 years, plenty of research has been done revealing fundamental structure-property relationships of these compounds.[13]

Molecular design of these compounds can be divided into different building blocks (see figure 1.3), depending on the desired properties. The building blocks can be divided into bridging moiety, heteroaryl rings, the R^1 substituents at the ring-closing carbons (reactive carbon) and the R^2 substituents in the periphery of the DAE's.[14]

1.2.1.1 Bridging Moiety

DAE's usually containing as bridging moieties a cyclic system. The reason behind is to prevent the photochemical E/Z isomerization, which would compete with the desired photocyclization reaction. Instead of having two isomers, we would have four isomers upon photoirradiation. In that way, the first DAE's derivatives were functionalized with rigid cyclic structures, like maleimide, cyclopentene or

perflurocyclopentene.[15,16,17] The last example is the most popular because the fluorine atoms increase the photochemical stability of the compounds.

In the last years, Feringa and co-workers developed synthetic pathways leading to DAE's with a non-fluorinated cyclopentene as bridging moieties, but still presenting a high stability. The use of non-fluorinated cyclopentenes extends the synthetic pathway flexibility, increasing the electrochemical properties in comparison to the "parent" structure while keeping the same photochemical mechanism.[18]

Another type of DAE's recently described in the literature include as bridging moiety a third heteroaryl moiety and are thus called "terarylenes".[19] The aromatic system in these compounds is delocalized over three heteroaryl moieties and this results in a weaker C-C formed upon photocyclization. This loss of aromaticity also promotes a thermal reversible reaction not observed in traditional DAE's. Although they present some thermal instability, these derivatives possess an extraordinary large quantum yield for the cyclization reaction.[20]

1.2.1.2 Hetaryl rings

The use of heteroatoms in aromatic systems lead to heteroaryl (hetaryl) rings. DAE's with hetaryl rings show a smaller energy difference between both isomers (see table 1.1). A large group of DAE's found in literature possess thiophene or benzothiophene as hetaryl rings but a variety of other heteroaryl structures can be used for this effect. Structures like furan, thiazole, imidazole or pyrrole as well as their benzannulated analogues have been used.

1.2.1.3 R^1 Substitution

Substitution of the reactive carbon is obligatory to avoid oxidation of the closed-isomer to the phenanthrene analogues.[21] In most reported DAE's, reactive carbons are substituted with methyl groups. The molecular behaviour is modulated by using a variation of substituents, for example, using a bulky substituent increases the photocyclization reaction quantum yield due to the enhancement of the antiparallel conformer in the ground state of the open isomer.[22] However, thermal reversibility is induced as well due to the weakness of the formed C-C bond by increased steric strain.[23] The use of electron donating groups (EDG) on the reactive carbon will stabilize the closed isomer, resulting in a decrease of quantum yield for the cycloreversion reaction.[24,25] On the other hand, using electron withdrawing groups (EWG) have been shown to accelerate the photochemical cycloreversion reaction.[26]

1.2.1.4 R^2 Substitution

Peripheric substitution may have a considerable influence on photochemical and thermal properties, more specifically thermal reversibility. There is a vast variety of DAE's substituted on the α-position, opposite to the reactive carbons. With all the different variety of substitution that can be made, literature data revealed that EWG decrease the thermal stability of the ring-closed isomer, while the opposite is observed when is substituted with EDG. Besides the fine-tuning of the photochromic properties, the peripheric substituents serve as an anchoring point for the connection for other moieties, to obtain for instance covalently linked structures.[27]

1.3 SUPRAMOLECULAR CHEMISTRY

Supramolecular chemistry is the field that studies molecular assemblies and intermolecular bonds between molecules.[28] This field was mentioned for the first time by Jean-Marie Lehn in 1988.[28] Lehn also named this field as "the chemistry beyond the molecule" bearing on the organized entities of higher complexity that result from the association of two or more chemical species held together by intermolecular forces. This field studies not only an isolated molecule but also the assembly of at least two molecules.[29] In opposition to conventional synthetic strategies where formation and rupture of covalent bonds occur under kinetic control, the supramolecular approach is based on thermodynamically controlled noncovalent interactions and dynamic covalent bonds.[30] The main targets of supramolecular research are the molecular assemblies based on weak intermolecular interactions, such as hydrogen bonds (H-bonds), van der Waals interactions and π-π stacking. Properties of these supramolecular systems are greater than the sum of the properties of the contributing parts. A variety of noncovalent interactions can be used to bring the building blocks together to prepare supramolecular structures. These noncovalent interactions are characterized by low energies and poor directionality, with exception of H-bonds.

Molecular recognition and self-assembly are concepts that have to be considered when supramolecular chemistry principles are discussed.[29] Molecular recognition is a crucial process in biologic systems. If pieces of the puzzle are not well designed, these pieces will never fit together, and the puzzle cannot be made. It was pointed out that the selected pieces do not have to be the most stable one, but the energy balance of the whole system must be minimized. [31] The reversibility of bonds formation is essential for molecular recognition and self-assembly, and in this way, errors can be fixed during the building block. That reversibility makes these materials (supramolecular materials) useful in different areas, such as biologic sensors, drug delivery, cell recognition, and so on. This property can be controlled by the addition of different functional groups.[32,33]

Molecular recognition principles are from an early 20th century when being introduced two different terms, "lock and key" and "receptor/substrate". Principles describe the fit of a rigid substrate to a receptor. Lock and key principles laid the foundation for host-guest chemistry, however, the lock and key principles must be considered in the context of "induced-fit-mechanism". Stimuli-responsive supramolecular assemblies formed by host-guest interactions has been well established in solution.[34]

Host-guest chemistry has become a broad discipline witch not only cations or anions, but also neutral guests are investigated. The focus of host-guest chemistry is the selective interactions between host and guest molecules. Generally, hosts are molecules that contain a large cavity volume, to encapsulate guest molecules. There is a vast example reported in the literature using host molecules such as cyclodextrins (CD), cucurbit[n]urils (CB), calixarenes, carcerands, zeolites, among others.[35] Guests typically have both a complementary shape and interaction with host macromolecules, thus allowing for selectivity between both (host and guest), which is denoted as molecular recognition, introduced above. These (host-guest chemistry) can include various noncovalent interactions. Molecular recognition properties of hosts for inclusion appropriate guest can be utilized in designing sensors, switches and nanoscale components.

1.3.1 Cucurbit[n]urils

1.3.1.1 Synthesis

Chemistry of cucurbit[n]urils (CBn) was a rapidly developing field. More recently, the synthesis of functionalized derivatives has been progressed. Synthesis of these compounds is described in figure 1.5. CBn results by condensation of glycoluril (1 in figure 1.4) and formaldehyde in acid conditions.[36] Over the years, different conditions, and methods of synthesis were published. The first synthesis was performed in 1905 by Behrend and coworkers.[36] The name of cucurbit[n]uril was denominated by Mock, due to the similarity of a pumpkin structure, which botanical family name is *Cucurbitaceae*.[37]

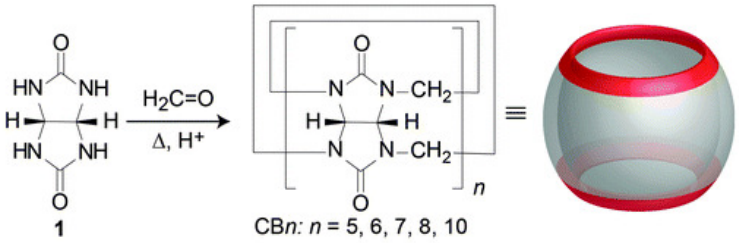

Figure 1.5 Synthesis of CBn by condensation of glycoluril (1) and formaldehyde under acid conditions.[38]

1.3.1.2 Properties

CBn presents a highly symmetric structure, with carbonyl portals containing considerable negative charge density and a hydrophobic cavity. When guest compounds are encapsulated in the inner cavity, their physical properties (absorption, fluorescence and NMR spectra) change.[39,40,] The complexation induces a spectral shift due to the surrounding electronic and/or magnetic environment of CBn units. Although CBn have a nonpolar inner cavity and are not dipolar, due to symmetric structure, they exhibit a very higher quadrupole moment.[41]

A variety of uses for CB5 to CB8 have been reported due to their ability to form binary and ternary host−guest complexes, such as complexes between methyl viologen and azobenzene derivatives, and therefore impacted a wide variety of scientific applications,.[42,43]

1.4 POLYMERS

A polymer is defined as a macromolecule built up from numerous small molecules, repeating units (monomers), connected by a covalent bond. These units can be connected in diverse ways. Monomers may be connected linearly (a in figure 1.6, simplest way) or branched (b). The branched polymers also show different structural ramifications, like star-shaped (c) or comb-shaped (d). There are also polymers call ladder polymers (e) or semi-ladder polymers (f), that shows a double-stranded structure. The most complex structure of branched polymers are the network polymer (g), where the units are connected in a three-dimensional way.[44,45]

If polymers chains are built with two or more different structural units, the term used is copolymer instead of polymer. Different monomers can be used to build these macromolecular structures. Different monomers incorporate different physical and chemical properties in the build polymer.[45]

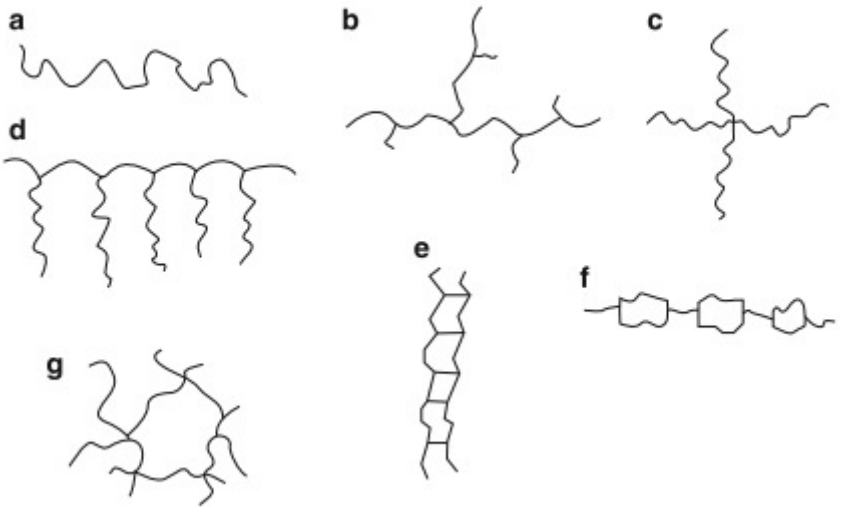

Figure 1.6 Shapes of polymer molecules. A) Linear B) branched C) star-shaped D) comb-shaped E) ladder F) semi-ladder G) network structure. [44]

Several examples of polymers using DAE's as structural unity have been published over the years. The examples come from using the DAE's as a monomer (main chain) or as a residual group (side chain), figure 1.7 a and b, respectively.[5] The main idea when DAE's are incorporated in polymers structure is to give different properties such as photochemical, electrochemical, fluorescence, and so on.[46,47] These photochromic polymers show an increment of cyclization quantum yield.[48] Bertarelli and co-worker prepared polyurethanes and polyesters having DAE's in the main chain, and observe that the photochromic reactivity, of these formulated polymers, remain similar to the free molecules in solution because of the relatively low glass transition (T_g).[49]

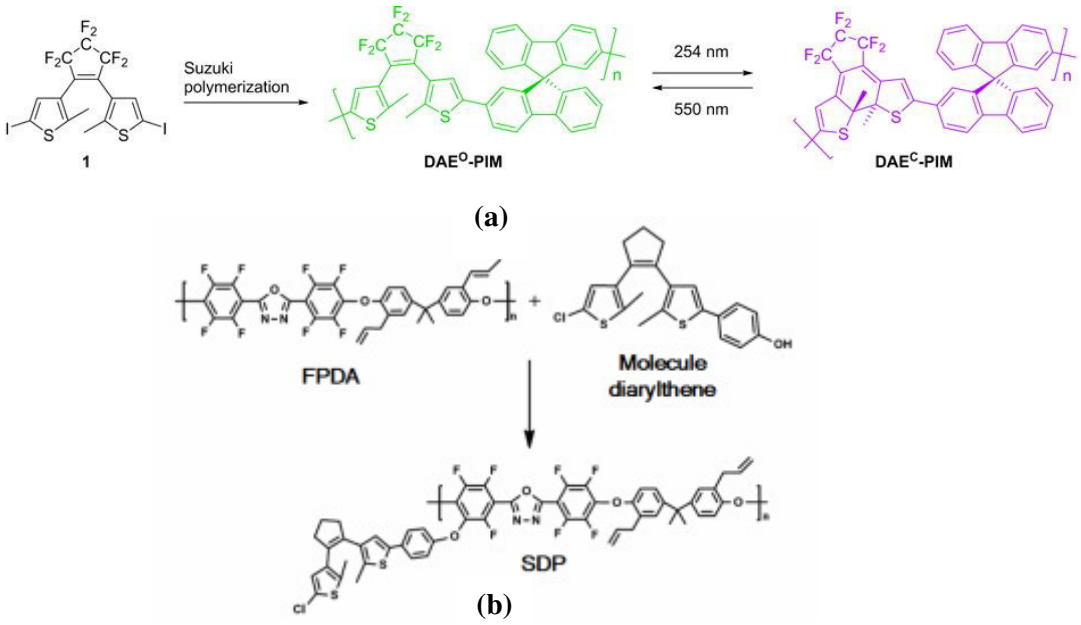

Figure 1.7 (a) Polymer with DAE in the main chain;[50] (b) Polymer with DAE in the side chain.[51]

The main difference between polymers and supramolecular polymers is the interaction between monomers. In the first case, monomers are connected by a covalent bond (C-C, C-O, C-N) while monomers of supramolecular polymers are linked by noncovalent bonds, such as π-π stacking and hydrogen bonds. A representation of each polymer can be seen in figure 1.8.

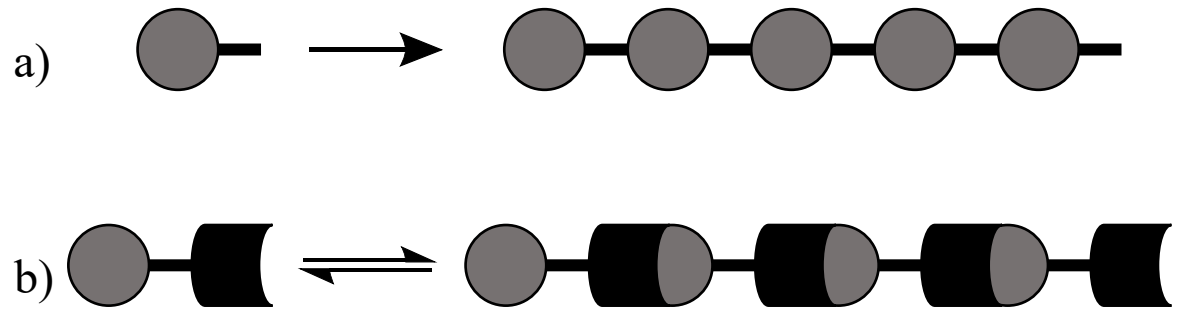

Figure 1.8 (a) Polymer; (b) Supramolecular polymer.

1.4.1 Supramolecular polymers

Supramolecular polymer emerged from the combination of supramolecular chemistry and polymer science. These polymers are based on monomeric units held together by directional and reversible noncovalent interactions.[52] These supramolecular polymers are defined as polymeric arrays of monomeric moieties that are linked by reversible and highly directional secondary interactions, as mentioned above. The directionality and strength of the supramolecular bonding are key features of systems that can be regarded as polymers that behave according to well-established theories of polymer physics. The nature of noncovalent interactions, structure and/or properties of the used building blocks employed in these supramolecular systems, determines the responsiveness of the resultant material to surrounding environment. This way a wide range of possibilities can be taken into account during the formulation of supramolecular structures.

Polymerization reactions involving covalent bond formation usually occur under kinetic control, as the potential barrier for the back reaction is generally much larger than the forward reaction. Supramolecular polymers, due to reversibility, have it is growth dependent on thermodynamic parameters, such as concentration, temperature, and pressure.[53] Three major growth mechanism can be assigned, namely, isodesmic, ring-chain, and cooperative.[54]

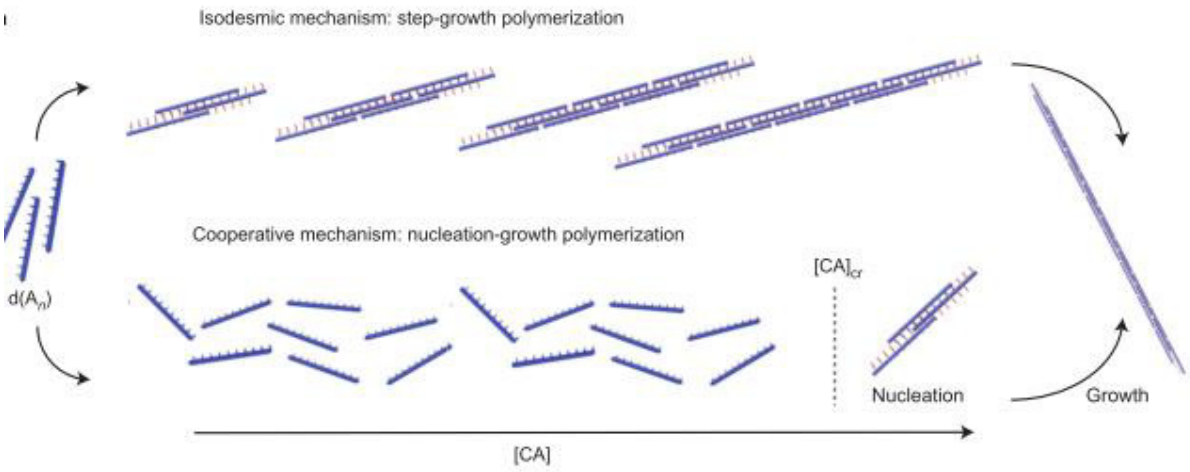

Figure 1.9 Representation of isodesmic versus cooperative supramolecular polymerization mechanism.[55]

Isodesmic polymerization is like to the step polymerization, that is characterized by a high polydispersity, which assumes that the association affinity of the monomers end-groups does not change during the supramolecular polymerization process. The second mechanism (ring-chain) is represented by the reversible polymerization where each linear aggregate is assembly with it cyclic counterpart. The cooperative mechanism is characterized by nonlinear growth, it can be distinguished in two stages, the accumulation of nuclei followed by the start of fibre growth.[55] A comparison between Isodesmic and Cooperative mechanism is represented in figure 1.9. A few examples of supramolecular polymers have been published in the literature, in the last decade. In the reported examples, it is possible to verify the use of more than one non-covalent interactions to link monomers, which increases the stabilization of the formed supramolecular structures.[52]

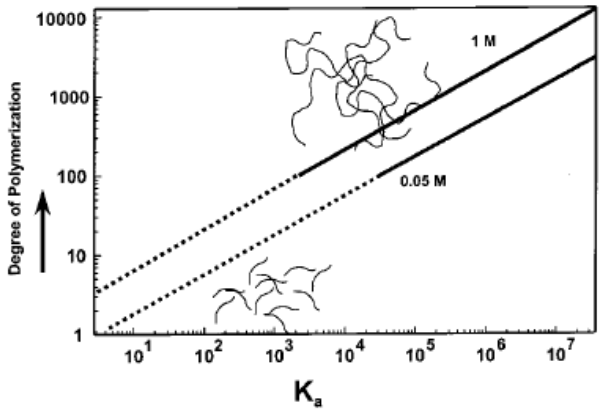

Figure 1.10 Theoretical relationship between the association constant (K_a) and DP. [56]

There is already a well-established relationship between the polymerization degree (DP) and the association constant (K_a). This relation is represented in figure 1.10, where is also able to verify a concentration dependence for this type of systems, as mentioned and illustrated in figure1.9.

Of all examples reported in the literature, just a few obtain a rigid material, as the final product. The following example represented in figure 1.11, was reported by Yiliu Liu and co-workers, where they obtained a rigid supramolecular structure, using host-guest interaction methodology. In the reported case acceptor-donor systems are used to interact and this way occurs the polymer growth. CB8 macromolecules are used to hold together all molecules, encapsulating monomers. [57]

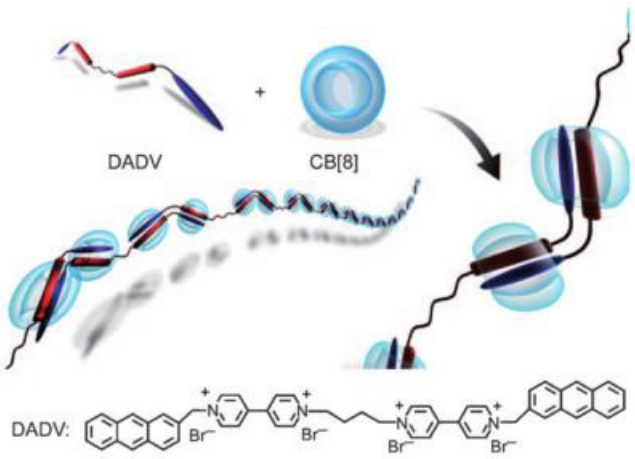

Figure 1.11 Schematic representation of the formation of the supramolecular polymer based on multiple host-stabilized charge-transfer interactions. [57]

Having in mind all mentioned concepts, during the molecular design profiles of molecules, was possible to design the system using donor and acceptor moieties, naphthalene and pyridinium, respectively. To increase this π-π interaction between the moieties, cucurbit[n]uril (CBn) will be used as Host macrocycle. These macrocycles were chosen due to their high-affinity constants, K_a around $10^6/10^7$ M^{-1}, and due to the examples reported in the literature. This way supramolecular polymers with photochromic behaviour will be created and studied. Supramolecular assemblies that combine photochemical properties of the chosen guest, host-guest properties between the molecules used and the formation of a supramolecular photochromic polymer, are the focus of the presented work. The materials have a large interest in optical and electronic applications. Once photochromic molecules change their properties upon an electromagnetic stimulus, these molecules can be used to make or break molecular assemblies, creating this way smart materials and devices.

2 RESULTS AND DISCUSSION

2.1 DESIGN AND SYNTHETIC PATHWAY

Molecular design of synthesized molecules was made having in mind the photochemical properties of DAE's, donor-acceptor and Host-Guest interactions. The main idea is to form monomers capable of fit inside CBn molecules and capable of interacting with another monomer to make the polymer growth. A first approach represented in figure 2.1, donor and acceptor moieties were placed on peripheric carbon of thiophene ring, creating this way asymmetric molecules. Using asymmetric DAE's for supramolecular polymer formation, two possible species could be observed in solution. Both possibilities are represented in figure 2.1, dimer (I) and the desired linear polymer (II).

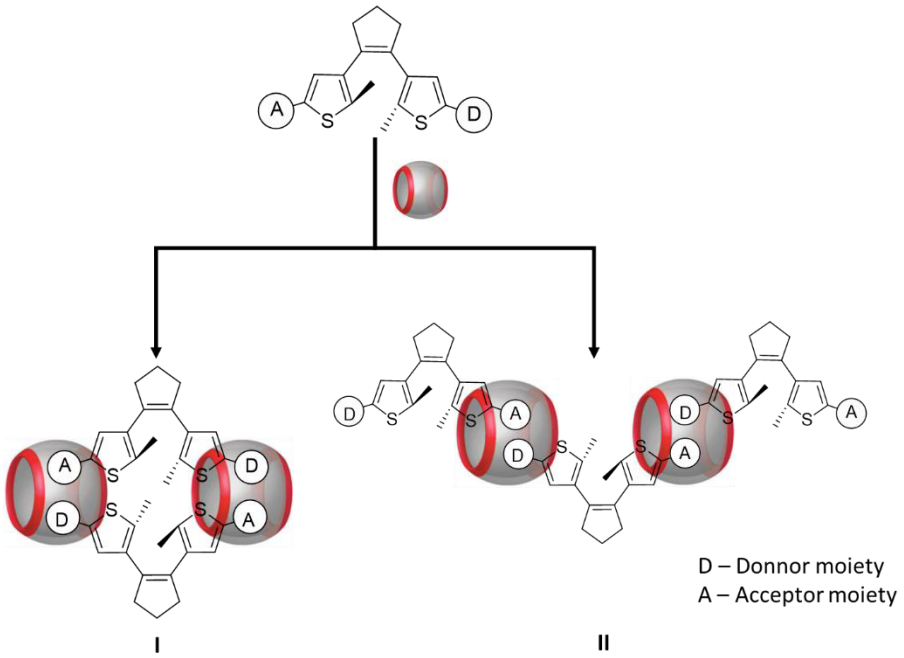

Figure 2.1 Scheme of the first approach for the molecular design of monomers used for supramolecular polymerization. (I) dimer (II) linear supramolecular polymer.

Formation of dimer species (I) would work as a "stopper" for supramolecular polymer growth and the reaction yield would be low, due to a competition between both species. To solve this problem a different approach was reformulated, represented in figure 2.2 In the second approach the peripheric carbons of the thiophene rings were substituted with a group having acceptor and donor moieties side by side. This substitution increases the polymer growth and decreases the dimer formation, once the π-π interaction between two DAE's is only possible from one side of the molecule, due to the relative position of these groups inside the structure, creating this way symmetric compounds. Superposition of thiophene ring with pyridinium (forming this way a dimmer species) can also be taken account, but it is less favourable the formation of this species compared with the linear polymer. Being symmetric, the synthetic process will be easier and faster. Pyridinium as acceptor and naphthalene as donor moieties were chosen due to previous work reported in literature the presence of positively charged compounds is interesting and required, in a design point of view, because of the host carbonyl portals, having an electronegative

character, can establish attractive ion-dipole interactions that increase the stability of the resulting complexes.

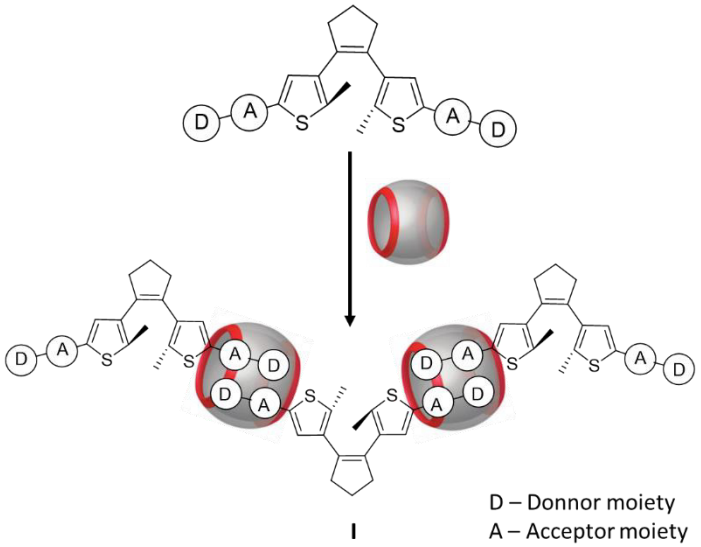

Figure 2.2 scheme of the second approach for the molecular design of monomers used for supramolecular polymerization. (I) linear supramolecular polymer.

With the molecular design established, retrosynthesis was performed to decide the synthetic pathway to follow. The pathway followed to prepare DAE's derivatives were based on the one described in the literature, and it is outlined below (figure 2.3).[18] **PF20** does not show acceptor-donor moieties, once this compound served as a model to have a better understanding of host-guest interaction, while **PF7** is designed to be used in supramolecular polymerization.

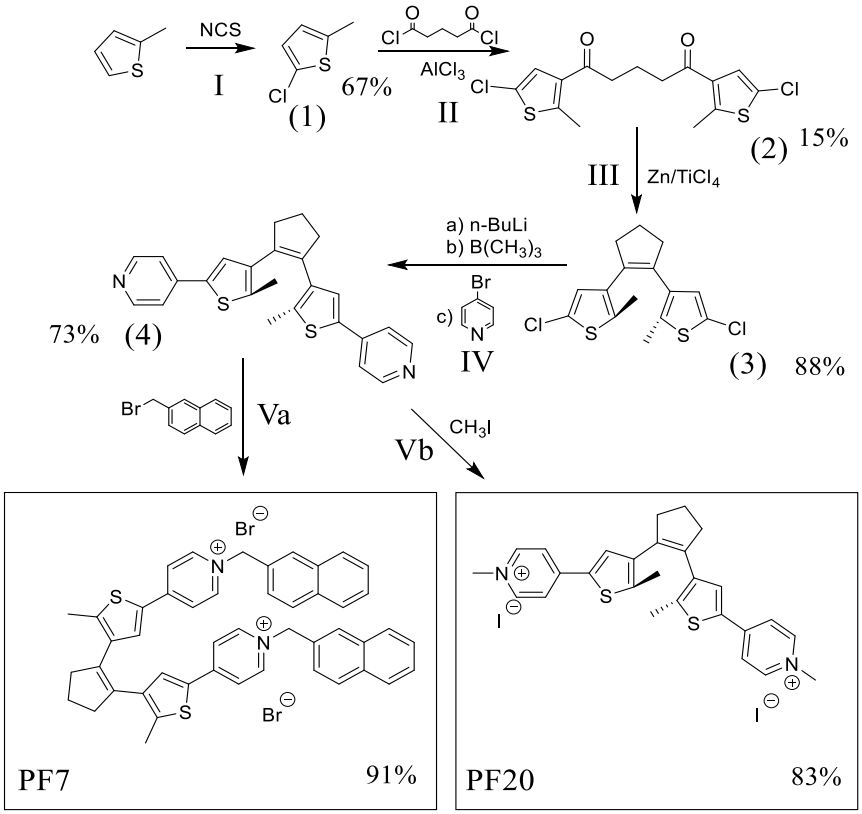

Figure 2.3 Synthetic pathway of diarylethene derivatives.

All products obtained were purified and characterized by NMR spectroscopy and elemental analysis (EA) was performed for the interest compounds. The synthetic pathway was optimized, always that a reaction was repeated, to increase the reaction yield of each step.

A third compound **(8)** was designed with PEG units to increase their solubility in water, once it analogue **PF7** shows poor solubility. Synthetic pathway of this new compound is illustrated in figure 2.4. (8) derivative from (4), as **PF7** and **PF20**, the difference is that in the donor moiety, a PEG derivative unity was incorporated. Different approaches were performed, with different starting materials, but the successful one is represented in figure 2.4 when the starting material is dimethyl naphthalene (5). Compound (7) was obtained in a mixture of mono- and di-substituted. PEGylation of (6) is an easy reaction, but obtaining di- as major compound seems to be a problem, once desired product is the mono-substituted.

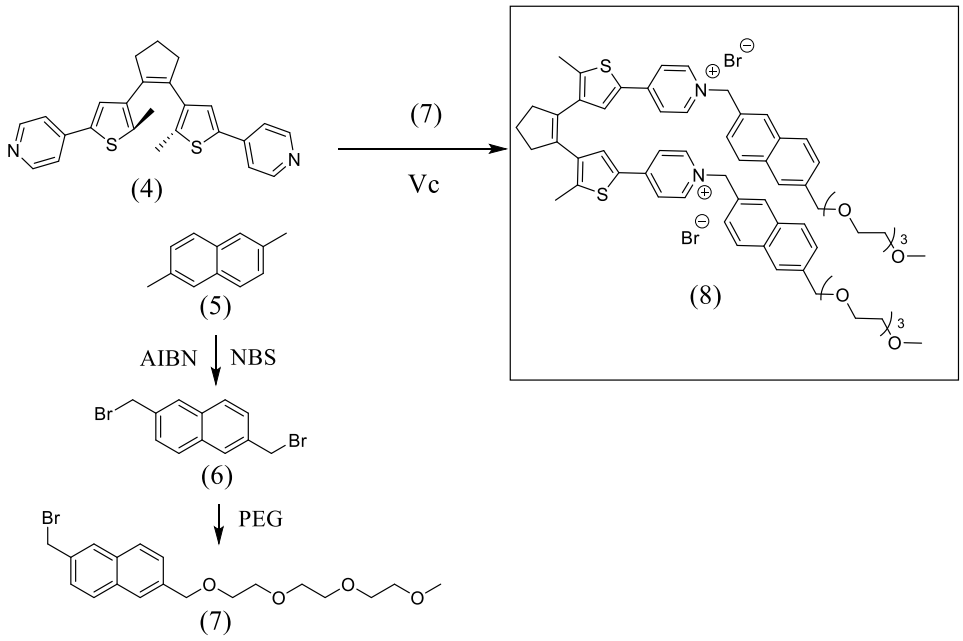

Figure 2.4 (continuation) Synthetic pathway of Diarylethene derivatives.

To finalize the synthesis of the new compound (8), an optimization of PEGylation reaction must be performed, in a way to obtain mono- with a considerable yield, and then make the last step that is an SN_2 reaction, between (4) and (7).

2.1.1 Halogenation Reaction

The first step is a nucleophilic substitution of the thiophene ring (halogenation reaction, I in figure 2.3). For this propose a chlorination was done, using NCS as chlorination agent. The acetic acid was as polar protic solvents increase the yield of this reaction. The acidic conditions catalyze the reaction, protonating the *N*-chlorosuccinimide and forming the O-Cl bond between the oxygen of the acetic acid and the chloride cation. This formation is forced by the migration of the proton from the oxygen to the nitrogen that stabilizes the system, as illustrated in figure 2.5, the C=O bond decreases the energy of the system.

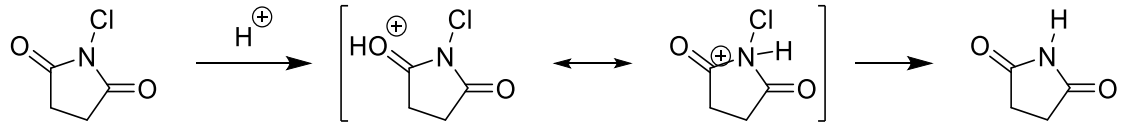

Figure 2.5 Mechanism of NCS in acid conditions.

Looking for the conditions of the reaction, it is possible to admit a cyclic reaction between the catalyst and the reagent, NCS and methylthiophene respectively. The chloride cation forms a bond with oxygen from acetate, forming this way the acetyl hypochlorite.[58] The reaction mechanism is described in figure 2.6. Chlorination is preferential on 2-position of the thiophene ring than in 3-position because the intermediate formed. In the first case, it can be stabilized by charge delocalization more efficiently than in the other case. After the electrophilic attack on the thiophene ring, the acetate formed to remove the proton to restore the aromaticity of the ring by the formation of the conjugated acid. The workup of the first step consists in the neutralization of the formed and remained acid with sodium hydroxide. This product was isolated and obtained with a yield of 67%.

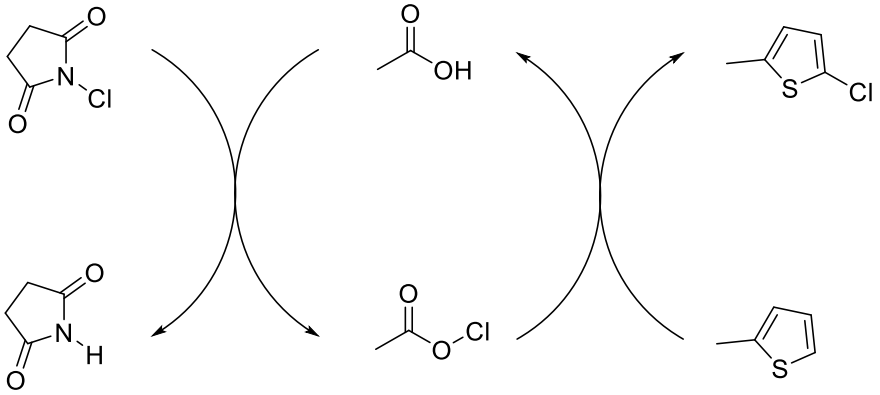

Figure 2.6 Catalytic cycle of Halogenation reaction.

2.1.2 Friedel-Craft Acylation

The second step is a Friedel-craft acylation (II in figure 2.3). The product formed contains aromatic ketones that are obtained by the combination of an aromatic substrate with an acyl component, typically in the presence of a catalyst. This reaction can also take place without any catalyst but in severe conditions. The first step is the creation of the electrophile via complexation of an acyl chloride with Lewis acid used (aluminium chloride). The mechanism of this step is the complexation between the oxygen of the carbonyl group and the aluminium atom (figure 2.7 a) and not the complexation of the chloride with the aluminium (figure 2.7 b). This mechanism (see figure 6.32 in appendix) was reported in the literature and was confirmed by X-ray spectroscopy.[59]

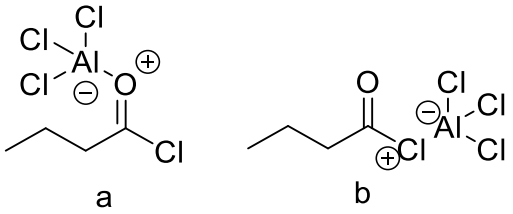

Figure 2.7 Intermediate structure for Friedel-Craft Acylation.

This suggests an intermolecular rearrangement of the **a** complex.[60] After formation of the acylium ion, there is an attack on the positive charge by the aromatic ring, formatting a new σ bond. Then occurs the de-protonation leading to the re-aromatization of π-system, HCl gaseous is also formed during the reaction. The neutralization of the acid formed is required, followed by purification of the product with a yield of 15%. The low yield it is due to the losses occurred during the reaction, as well during the purification process.

2.1.3 McMurry Coupling

Also known as McMurry Cyclization (III in figure 2.3), consist on a reductive coupling between two ketones or aldehyde to form an alkene, using a titanium (Ti^{3+}) as a catalyst and as reducing agent. The reaction was named after McMurry and Fleming described a "new method for the reductive coupling of carbonyls to olefins".[61]

McMurry Coupling mechanism remains unknown.[62] However, most mechanistic studies reported suggest that the mechanism is composed of two steps, without considering the reduction of the titanium species. Firstly, preparation of the valent titanium species, for this purpose it is usually used $TiCl_4$ or $TiCl_3$ as titanium species, and Zn powder or $LiAlH_4$ as reductive agent (see the mechanism in the appendix, figure 6.33).[63]

The first step of the mechanism is the formation of pinacolate intermediates (figure 2.8). followed by the deoxygenation of these pinacolates (figure 2.3.1 2). Two-step mechanism is supported by literature results.[62] Pinacol product can be separated if the reaction takes place at low temperatures.[64]

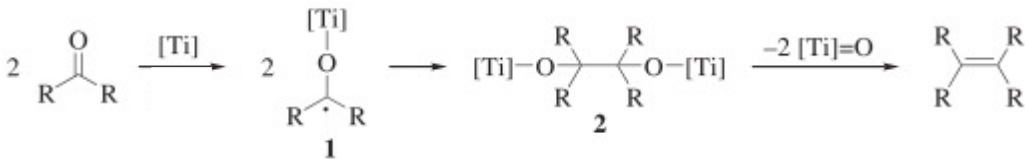

Figure 2.8 McMurry coupling mechanism.[62]

The product was obtained in 88% yield.

2.1.4 Suzuki coupling

The next reaction is the Suzuki coupling also known as Suzuki-Miyaura reaction, due to the shared publication in 1979, when this reaction was published for the first time.[65] The reaction consists on the coupling between an organoboron species and an organohalide catalyzed by a palladium (0) and base.[66]

The mechanism involves three steps (cyclic mechanism of the realized reaction described in figure 6.34 in the appendix). The first step consists in an oxidative addition of palladium to halide species, forming the organometallic compound. Then a transmetallation process with borate, followed by the reductive elimination. The catalytic cycle is illustrated in figure 2.9.

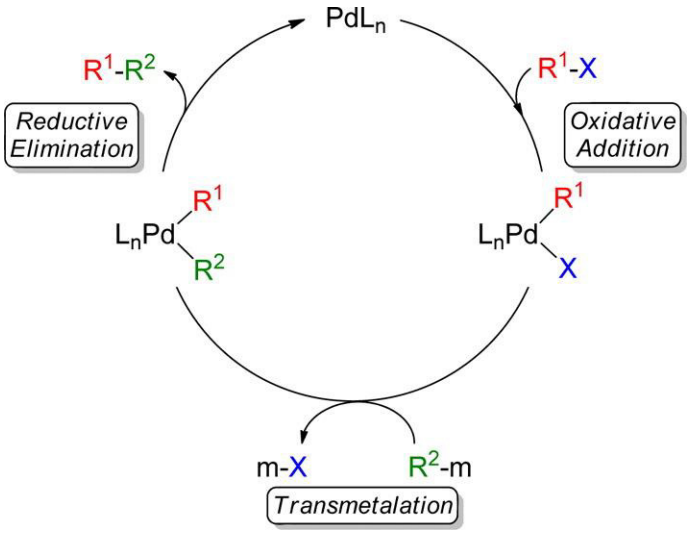

Figure 2.9 General catalytic cycle for Pd-catalyzed C-C cross-coupling reactions, such as Suzuki coupling.[67]

The base has three roles in the mechanism: i). Formation of palladium complex, ii) formation of trialkyl borate and iii) the acceleration of the reductive elimination.[68]

A few optimizations were made for this step. In the first trial was used few drops of ethylene glycol, them was replaced by PEG 400 because was reported in literature the improvement of the reaction yield, as observed, the yield increase from 48% to 73%.[69] The role of PEG is not clear yet, but it is reported in literature the possibility of the terminal hydroxyl group in PEG is acting as reductant agent.[70] The key role of this reductant species in the palladium-catalyzed couplings is also described in literature.[71]

The last reaction is an SN_2. Diarylethene containing anthracene moiety (**PF7**) and methyl groups (**PF20**) were obtained in 91% and 83%, respectively.

2.2 DETERMINATION OF ASSOCIATION CONSTANTS

Formation of supramolecular complexes was observed by different methodologies. Structures of supramolecular assemblies were determined (chapter 2.3) and the photochemical behaviour was studied (chapter 2.4). In this chapter, a mathematical model was used to determine association constants of each complex. Due to the small cavity of CB7, the supramolecular polymer is not expected, only the formation of [11] (one host for one guest) and [21] (two host for one guest) host-guest complexes. Studies with these macrocycles (CB7) will give a better understanding of the interactions between CBn and guest molecules. The size of CB8 cavity is larger and can encapsulate two small organic molecules, so the mathematical model used will be different in this case. **PF20**, unlike **PF7,** does not have donor acceptor moieties to interact one each other, and supramolecular polymer formation is not expected.

PF20.CB7

Spectrophotometric titration of **PF20** (open isomer) with CB7 is represented in figure 2.10, where the course of the experiment is defined with the narrow. As the complex is formed the absorbance decreases and the λmax shift to lower energy region (redshift).

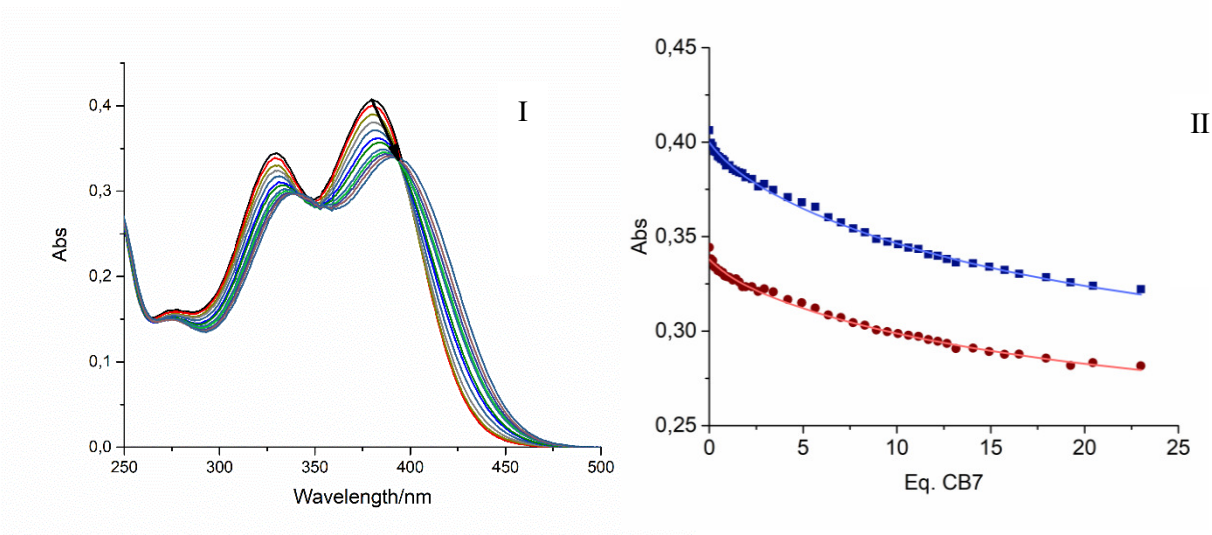

Figure 2.10 (I) Spectrophotometric titration of PF20 with CB7, (II) experimental data (blue) 380 nm; (red) 330 nm, the solid line represents the best least squares fit of data to a 2:1 association model. Conditions [PF20] = $2x10^{-6}$ M;

For this experiment, the range of titrant was from 0 equiv. to 23 equiv. of CB7 (as shown in figure 2.10 II). Association constants of these complexes were determined by fitting the experimental data using best least squares fit with 2:1 binding model (solid lines in figure II 2.10). This model was used instead of 1:1 due to the bivalency of guest used. The same experiment was performed for the closed-isomer (figure 6.6 in the appendix), to verify if the affinity between molecules changes with the structural change of **PF20**. The determined constants for both isomers are listed in table 2.1. The conditions used were the same for both experiments.

As stated before, the data analysis was performed using a 2:1 binding model. The binding model is explained on section 4 Equation (33 and 34) was used to fit the data and this way, K11 and K21were determined.

Association constants were determined using a different technique to compare and/or confirm the obtained constants. NMR titration was performed, and results were fitted with the 2:1 binding model, as previously. RMN titration of **PF20** (open isomer) with CB7 is illustrated in figure 2.11, where the obtained results and the best least squares fit a 2:1 binding model are represented by dots and solid lines, respectively. The blue colour indicates the positive shifts, while red colour is ascribed to negative shifts, of guest protons. The shifts were calculated by the difference between the initial and the shift at each equiv. The positive (blue) shift mean that guest region is encapsulated inside the cavity of CB7, meanwhile negative (red) shifts represent the protons near the portal region of CB7, see spectra fig 2.19.

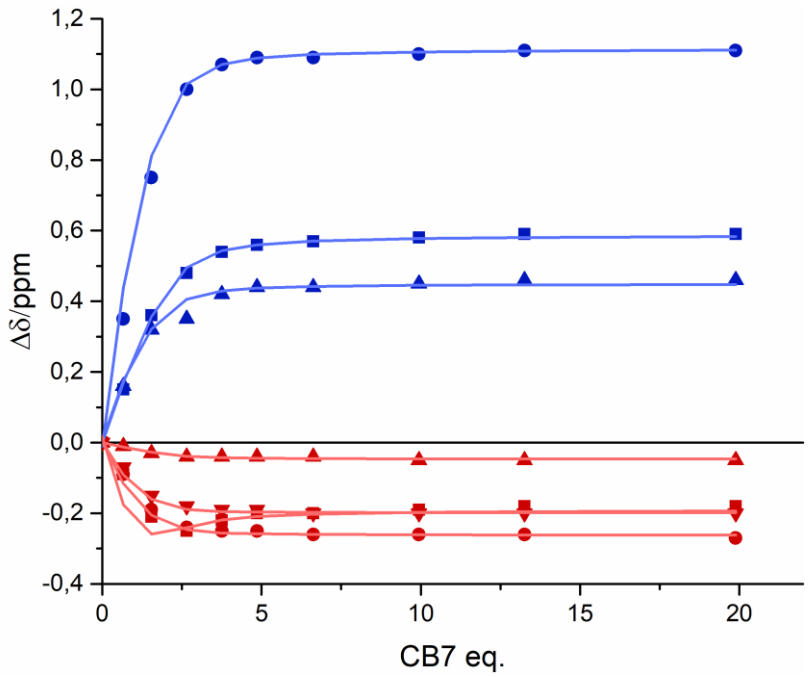

Figure 2.11 Plot of the chemical shift of PF20 (closed isomer) titration with CB7. Solid lines correspond to the best fitting of the experimental data.

Association constants listed in Table 2.1 were determined by different methods for open- and closed-isomers of **PF20**. The constants K_{11} are the same for both isomers, the only difference is related to K_{21} of closed-isomer, where the value obtained by NMR seems to be higher than the one determined by spectrophotometric titration. This difference can be explained by the conditions used for both methods, and the error associated with each technique. With the obtained values it is possible to verify a preference for the [11] complex when **PF20** is in the open isomer, the higher association constant, while [21] complex formation is more visible for the closed form. Molar fraction (figure 6.8 and 6.9 in the appendix) help to have a better perception of each complex in solution versus the equivalents of CB7. This can be explained, due to the delocalization of the π-system when the compound is in the closed form and this way the charge is more stabilized by CB7.

Table 2.1 Association constants determined by UV-Vis and NMR spectroscopy for PF20 (open and closed form) with CB7.[a]

	UV-vis		NMR	
	K_{11} (M^{-1})	K_{21} (M^{-1})	K_{11} (M^{-1})	K_{21} (M^{-1})
Open - isomer	$1.00x10^5$	$2.50x10^3$	$1.00x10^5$	$5.00x10^3$
Closed - isomer	$4.00x10^4$	$1.09x10^4$	$4.00x10^4$	$1.09x10^4$

[a] error in data is 20%

PF20.CB8

Once the system with the CB7 was studied and association constants were determined, CB8 titrations were performed. In figure 2.12 is represented the spectrophotometric titration of **PF20c**, with CB8, from 0 eq. to 2equiv. The complexation behaviour followed by UV-Vis it very similar with CB7.

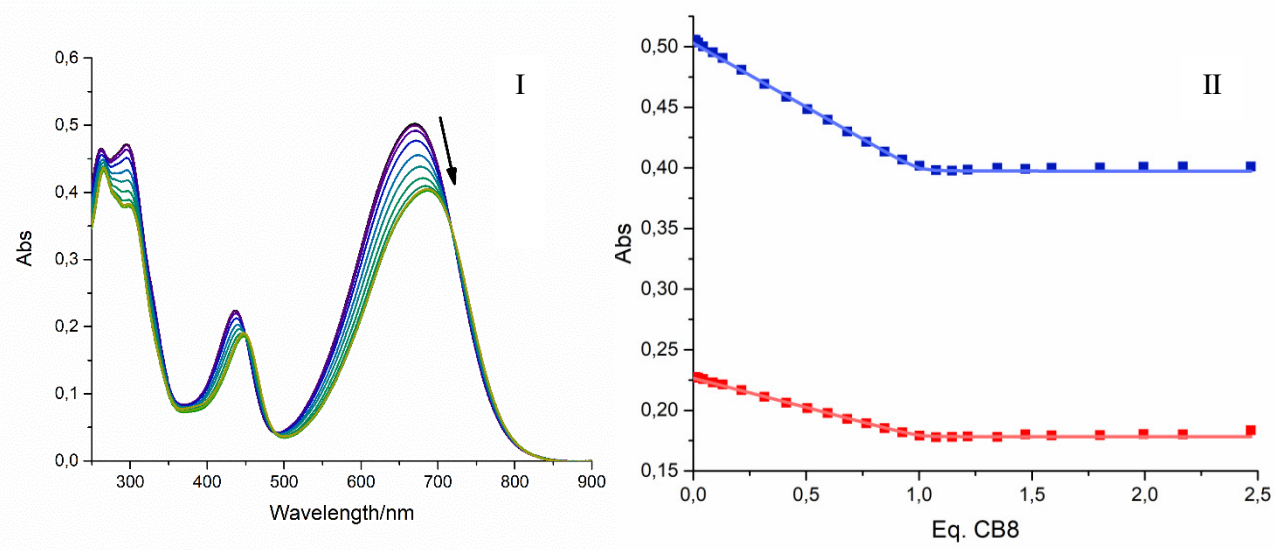

Figure 2.12 (I) Spectrophotometric titration of PF20 with CB8, (II) experimental data (blue) 670 nm; (red) 438 nm, the solid line represents the best least squares fit of data to a 1:1 association model. Conditions [PF20] = $2x10^{-6}$ M;

As previously used for CB7 studies, **PF20** was studied in both isomers and used another technique to confirm the results obtained by UV-Vis spectroscopy. In the studies with CB8 Isothermal titration calorimetry (ITC) was performed instead of RMN titrations, although NMR was performed to determine the structure of the supramolecular complexes (following chapter). Within ITC technique was possible to determine thermodynamic parameters of the host-guest interactions. Bellow, in figure 2.13, is represented the experimental values obtained for this technique for both isomers. Data were fitted with 1:1 binding model, used Equation (17) for this effect. The mathematical model is represented in section 4. The fitting is represented by a line in figure 2.13 and was used to obtain the thermodynamic and association parameters as well.

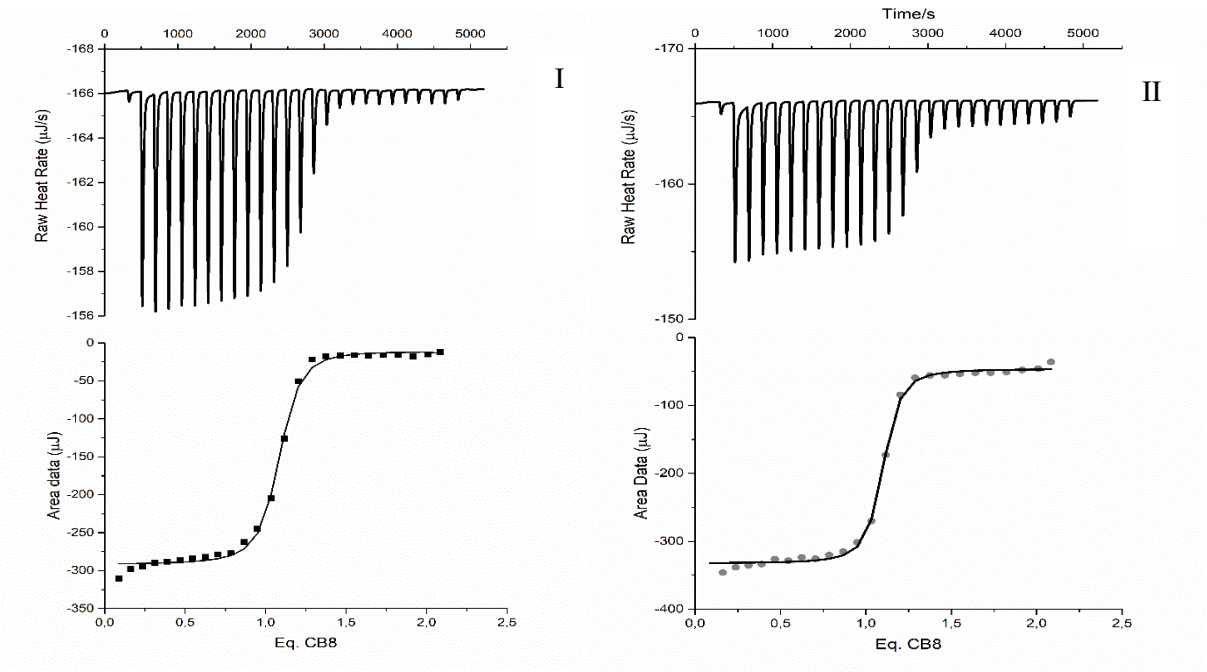

Figure 2.13 (I) ITC of PF20 (Open isomer) with CB8 (II) ITC of PF20 (closed isomer) with CB8. ▪experimental data, (black line) best fitting of the experimental data with a 1:1 binding model.

Listed in table 2.2 are the results obtained for both methods, reported above. The association constants are different for both isomers, as in previously complexes (**PF20** with CB7). Using CB8 as host macrocycle, it is not visible the formation of [21] complex only [11] complex. This fact is due to the structure of the supramolecular complex **PF20.CB8,** determined by NMR spectroscopy (see 2.3 topic). The interaction between the host and the guest molecules is localized on the centre of **PF20** and is very difficult fit two molecules inside the cavity of CB8 due to steric impediments. [21] complexes would be possible if CB8 was in the side "arms" of DAE, as CB7. Obtained values change conforming the technique, but the different conditions, such as different concentration, may explain this effect.

Table 2.2 Association constants determined by UV-Vis spectroscopy and ITC for PF20 (open and closed form) with CB8.[a]

	UV-vis	**ITC**	
	K_{11} (M^{-1})	K_{11} (M^{-1})	ΔH (kJ/mol)
Open	$8.00x10^5$	$2.868x10^6$	-40.21
Closed	$7.00x10^6$	$4.88x10^6$	-40.91

[a] error in data is 20%

PF7.CB7

Once **PF20** systems were understood, Host-Guest studies were performed for another compound, with donor and acceptor moieties (**PF7**). Complexation studies were performed in the same order as performed for **PF20**. CB7 was first made, due to the small cavity it is not possible to include two guests inside the same macrocycle. By UV-Vis titration, it is possible to observe the formation of two complexes, [11] and [21], as in the previously compound. The association constants were determined by best least squares fit of the data to a 2:1 binding model.

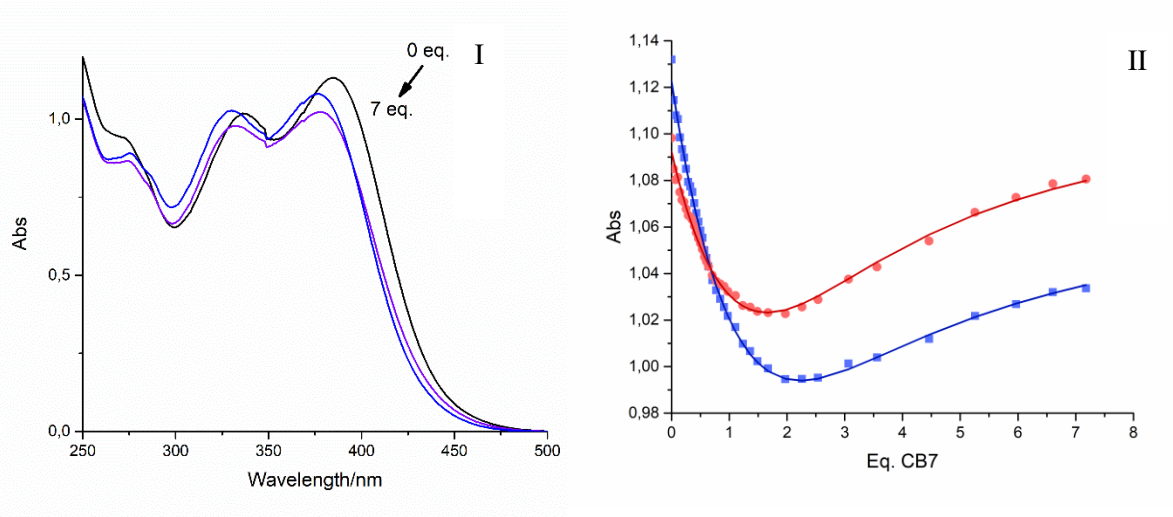

Figure 2.14 (I) UV-Vis titration of PF7 with CB7, (black) 0 equiv. CB7; (violet) 2 equiv. CB7;(Blue) 7 equiv. CB7. (II) Plot of experimental data (red points) 377 nm (blue points) 385 nm, (lines) best least squares fit of the data to a 2:1 association model. Conditions: [PF7] = $2.5x10^{-5}$ M;

Figure 2.14 (I), represents the spectrophotometric titration of **PF7o** with CB7, in the figure, there is not represented all points to have a better perception of spectral differences. In (II) is represented the best fit for the experimental data, (red) 377 nm (blue) 385 nm. The obtained association constants are listed in table 2.3. Comparing the constants with **PF20.CB7** it is possible to verify a similarity, but **PF20** system shows a higher K_{11}, while K_{21} is higher in the discussed system. This means that is more favourable the formation of [21] complex using **PF7** instead of **PF20**. This fact can be explained, once **PF7** has a large π-system, compared with **PF20**. Association constants for [11] complex between CB7 and bipyridinium and pyridinium naphthalene analogue of $1x10^7$ and $3x10^7$ M^{-1}, respectively, were reported in the literature.[72] This data support the previous that the increase of the π-system increases the association constant.

Table 2.3 Association constants determined by UV-Vis spectroscopy for PF7 (open form) with CB7.[a]

	UV-vis	
	K_{11} (M^{-1})	K_{21} (M^{-1})
Open	$7.50x10^4$	$2.50x10^4$

[a] error in data is 20%

The statement above is supported by the molar fraction of each complex in solution versus the equivalent of CB7 (Figure 6.10), where it is possible to verify the presence of at least 50% of these complex ([21]) in solution, using fewer equivalents of CB7.

PF7.CB8

Next has performed the same experiment but with CB8, where supramolecular polymers were expected, due to the donor-acceptor moieties of **PF7** and the large cavity of CB8, that can encapsulate two guest compounds. Obtained data for spectrophotometric titration are represented in figure 2.15. The spectral changes are similar for both compounds (**PF20** and **PF7**), the major difference is the shifting of the maximum wavelength, in this case, a blue shift is observed (shift for a high energetic region) and there is a disappear of a band at 340 nm.

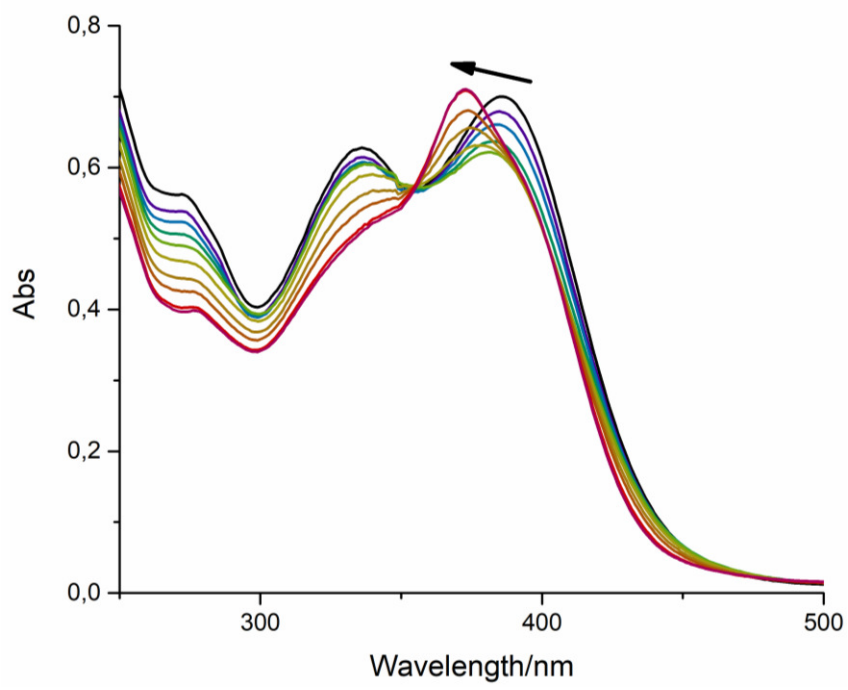

Figure 2.15 UV-Vis titration of PF7 with CB8. Narrow represents the progress of the experiment. Conditions: [PF7] = 2.5×10^{-5} M

Once supramolecular polymers are expected, the data were fitted using a new model. The new model is the modified isodesmic model. As explained below (chapter 1) isodesmic polymerization is similar the step polymerization where the degree of polymerization (DP) is dependent on the association constant of the linking supramolecular unity. In this model, the reactivity of the end groups does not change during the polymerization process, due to neighbouring group effect. Isodesmic supramolecular polymerization is characterized by a single association constant (K) for each reversible step in the assembly pathway, as represented by following equations and in figure 2.16. M_1 represents the monomer and K molar equilibrium constant.[54] The model is also called free association model or multistage open association model.

$$M_1 + M_1 \leftrightarrow M_2 \qquad [M_2] = K[M_1]^2 \qquad (1)$$

$$M_2 + M_1 \leftrightarrow M_3 \qquad [M_3] = K^2[M_1]^2 \qquad (2)$$

$$M_{I-1} + M_1 \leftrightarrow M_i \qquad [M_i] = K^{-1}(K[M_i])^i \quad i = 1,2,\dots,\infty \qquad (2)$$

In the case of **PF7.CB8** compound, the polymerization mechanism is not that linear. Due to the bivalency of guest and the large cavity of CB8, after the first step of polymerization, two pathways may be occurring. One where a new host is added and the other where is added a new guest to the previously formed complex. In the figure 2.16 is schematized the supramolecular polymerization of **PF7** up to [44] complex. A-B represents the acceptor-donor system incorporated into the **PF7** structure, (pyridinium and naphthalene, respectively) and CB8 is represented by the curved box.

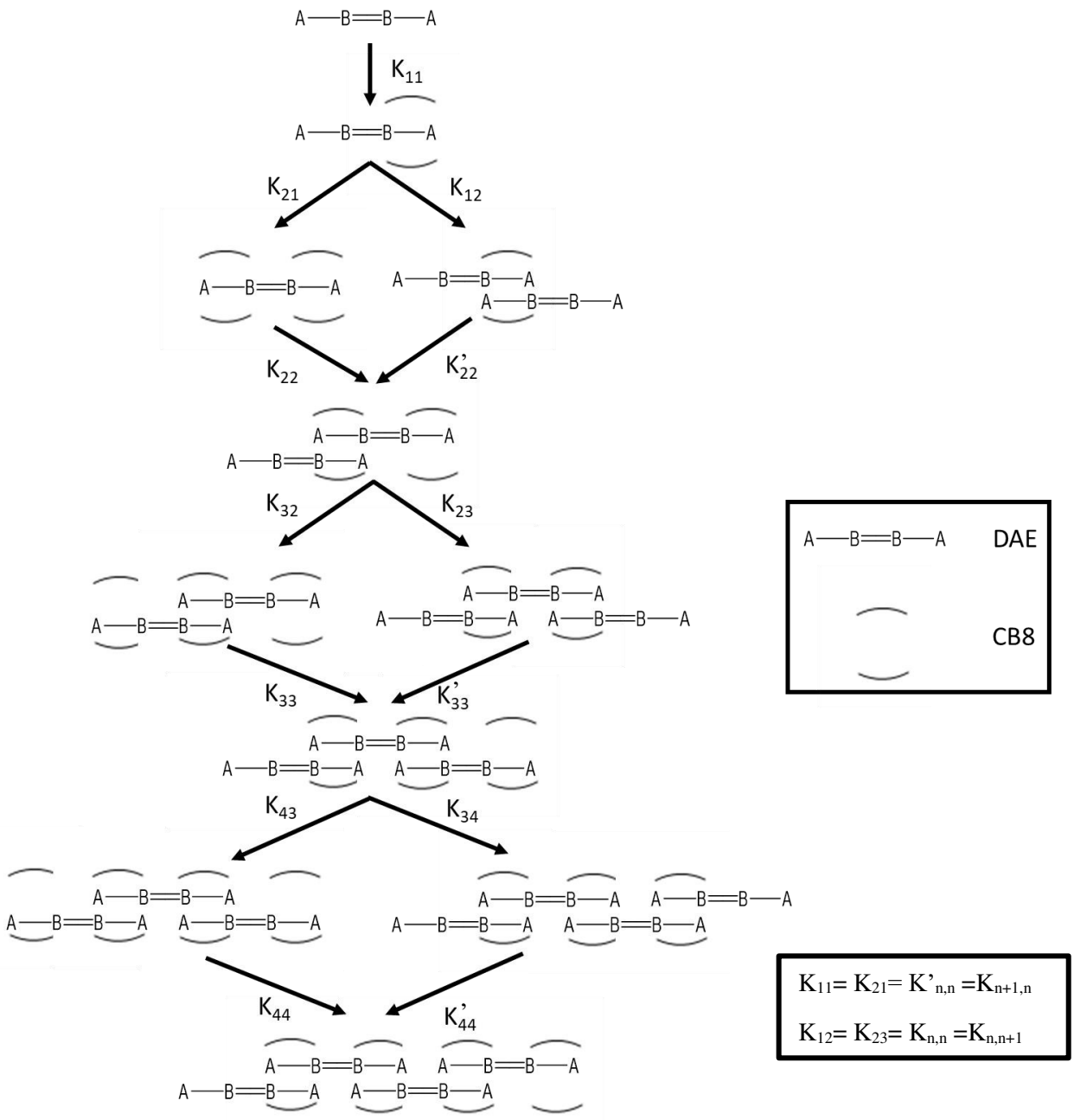

Figure 2.16 Schematic figure of supramolecular polymerization using PF7 as monomer units.

The obtained data were fitted with the modified isodesmic model and in the figure 2.17 are represented the experimental points of PF7 titration with CB8 for different wavelengths (dots), solid lines represent the best least squares fit of the data with the model introduced above. In this way was possible to determine the association constants for [11], [12] and [21] complexes. The values are listed in table 2.4.

Table 2.4 Association constants determined by UV-Vis spectroscopy for PF7 (open isomer) with CB8.[a]

	K_{11} (M^{-1})	K_{12} (M^{-2})	K_{21} (M^{-1})
PF7.CB8	$5.00x10^{7}$	$1.00x10^{5}$	$1.25x10^{7}$

[a] error in data is 20%

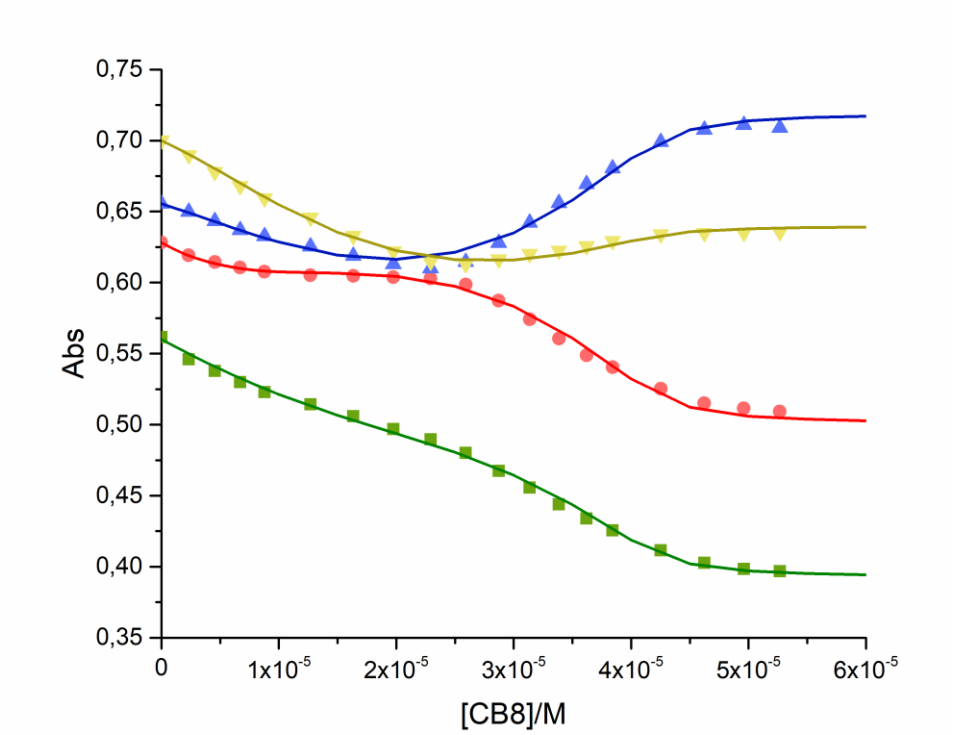

Figure 2.17 Plot of experimental data (points), (lines) best least squares fit of the data to an isodesmic polymerization model. Blue – 374 nm; Yellow – 386 nm; Red – 336; Green 273 nm.

In figure 2.17 is possible to observe two inflexion points, represent the [12] and [21] complexes, respectively. With the increase of CB8 in solution high complexes [12] start to dissociate due to the affinity of **PF7** to CB8. K_{21} is higher than K_{12}, see table 2.4. With the association, constant determined was possible to determine the molar fraction of each species in solution. In the figure 2.18 are represented the molar fraction of each species in solution, up to [55] complex. Grey dotted line represents the sum of the high complexes in solution ([22], [23], [32], [33], [34]; [43]; [44]; [45]; [54]; [55]). It is reported in the literature and discussed above in the introduction chapter of this thesis (chapter 1) that when guest concentration increases polymerization degree (DP) also increases. In the discussed case the formed polymers show short size due to the poor solubility of **PF7** in water. Increasing the solubility of the compound in water will increase the size of the supramolecular polymer formed, that is one of the reasons why a new compound (8) with theoretically high solubility in water is being prepared. Another aspect that may lead to short polymers chain formed is the weak interaction between donor-acceptor moieties of **PF7**.Replacing these moieties by higher affinity pairs to intensify these interactions could improve the growth of the supramolecular polymer in solution.

Figure 2.31 shows the proposed structure of **PF7** with CB8 in solution. That structure represents the majority species in solution, this affirmation is supported by mass spectroscopy (see the following

topic). As NMR spectroscopy was not performed for this compound, the region where π-π stacking take place, and the encapsulation by CB8 is not known. But theoretically π-π interaction take place between the donor and the acceptor moiety (pyridinium and naphthalene), so is to expect the superposition of these two moieties, and the portal region of CB8 should be located near the positive charge of the pyridinium moieties so this way there is a stabilization of the positive charge.

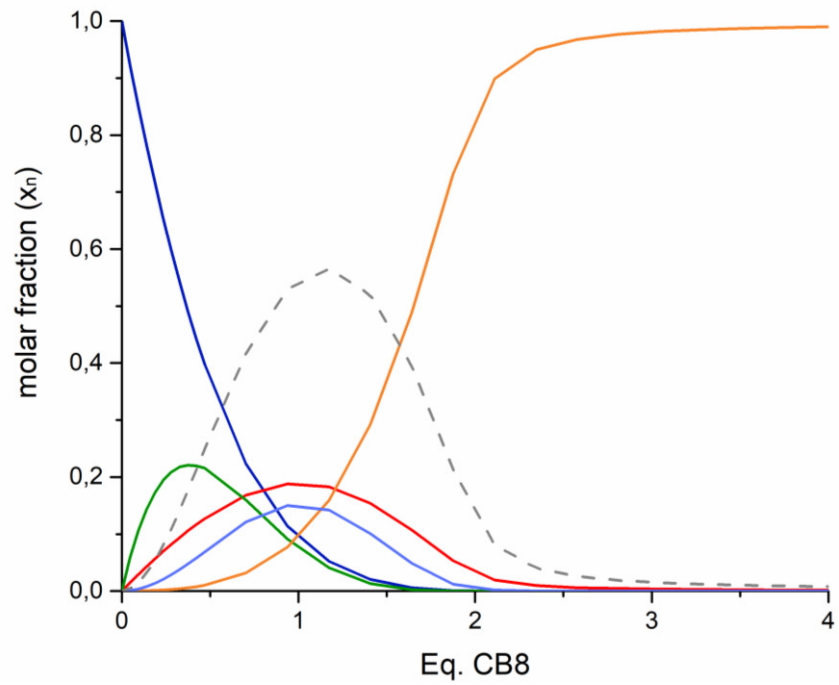

Figure 2.18 Molar fraction of each species in solution. Dark Blue - Guest; [11] – Red; [12] – Green; [21] -Orange; [22] – Light Blue; Dotted line – sum of molar fraction from [22] to [55].

From the molar fraction graph (figure 2.18) is also possible to propose a structure for the majority species in solution determined by UV-Vis. In the case of [12] complex (green line) is assumed that the host is located on the acceptor-donor moieties region, the same for the [21] complex (orange line). In the case of **PF7** with CB8, the supramolecular structure is different from the previously compound (**PF20**), where the host is located on the centre site of DAE (photoactive site). The value of cyclization quantum yield can support affirmation (table 2.5). In the **PF20** system is verify an increment of quantum yield, while in the case of **PF7** the opposite is verified.

2.3 STRUCTURE OF SUPRAMOLECULAR COMPLEXES

To determine the supramolecular complexes structure NMR spectroscopy was performed to have a better perception, where the interactions between both molecules take place (determine the geometry of the complex). In the figure below (figure 2.19) are represented the NMR spectra for the titration of **PF20** with CB7, where is possible to observe that as soon as CB7 was added a significant shift for a shielded region from the pyridinium protons (H2 and H3 in figure 2.20) is observed. The opposite effect was observed for aliphatic and the aromatic protons of the thiophene rings (H4), being the thiophene rings protons the ones that shift the most for the deshielded region, due to the proximity with the portal region of CB7.

PF20.CB7

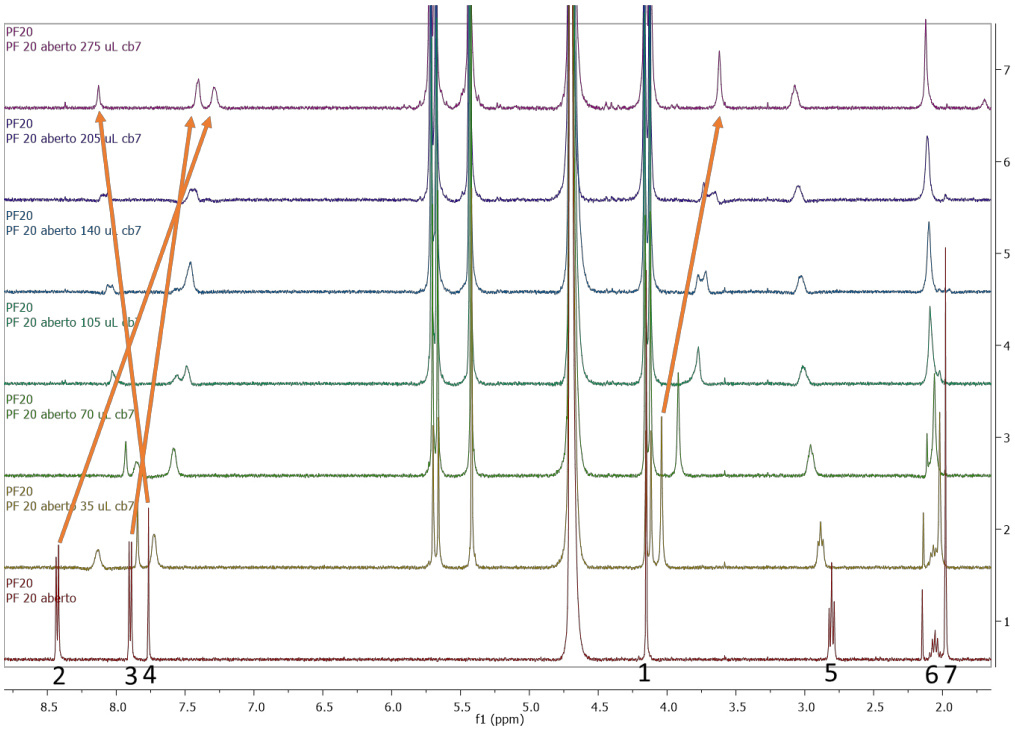

Figure 2.19 ^{1}H NMR titration spectra of PF20 (open isomer) with CB7 (red 0eq, violet 5eq), [PF20] = $5x10^{-4}$ M in D_2O.

In the literature is reported that when organic moieties are encapsulated by CBn a shift for a shielded region is observed, due to the different magnetic environment inside CBn cavity. A contrary effect is observed when organic molecules are localized near the portal region of these macrocycles, so positive or negative shifts must result from the relative position of the hydrogens with respect to the carbonyl group of the portals of CBn (figure 1.7).[38] These processes are observed for this system, and this way supramolecular structure can be determined. This complex adopts a structure where the macrocycle is in the pyridinium region, as represented in figure 2.20., the same structure was determined for **PF20** closed isomer.

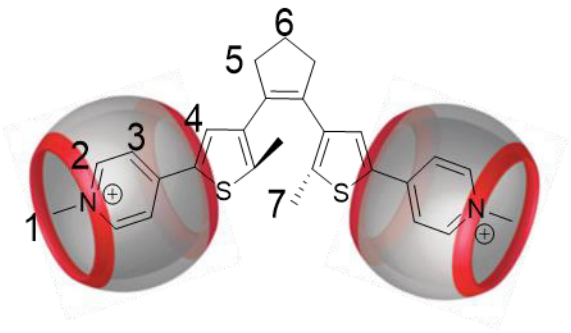

Figure 2.20 Propose structure of PF20.CB7 complex.

ESI-MS was performed on both host and guest molecules. Figure 2.21 shows the obtained spectrum for **PF20** with CB7. Two major signals at m/z 803 and 571 were observed for the complex [11] and **$PF20^{+}I^{-}$** , respectively. Closer analyses of the isotopic distribution indicate a Δm/z = 0.5 charges ion, for the major signal (insets of figure 2.21), indicating a double charge system who confirms the [11] complex.

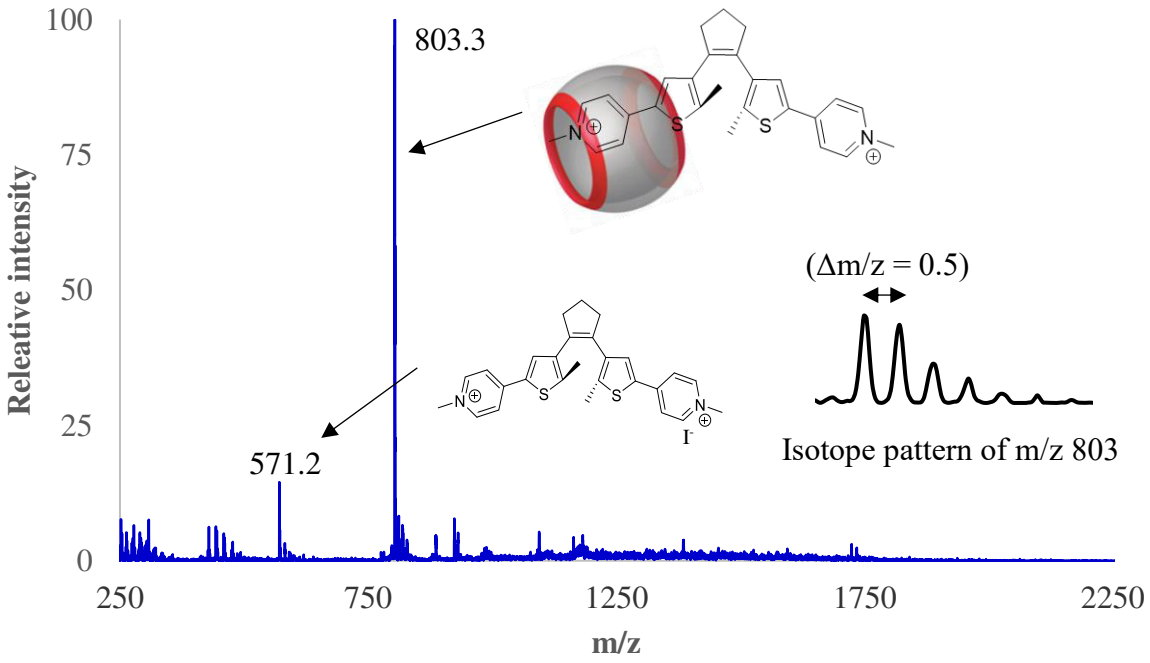

Figure 2.21 Full ESI-MS spectra for PF20 with CB7; [PF20] = 50μM

MS^2 was performed for 803m/z signal obtained spectra (appendix figure 6.12) indicates a high association of host and guest molecules in gas phase, once the complex is whole fragmented upon fragmentation and no other signals are detected.

PF20.CB8

The same technique was performed to determine the structure of **PF20.CB8** supramolecular complex. In figure 2.22 are represented the NMR spectra of **PF20** with CB8. The acquired spectra show that CB8 is complexed on the photoactive site of the organic molecule (**PF20**), cause aliphatic protons (H5-H7) shifted to high field, meanwhile the aromatic proton, namely the pyridinium proton, shift to the low field, opposite effect of CB7 complexation. With the experimental data, a proposed structure illustrated in figure 2.23 was formulated.

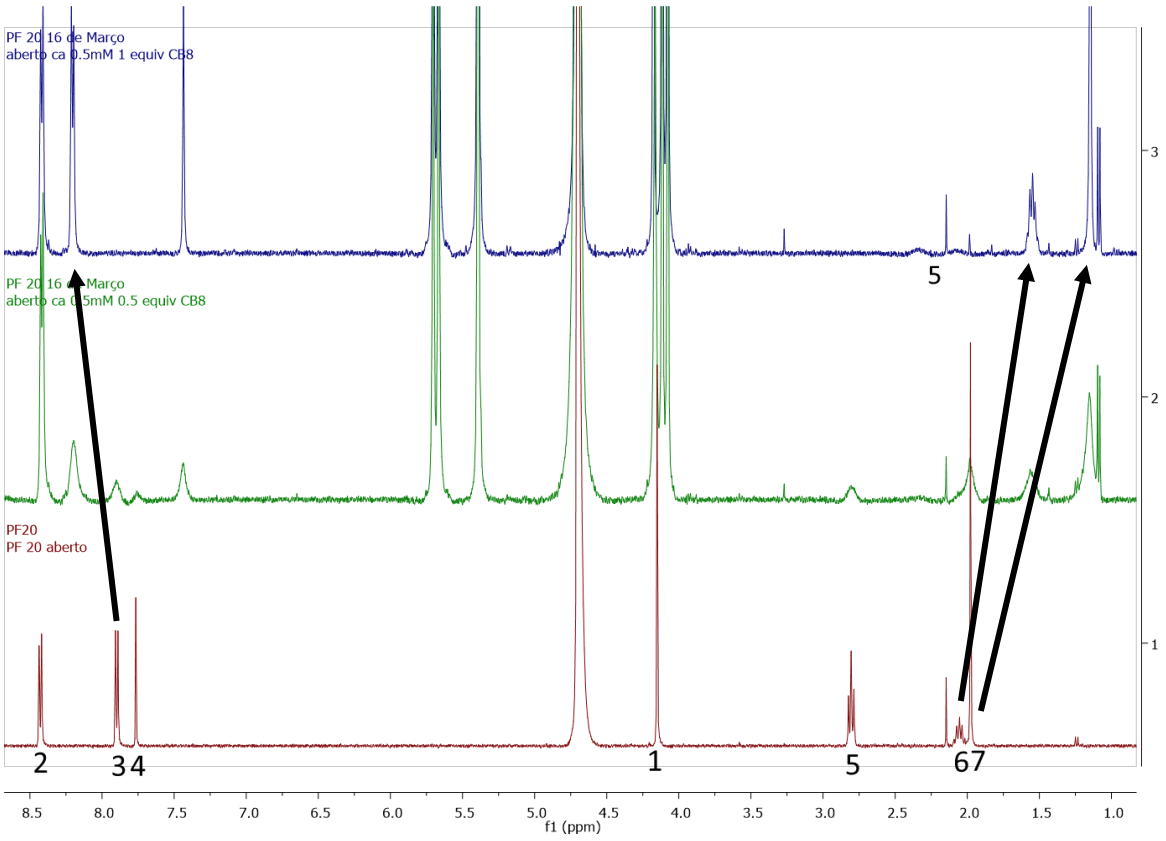

Figure 2.22 ^{1}H NMR titration spectra of PF20 with 0 (red), 0.5 (green) and 1 (blue) eq of CB8, [PF20] = $5x10^{-4}$ M in D_2O.

The high quantum yield of the cyclization reaction and the conversion reactions when the molecules are complexed with CB8 (topic 2.4), might be explained due to the structure of these supramolecular complexes. Due to the cavity size of the macrocycle (CB8), only the linear conformation of the open-isomer can fit in the macromolecule, and the parallel conformation shows a cubic structure, occupying more space. So, when the compound is complexed, and the macrocycles enclose the centre of the molecule, the populations between both conformations changes, and there is an increment of Ap compared with p, that is also the photoactive conformations, as said below. So, the encapsulation of the CB8 on the photoactive site of diarylethene improves the cyclization reaction.

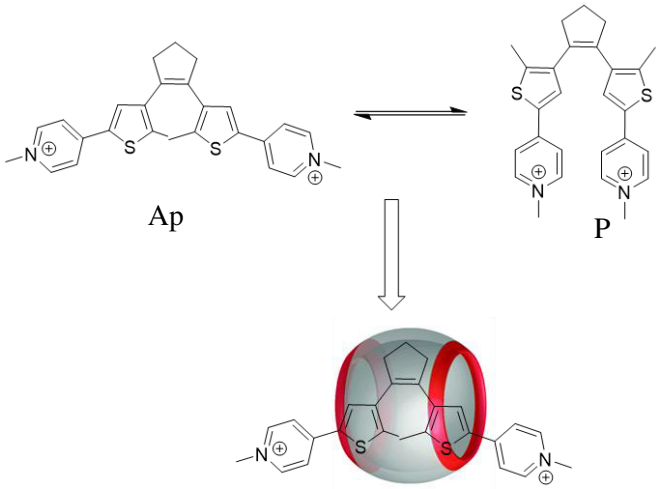

Figure 2.23 Both conformations of PF20 open isomer and the proposed structure of PF20.CB8 complex.

ESI-MS was performed for CB8, and in this case, four major signals were observed at m/z 1551, 1219, 886 and 571, corresponding to [21], [32], [11] and **PF20^{+}I^{-}** respectively, in figure 2.24. Supramolecular structures, namely [32], were detected with this technique but not by UV-Vis spectroscopy. MS^{2} was performed for major signals. For [11] complex the effect observed for CB7 is also observed for CB8, the whole complex is fragmented.

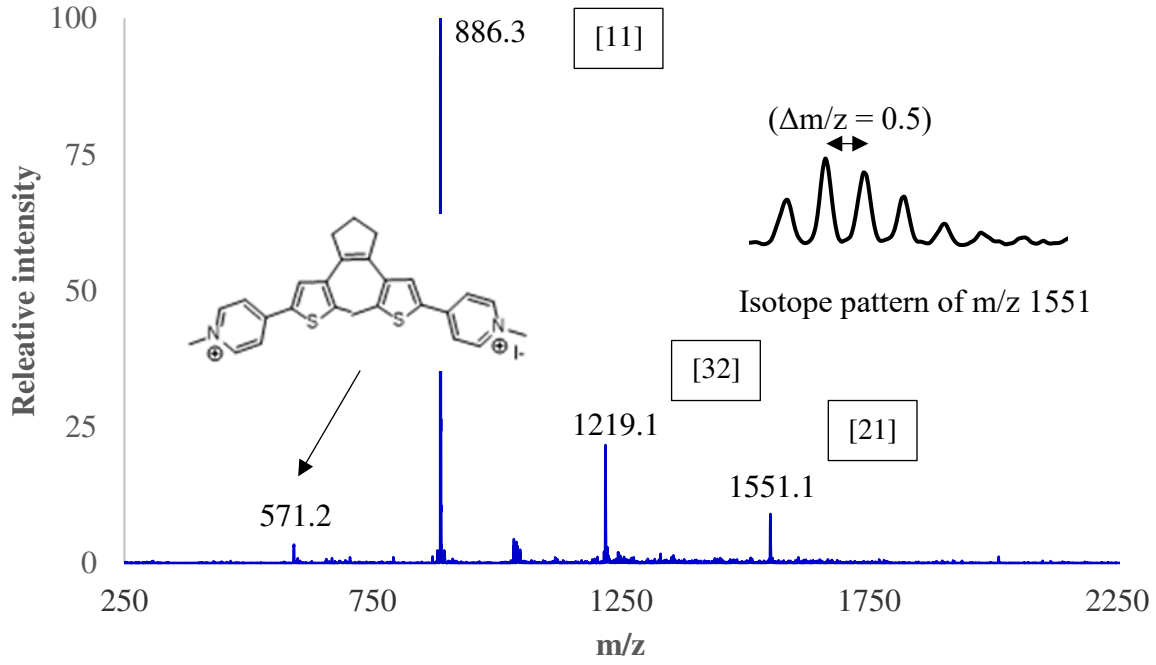

Figure 2.24 Full ESI-MS of PF20 with CB8. [PF20] = 50µM

Isotope distribution of 886 m/z signal is Δm/z = 0.5, which indicate a double charge ion, also observe in m/z 1551 signal. Fragmentation (MS^{2}) of [21] complex signal (m/z 1551) leads to [11] complex, fragmentation pattern indicates the signal at m/z 1551 correspond to a [21] complex (figure 6.13 and

6.14 in the appendix). Isotope distribution of m/z 1219 signal indicates four charge ions, this signal is correspondent to a supramolecular polymer [32], as mentioned above. Fragmentation of m/z 1219 (MS^2, obtained spectra in figure 2.26) shows that the fragmentation leads to [11] and [21] complex, m/z 886 and 1511, respectively.

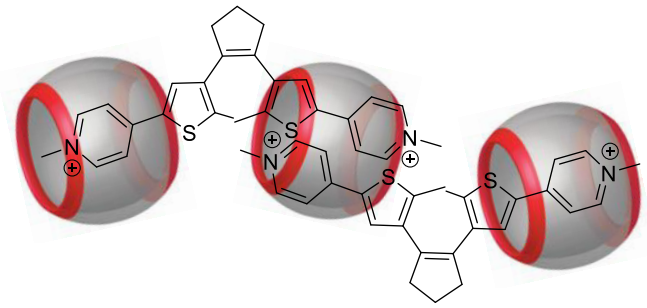

Figure 2.25 Propose structure of 3:2 supramolecular polymer

In figure 2.25 is illustrated a proposed structure of [32] supramolecular complex. Evidence of this supramolecular structure was not observed in other performed techniques, probably, due to the difference in interactions, for ESI-MS the molecules are in gas phase, while, in the other used techniques the essays were done in aqueous media. In the gas phase, there is no solvation by solvent molecules, for example. Another possible explanation is an intramolecular charge-transfer happening between thiophene ring and pyridinium moiety, that can be intensified in gas phase.[73]

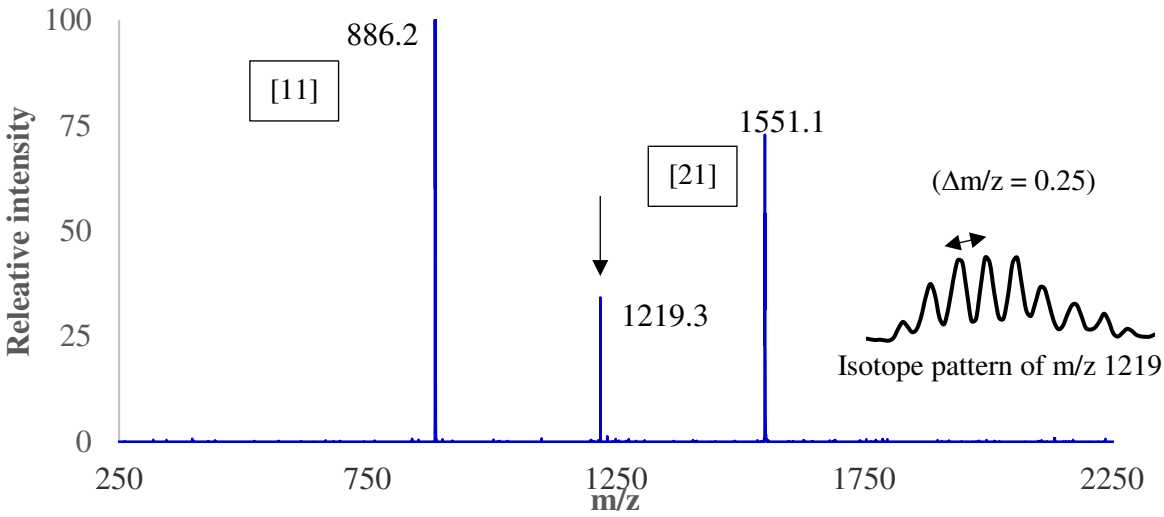

Figure 2.26 MS^2 of m/z 1219 signal, obtained for PF20 with CB8.

Job plots were performed for **PF20** to confirm the stoichiometry of the formed complexes. Figure 6.29 and 6.30 in the appendix, show the obtained results for PF20 with CB7 and CB8 in both isomers. By the obtained data 1:1 stoichiometry of host-guest complexes was determined. In the case of CB8 these results were expected, but for CB7 [21] stoichiometry was expected. This can be explained due to the low association constants for 2:1 complexes with CB7, and thus [21] complexes are more visible when the concentration of CB7 is high.

PF7

NMR spectroscopy was not performed for **PF7** due to the poor solubility in water but is possible to assume the same structure of **PF20.CB7** for **PF7.CB7,** once the behaviour is comparable to **PF20.CB7** and the structure of guest compounds are similar. Otherwise, **PF7.CB8** structure of the majority species in solution was determined to have been different from **PF20.CB8**, supramolecular polymers species are detected in solution (see topic 2.2 and 2.4).

PF7.CB7

Figure 2.27 shows the obtained spectrum for **PF7** with CB7 [11] equivalents, four major signals were observed at m/z 929, 555, 348 and 141. In the full scan is observed two signals from fragmentation of **PF7** due to the fragility of pyridinium naphthalene moieties bond. Isotope distribution of m/z 929 indicates a double charge compound, identified as [11] complex. Fragmentation of m/z 929 leads to three new species (figure 6.15 in appendix), m/z 1161 is the loss of a proton of CB7, m/z 1717 is CB7 with fragment detected at (m/z 555) and m/z 1303 is CB7 with the other fragment (m/z 141).[74]

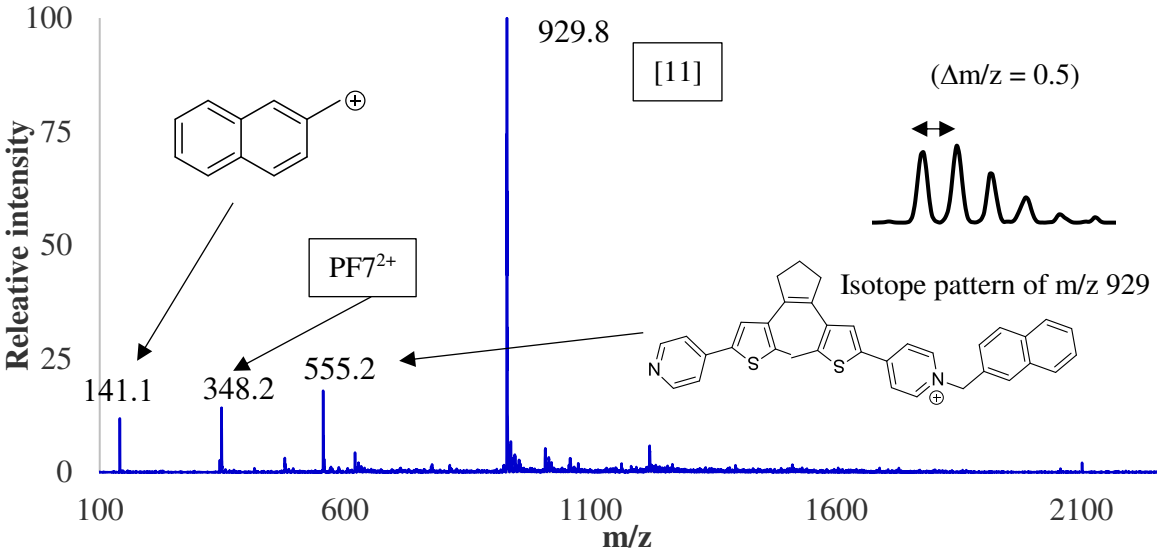

Figure 2.27 Full ESI-MS spectra of PF7:CB7 1:1

The same experiment was made with an excess of CB7 in the sample. Full obtained spectrum is shown in figure 2.28, under this condition [21] complexes are seen at m/z 1511, isotope pattern is consistent with double charged ions, and the signal at m/z 1764 is attributed to CB7 aggregation.[75] In the case of the signal at m/z 1395 was not possible to attribute a species, need further studies to be possible a right attribution. Fragmentation at m/z 929 was not performed, once was made in the previous experiment, with [11] stoichemistry of **PF7:CB7**. Fragmentation of [21] complex (m/z 1511) leads to CB7 with both mentioned fragments (m/z 1717 and 1304) and CB7 deprotonated (m/z 1161), figure 6.16 in appendix.

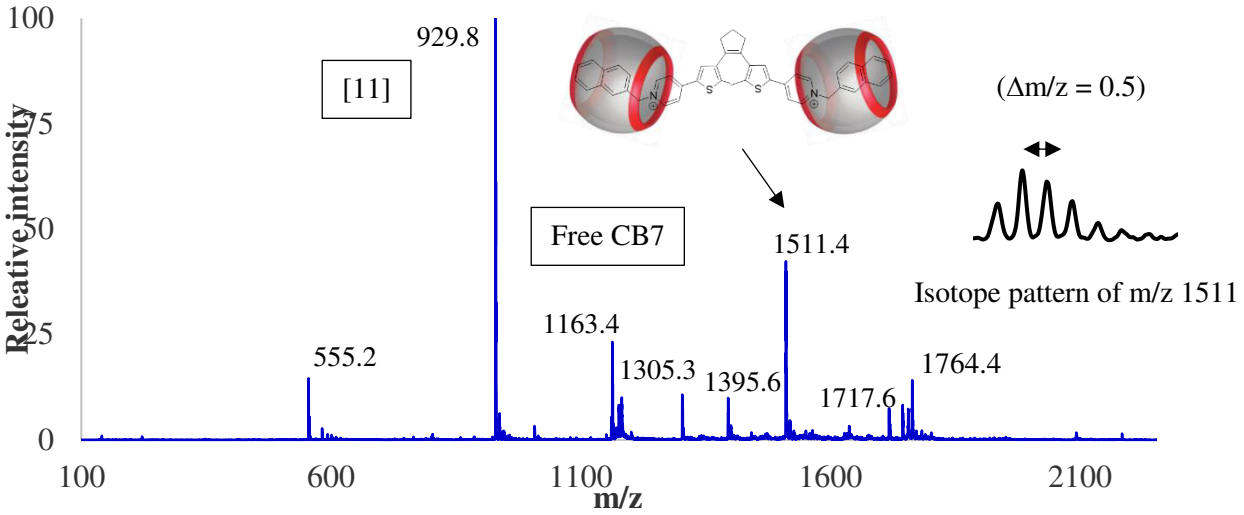

Figure 2.28 Full ESI-MS spectra of PF7 with CB7 2:1.

PF7.CB8

ESI-MS for PF7 with CB8 was performed using excess of guest and with an excess of the host. The results when **PF7** is in excess are similar to the assay made using an excess of CB8. In the last case represented in figure 2.29, a signal at m/z 1345 was observed and is assigned to [32] complex confirmed when fragmentation was performed, figure 2.30. Fragmentation leads to two signals at m/z 1677 and 1012, correspondent to [21] and [11] complexes. By the pattern of fragmentation was possible to confirm the attribution made for the signal at m/z 1345.

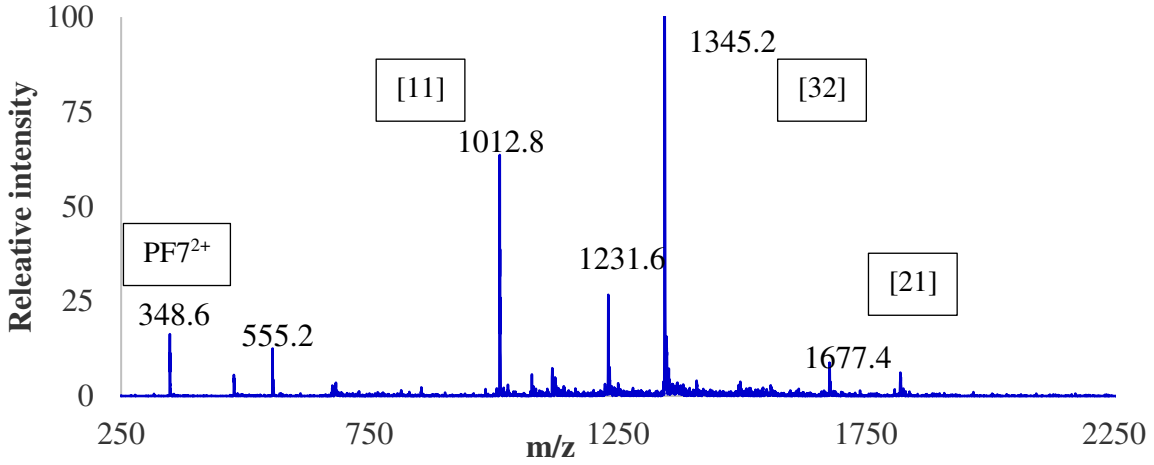

Figure 2.29 Full ESI-MS spectra of PF7 with CB8 [21] under very soft ionization conditions.

The signal at m/z 1231 (figure 2.29), is a multiple charge system but was not study in detail, the theoretical calculation was performed for the large supramolecular system, but determined values are different from obtained values, suggesting a more complex system. Isotope distribution of m/z 1012 and m/z 1345, indicates a double and a four-charge system, respectively, corresponding to [11] and [32] complexes. Structure of [32] supramolecular assembly should be like to the one proposes for **PF20**, figure 2.31.

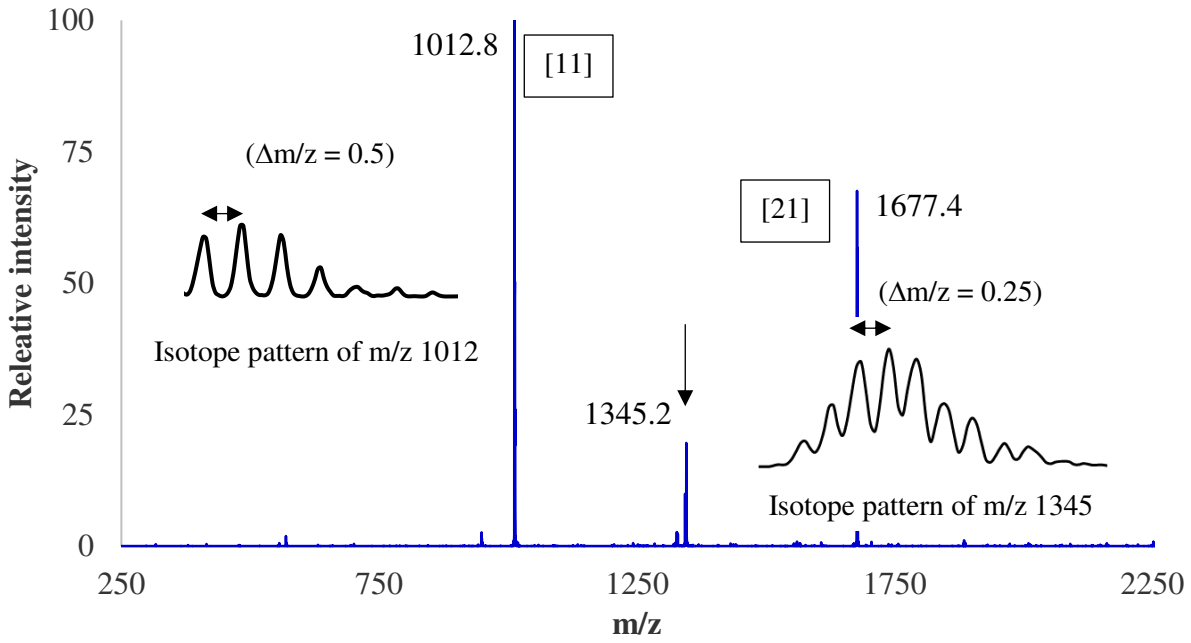

Figure 2.30 MS^2 of m/z 1345 signal, obtained for CB8 with PF7 (2:1).

NMR and MS techniques enable a better understanding of supramolecular structures formed for host and guest used. Oligomer [32] was observed in MS spectroscopy and the same species was not seen in other techniques, this could be explained by the different condition used for each technique. Poor solubility of **PF7** in water could also explain the differences between results. As stated above the interaction in the gas phase are different from the happened interaction in solution.

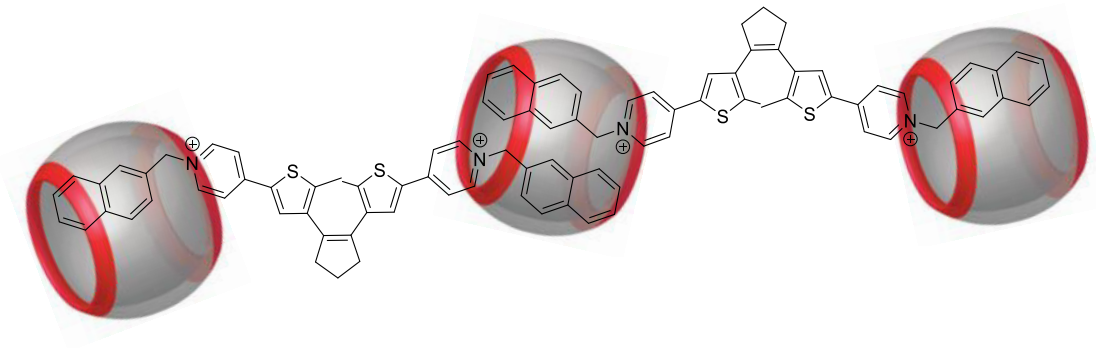

Figure 2.31 Propose structure of the major species of the PF7.CB8 polymer in solution.

*All ESI-MS signals were confirmed by theoretical calculations.

2.4 PHOTOCHEMICAL BEHAVIOUR

After host-guest interactions were studied, photochemical properties of these synthesized compounds were characterized, and this way is possible to verify if these properties are influenced by the supramolecular system. So photochemical properties will be studied with and without hosts compounds (CB7 and CB8) for both synthesized DAE's.

2.4.1 Free and complexation behaviour

Photochemical studies consist in the irradiation of an aqueous solution of the desired compound, with UV light, to convert the open isomer (I) to the closed isomer (II) (cyclization reaction, I and II in figure 2.32) and the inverse reaction (cycloreversion reaction) using visible light for this effect. Open and closed isomers are also known as open and closed forms, respectively. The photochemical reaction of **PF20** and **PF7** is shown in figure 2.32, wherein the red colour is indicated the chemical bonds responsible for the pericyclic reaction (cyclization and cycloreversion reaction). As indicated in chapter 1, these pericyclic reactions are characterized by the movement of six electrons of the π-system ($6\pi e^-$).

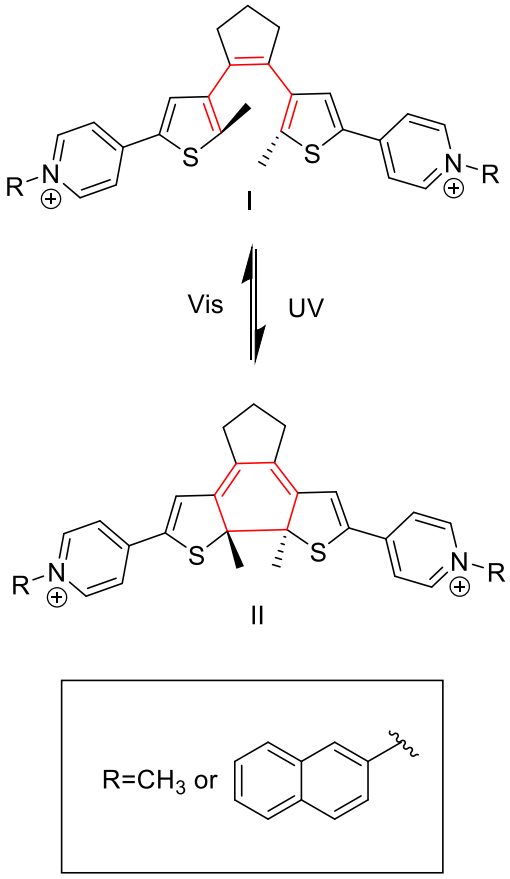

Figure 2.32 Photochromic reaction of synthetized DAE's, with different residual groups.

The type of reaction can be sub-named as an electrocyclic reaction, once there is a formation of a sigma bond (σ), and a loss of a double bond (π), As represented in red colour in figure 2.32.

Photochemical reactions (cyclization and cycloreversion) were followed by UV-Vis spectroscopy, as shown in figure 2.33. Obtained spectra for both molecules are very similar between them and between

derivatives compounds reported in the literature, see chapter one example. As the molecule is converted on the closed isomer a new band increase in the visible region, at the same time the band characteristic of open isomer decreases intensity. Once the process was studied for free molecules, the same experiment was performed with an excess of CB7 and CB8, to guarantee a total complexation. The determined values of quantum yields for cyclization and cycloreversion reaction are listed in table 2.5, the quantum yield was determined using equation (4), where only the first initial points (linear region) were used to determine *m*. V is the sample volume and I_0 was determined by chemical actinometry for each irradiation wavelength.

$$\phi = \frac{V.m}{1000.\Delta\varepsilon.I_0.(1-10^{-\Delta Abs})} \quad (4)$$

Comparing model compound system, it is possible to verify that **PF20** alone shows the lower value of cyclization quantum yield, while **PF20.CB7** and **PF20.CB8** show the higher ones. A possible explanation for the higher quantum yield for the cyclization reaction when the compound is complexed with CB8 is due to the supramolecular structure, DAE's included inside CB8 cavity are forced to have only the antiparallel conformation, as explained before (see figure 2.23). For the **PF7** system, there is a small decrease when it is complexed with CB8. Comparing both systems, **PF7** seems to be more efficient. When is complexed the quantum yield for cyclization reaction is the highest, and it might be explained due to the large π-system of **PF7**. Naphthalene is an electron donating group which increase the quantum yield, once EDG substituents in peripheric carbon of DAE's stabilizes the formed sigma bond. The low cyclization quantum yield is also due to the solvent polarity, have been reported in literature that apolar solvents increase the cyclization quantum yield.[7]

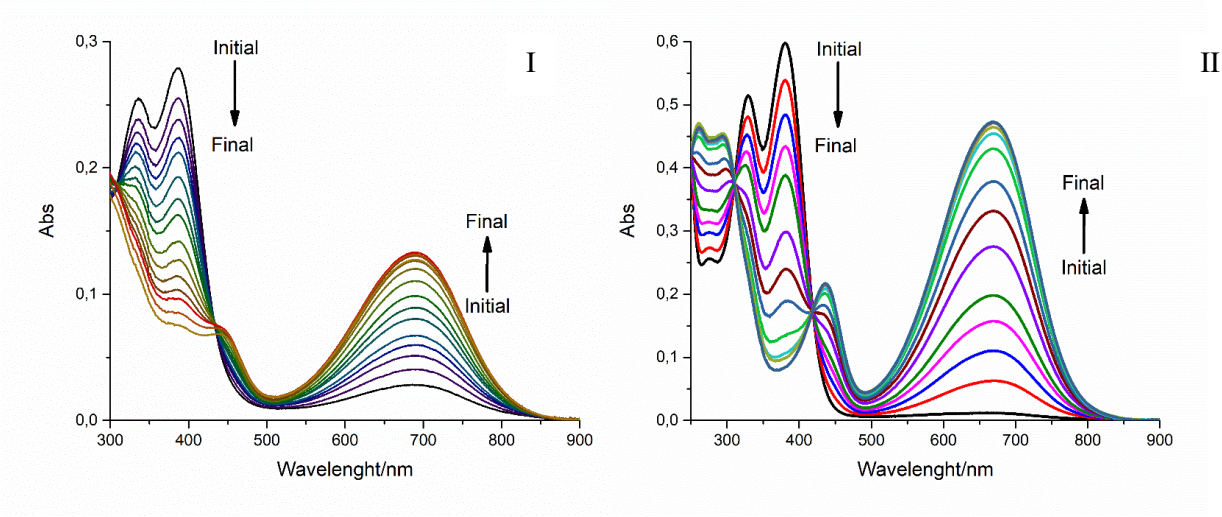

Figure 2.33 (I) Spectral variation of PF20 and (II) PF7 upon photoirradiation in water (PF20) with 1% methanol (PF7); conditions: [PF20] = $2x10^{-5}$ M; [PF7] = $2.5x10^{-5}$ M; T=20ºC; λirr=365 nm.

2.4.1.1 Kinetics

Kinetic constants of both reactions were determined. Cyclization reaction can be fitted by using an exponential function of the type of Eq. (5), where y is the experimental absorbance at the t time. *t* is the time, and a1, a2 and k are fitting constants.

$$y = a1 \pm a2e^{-kt} \quad (5)$$

The explanation for the kinetic behaviour of the cyclization process, is due to the existence of two conformers in the open isomer, as mentioned before. Both conformers represented in figure 1.4, where is also possible to observe the reaction selectivity. Cycloreversion reaction data were fitted with the same equation used for cyclization reaction Eq. (5).

The fitting is represented in figure 2.34, and the obtained constants are listed in table 2.5. As listed in the table, **PF20** show higher kinetic constant than **PF7**, but when both compounds are complexed with CB8, the constants become similar and an improvement of **PF7** cyclization reaction rate. Obtained values for kinetic constants, represented in table 2.5, are determined under the following irradiations conditions. $I_0 = 2.2x10^{-7}$ (365 nm), $I_0 = 1.7x10^{-7}$ (550 nm), [PF20] = $2x10^{-5}$ M and [PF7] = $2.5x10^{-5}$ M, T=20ºC.

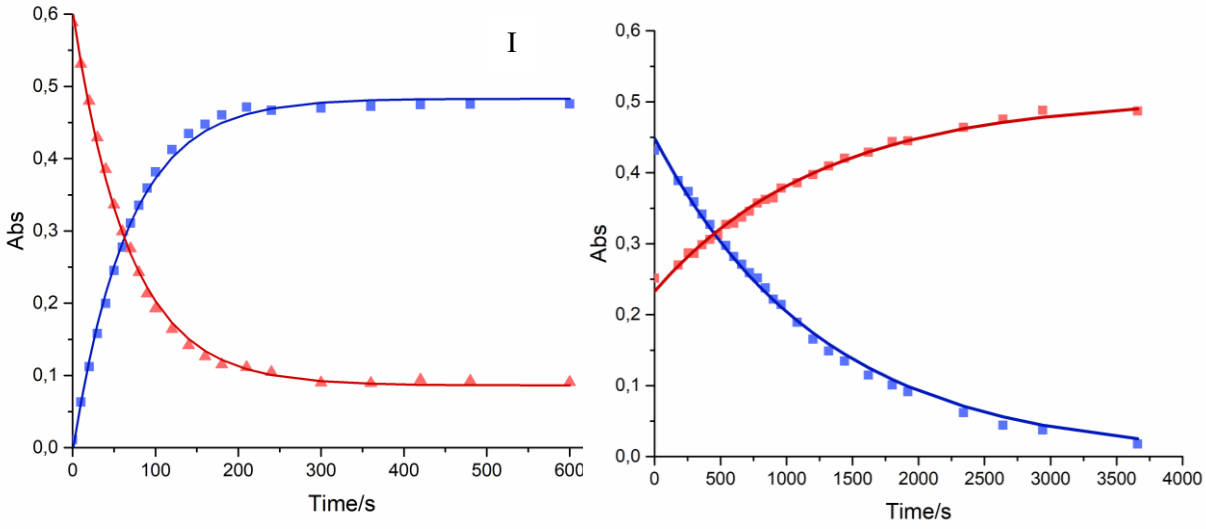

Figure 2.34 (I) Experimental data for cyclization reaction (II) Experimental data for cycloreversion reaction of PF20 (Blue) 655 nm; (red)385 nm. Solid lines represent the best least squares fit equation (5).

Table 2.5 Quantum yield and kinetic constants for ring-closure (cyclization) and ring-opening (cycloreversion) reaction.

	$\phi_{O\rightarrow C}$ (λ_{irr})[a]	$\phi_{C\rightarrow O}$ (λ_{irr})[a]	$k_{O\rightarrow C}$ (s^{-1})	$k_{C\rightarrow O}$ (s^{-1})
PF20	0.26 [365 nm]	0.019 [550nm]	1.50E-02	8.25E-04
PF20.CB7	0.35 [365 nm]	[b]	7.20E-02	[b]
PF20.CB8	0.60 [365 nm]	0.016 [550nm]	9.60E-02	7.74E-04
PF7	0.65 [365 nm]	[b]	3.04E-03	[b]
PF7.CB8	0.56 [365 nm]	[b]	9.62E-02	[b]

[a] I_0 was determined using ferrioxalate chemical actinometer. [b] not determined due to experiment time.

The kinetic constant for the cycloreversion reaction of the **PF20** system is lower in case of CB8 complex, this can be explained due to the stabilization of closed isomer inside CBn cavity, once this isomer shows a π system more delocalized, compared with the open isomer. When **PF20** is encapsulated with CB8 the π system is stabilized by the hydrophobic cavity of the host. The stability can explain the low rate of cycloreversion reaction.

2.4.1.2 Thermal stability

Once the DAE's are well known for their thermal stability, a simple experiment was performed to verify it. After irradiation with 365nm cut-off filter, the coloured solution was put in the dark, for one week. The experiment was followed by UV-Vis spectroscopy, spectra were made before and after one week. With both spectra was possible to prove the thermal stability, in the dark, of the free and the complexed species. Another interesting fact is the shift of maximum wavelength (λ_{max}) of the open-isomer in the presence of the complexing agent. The λ_{max} for all complexes are shown in table 2.6. Complexes with **PF20** show a redshift (Visible region) while **PF7** complexes show a Blue shift (UV region). **PF7** complexes show a high Gap energy compared to **PF20** complexes. The most visible difference is belonging to **PF20.CB7**, where the maximums wavelengths move for lower energy region, this can be due to the intermolecular CT interaction.[73]

Table 2.6 Maximum wavelength of DAE's in open and closed isomer.

	λmax	
	Open	Closed
PF20	385	655
PF20.CB7	404	706
PF20.CB8	398	690
PF7	388	688
PF7.CB8	373	686

The λmax of closed isomers change for higher wavelengths due to the delocalization system caused by the π bonds (compared with open-isomers). The formation of a covalent bond between thiophenes rings enables the extension of the π system for all the molecule. The value of the maximum wavelength for **PF7** can be explained by the electron donating group present in the structural backbone. The observed

shift indicates that the guest molecules are being encapsulated by CBn, once the cavity of these macrocycles shows a different electronic and magnetic environment.

By NMR spectroscopy was possible to determine the percentage of each isomer (open and closed) at the photostationary state (PSS), without and with a complexing agent. That values are listed in table 2.7. When **PF20** is not encapsulated 15% of molecules does not convert to the closed isomer, when **PF20** is complexed with CB8 100% of open form is converted to the closed isomer (Considering the detection limits of the instrument). The increment on cyclization reaction could be explained by the structure of the supramolecular complex formed, CBn is localized on the photoactive site od DAE, detailed explanation on chapter 2.3. For the **PF7** system, NMR spectroscopy was not performed for complexed compounds due to the poor solubility.

Table 2.7 Open and closed isomer in Photostationary state, for the PF20 system. [a]

	%OF[b]	**%CF[b]**
PF20	15	85
PF20.CB7	_[c]	_[c]
PF20.CB8	0	100

[a] This data was collected after irradiating the NMR tube at 365nm with a Cut-off filter, NMR spectra in figure 6.27 in the appendix; [b] determined by H^1-NMR; [c] undetermined due poor resolution.

2.4.1.3 Fluorescence

DAE's are also known for their fluorescence properties, in figure 2.28 are represented the emission spectra of studied compounds (**PF20** and **PF7** alone and complexed with CB7 and CB8). The behaviour is similar in both systems, with exception of **PF7.CB7** that shows a higher emission intensity, compared with analogue compound (**PF20.CB7**). Comparing both systems, **PF20** is more emissive than **PF7**, shows higher fluorescence quantum yield, values in table 2.8. This value also increases when the compound is complexed with CB8. From the values of table 2.8, it can be observed that the encapsulation of CBn exerts a dramatic influence on the fluorescence quantum yield. The increase of fluorescence quantum yield can be due to the minimization of the interaction between the guest and the solvent, as well the low mobilization of the guest inside the cavity of CB7. The organic molecules inside CB7 cavity are more confine compared with CB8 cavity.[76]In the case of **PF7.CB8** who show a lower value than **PF7.CB7**, the dimeric nature of the complexes ([32]) and the self-quenching effect due to the π-π stacking must be responsible for the decrease in fluorescence quantum yield. Closed-isomer emissions were not detected, but theoretical calculation shows an expected emission around 1300 nm. This emission was observed when transient absorption experiments were performed revealing an emission around 1300 nm with a short lifetime (~500fs) when excited at 650 nm.

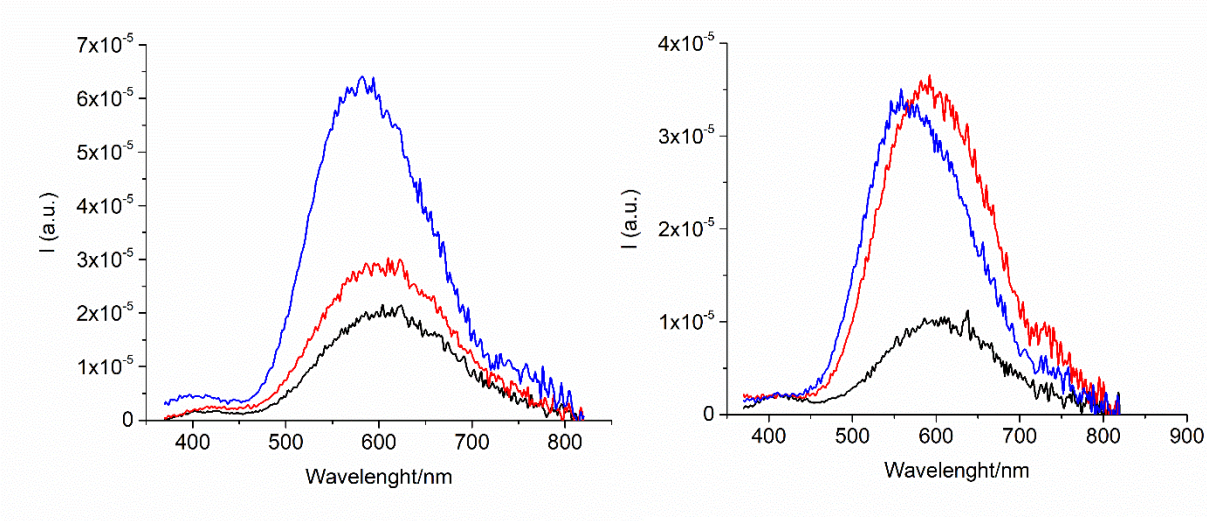

Figure 2.35 Emission spectra of PF (black); PF.CB7 (red); PF.CB8 (blue) for (I) PF20 and (II) PF7 compounds.

The high Stokes-shift value can be justified, by the structural changes between fundamental and excited state. Another determined property was the fluorescence lifetime (listed in table 2.8) of compounds under study. Lifetime titration experiments were also performed to determine the lifetime of each species in solution. The titrant range was 0-40equiv. for CB7 and 0-20equiv. for CB8. All the data was fitted globally with 3-exponential decays. During the global analyses was verified that when there is not a complexing agent in solution (CBn), the equation that best fits the data is a bi-exponential equation and not a mono-exponential equation. This effect is due to the two conformations of DAE's. To confirm the last affirmation Time-resolved emission spectra (TRES) for free molecules was performed. The excitation wavelength was 373nm. The obtained result was fitted well with a bi-exponential equation, which proves that the diarylethene show two different lifetimes ascribed to different conformations parallel and antiparallel (figure 2.23).

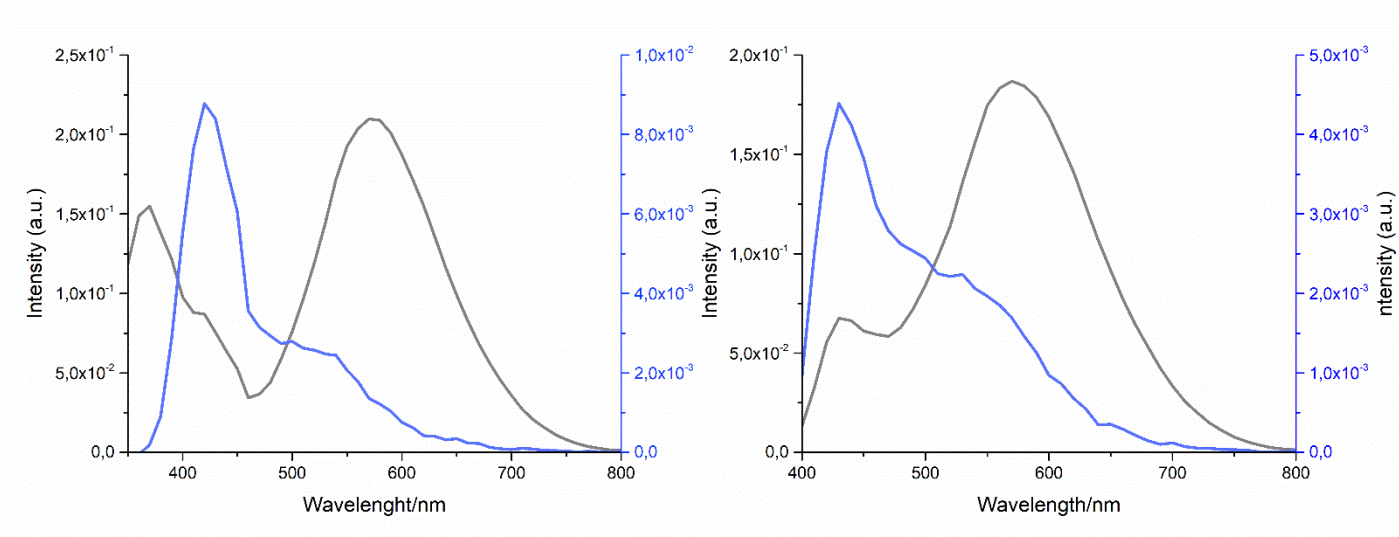

Figure 2.36 Emission spectra made based on lifetime titration data for PF20, (blue) p conformation; (black) ap conformation.

In figure 2.36 is represented the contribution of each lifetime of each conformation versus the wavelength. With this technique was also possible to determine the contribution of each component, something that by fluorescence spectroscopy was not possible to obtain due to the sensibility of this technique. The attribution of each conformation was given cause:

-Global analyses made at lifetime titration results show a fast decrease of a component with a lifetime similar to the one obtained by TRES, ~0.31 ns.

In this way the fast component was attributed to the antiparallel conformation, while the long one belongs to the parallel conformation, once in lifetime titration, one component with a lifetime similar to Ap decrease with the addition of CBn, as illustrated in figure 2.37 and 6.31 in the appendix. From the analysis of these graphics is possible to determine the lifetime of each component. Supramolecular complexes show longer lifetime, these results indicate that the complexes suffer more conformations changes in comparison to non-complexed species.

Table 2.8 Fluorescence quantum yield and lifetime for synthetized DAE's

	Φ_f[a]	λmax/nm	τ/ns
PF20	0.00366	618	0.22
PF20.CB7	0.00521	618	1.27 [11] 2.92 [21]
PF20.CB8	0.0105	586	0.69 [11]
PF7	0.0019	607	0.28
PF7.CB7	0.00619	588	0.74 [11] 1.83 [21]
PF7.CB8	0.00561	555	0.66 [11] 1.70 [12]

[a] quantum yield;

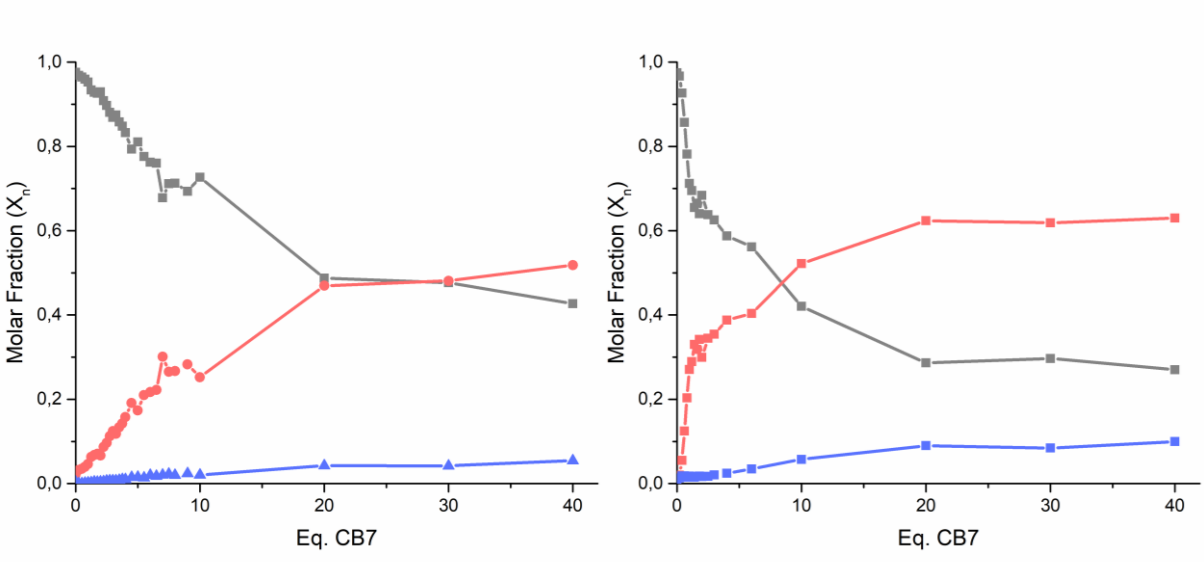

Figure 2.37 Molar Fraction versus Equiv. of CB7 for (I) PF20 and (II) PF7, determined by Lifetime titration. (Black) Guest; (RED) [11]; (Blue) [21]; Conditions: [guest] = $5x10^{-6}$ M; λ_{ex} 373 nm.

3 CONCLUSIONS AND FUTURE WORK

Based on the methodology applied, photochromic dithienylethene monomers were synthesized and characterized by UV-Vis, fluorescence and NMR spectroscopy. Design of a different synthetic pathway should be taking account to increase the yield and eliminate (if possible) the number of steps to obtain the final compound. The photochromic behaviour of synthesized compounds was studied by irradiating an aqueous solution and is possible to verify that the cyclization quantum yield increase when the peripheric carbon is substituted with electron donating groups (naphthalene moieties).

Supramolecular assemblies were made by complexation with CB8 to formed supramolecular polymers, and a small analogue CB7 to compare and have a better understanding of interactions between both molecules, (Host-Guest interaction). Photochromic properties remain intact when DAE's were complexed with CB7 and CB8, and an increase in emission is observable when DAE's are complexed with CBn.

Structures of supramolecular assemblies were determined by NMR and ESI-MS. When CB7 is used host-gest interactions take place in the pyridinium region with the positive charge being stabilized by the portal region of CBn. A surprising migration of CB8 for the photoactive centre of DAE's was detected, reducing this way the population difference between conformations, and consequently increasing the cyclization quantum yield. An increase of fluorescence properties was also observed due to the different electronic and magnetic environment inside CBn cavities. Supramolecular polymers were detected by ESI-MS for model compound although this does not have donor acceptor moieties in the backbone structure. This could be due to an intermolecular charge transfer between pyridinium and thiophene moieties, as reported in the literature.

Association constants were determined by different methods, for both synthesized compounds (PF7 and PF20) for CB7 and CB8. Both isomers of DAE's were studied to verify if the affinity change with the electronic and structural change of each isomer. Complexation was followed firstly by UV-Vis spectroscopy, once the encapsulation changes the electronic properties of monomers used. Supramolecular polymeric species were detected for both compounds, but only when compounds were in the gas phase (ESI-MS). In aqueous media, supramolecular polymers were only detected for PF7, compound who exhibit donor acceptor moieties.

Designed monomers were shown to be capable to interact and formed supramolecular polymers, detected for both molecules by different techniques, although these supramolecular structures were not expected for PF20 compound.

Aiming to create photochromic supramolecular polymers with larger chains the continuation of last compound (8) synthesis should be done. Larger supramolecular polymers will enable the use of other techniques such as DLS, NMR spectroscopy, imaging microscopy as TEM or SEM to analyze and prove the structures and obtain evidence of these assemblies.

The design of monomers with different functional groups will be considered for the formulation of supramolecular structures with specific properties and different responsiveness will occur. Substitute DAE's with stronger acceptor donating groups will increase the interactions between monomers and the strength of polymers chains will be higher, also develop modulated supramolecular assemblies with photochromic properties has a great interest for optical and electronic devices. The study of this system in order to create molecular machines has great interest due to the system reversibility and modulations.

4 EXPERIMENTAL PART

4.1 SYNTHESIS

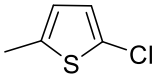

2-Chloro-5-methylthiophene (1): To a stirred solution of Benzene and Acetic Acid was added 2-methylthiophene (10 mL, 0.103 mol) and N-chlorosuccinimide (17 g, 0.124 mol). The suspension was stirred for 4h heated in reflux. After that, 30 mL of an aqueous solution of 3M of sodium hydroxide was poor in the cooled mixture. The organic phase was washed with a 3M aqueous solution of sodium hydroxide, dried with Na_2SO_4, filtrated and the solvent evaporated in vacuo to give a yellow liquid (11 g). The compound was purified by vacuum distillation afforded a colourless liquid (9.3 g) with a yield of 67%.

^{1}H NMR (400 MHz, $CDCl_3$) δ (ppm) = 6.69 (d, *J* = 3.6 Hz, 1H), 6.57 - 6.50 (m, 1H), 2.41 (s, 3H).

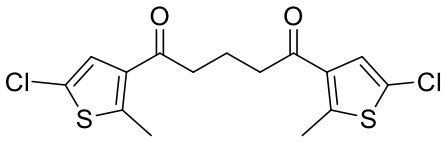

1,5-Bis(5-Chloro-2-methythien-3-yl)pentane-1,5-dione (2): under vigorous stirring $AlCl_3$ (10 g, 0.084 mol), previously crushed, was added, slowly, in portions to an ice-cooled solution of **(1)** (8.37 g, 0.063 mol) and glutaryl chloride (4.5 mL, 0.032 mol) in 80 mL of CS_2. The mixture was stirred at room temperature until the consumption of the starting material. Then ice-cooled water was added, very slowly, to the mixture and extracted with diethyl ether. The organic phases were washed with water, dried with Na_2SO_4, filtrated and the solvent was evaporated in vacuo to obtain a black tar (12 g). The black tar was purified by flash chromatography, using a mixture 9:1 of hexane/ethyl acetate as eluent, to provide a white solid (3.4 g, 0.009 mol) with a yield of 15%.

^{1}H NMR (400 MHz, $CDCl_3$) δ (ppm) = 7.18 (s, 2H), 2.86 (t, *J* = 6.9 Hz, 4H), 2.66 (s, 6H), 2.07 (m, *J* = 13.8, 6.9 Hz, 2H).

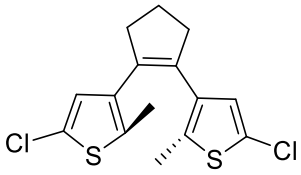

1,2-Bis(5-chloro-2-methylthien-3-yl)cyclopentene (3): Zn (1.2 g) dissolved in dry THF was placed in a two-necked flask under nitrogen. $TiCl_4$ was added very slowly, the mixture turns a yellow colour, and refluxed for 1h. An ice cooled solution of **(2)** was added to the mixture using a metal cannula, the mixture was refluxed for 3h. An aqueous solution of 10% K_2CO_3 was added, and the solution was filtrated with celite and extracted with diethyl ether. The organic phase was dried over Na_2SO_4 and the solvent was evaporated in vacuo to yield a yellow solid (2.67 g, 8.11 mmol). the compound was purified by flash chromatography (silica), in pure hexane, to yield a yellow solid (88%).

^{1}H NMR (400 MHz, $CDCl_3$) δ (ppm) = 6.57 (s, 2H), 2.71 (t, *J* = 7.5 Hz, 4H), 2.02 (m, *J* = 14.7, 7.4 Hz, 2H), 1.88 (s, 6H).

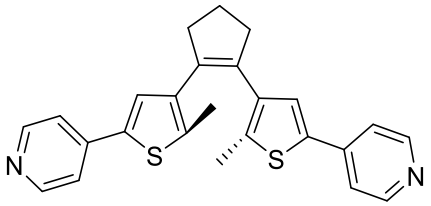

1,2-bis(2-methyl-5-(pyridin-4-yl)thiophen-3-yl)cyclopentane (4): to a two-neck round bottom flask, **(III)** (0.301 g, 0.914 mmol) and 20 mL of dry THF were added under nitrogen atmosphere. The resulting mixture was cooled with an ice bath and 3 mL of n-BuLi 1.6 M was slowly added, the mixture turned dark after the addition. The solution was stirred for half hour (30 min), the solution change from dark to orange. To the resultant mixture was added 1.5 mL of trimethyl borate ($B(OCH_3)_3$), and the solution was allowed to warm up to room temperature and stirred for 1h. At the same time in another two-neck flask equipped with a condenser, $Pd(PPh_3)_4$ (0.080 g), was suspended in 10 mL of dry THF, and the mixture was refluxed at 70ºC. after 30 min of reflux, was added to the mixture 10 mL of an aqueous solution 2.5 M K_2CO_3, 5 drops of PEG 400 and 4-bromopyridine hydrochloride (0.4 g, 2.5 mmol). The previous mixture was slowly added to this solution, using a cannula for the effect. The mixture was refluxed overnight. After the complete consumption of starting material (**3**), the mixture was cooled to room temperature followed by addition of water (30 mL). The resulting crude was extracted with diethyl ether and the combined organic phases were dried over anhydrous Na_2SO_4, the mixture was concentrated and purified by column chromatography (silica) using a mixture 1:1 of acetone/dichloromethane. The product was obtained as a violet solid in 73% yield (0.276 g).

^{1}H NMR (400 MHz, $CDCl_3$) δ (ppm) = 8.53 (d, *J* = 5.8 Hz, 4H), 7.32 (d, *J* = 12.2 Hz, 4H), 7.21 (s, 2H), 2.85 (t, *J* = 7.4 Hz, 4H), 2.11 (m, *J* = 7.5 Hz, 2H), 2.02 (s, 6H).

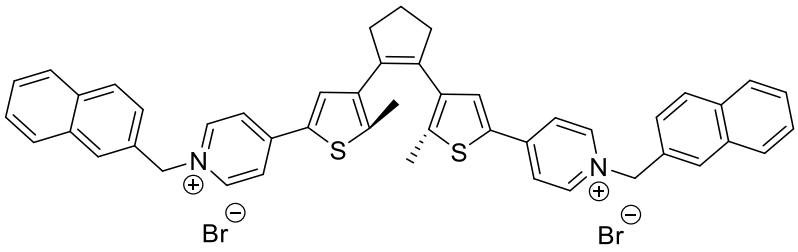

4,4'-(cyclopent-1-ene-1,2-diylbis(5-methylthiophene-4,2-diyl))bis(1-(naphthalen-2-ylmethyl)pyridin-1-ium) bromide (PF7): 2-bromomethyl naphthalene (0.35 g, 1.6 mmol) was dissolved in 40 dry ACN on one neck-flask under nitrogen atmosphere. **(4)** (0.276 g, 0.665 mmol) was added to the mixture. The mixture was stirred at room temperature, until the complete consumption of the starting material. Then the solvent was removed under vacuum, and the crude was washed and filtrated with diethyl ether to obtain a green solid in 91% (0.420 g).

^{1}H NMR (400 MHz, CD_3OD) δ (ppm) = 8.88 (d, *J* = 6.9 Hz, 4H), 8.12 (d, *J* = 7.0 Hz, 4H), 8.07 (s, 2H), 8.03 – 7.84 (m, 8H), 7.64 – 7.49 (m, 6H), 5.88 (s, 4H), 2.92 (t, *J* = 7.4 Hz, 4H), 2.23 – 2.14 (m, 2H), 2.10 (s, 6H).

^{13}C NMR (101 MHz, CD_3OD) δ (ppm) = 149.24, 145.10, 144.12, 139.07, 135.42, 133.61, 133.33, 133.23, 133.17, 130.79, 129.33, 128.62, 127.91, 127.49, 126.99, 126.71, 125.06, 121.79, 63.14, 48.26, 48.05, 47.83, 47.62, 47.41, 47.20, 46.98, 38.03, 22.59, 13.78.

EA: Calculated for $C_{47}H_{41}Br_2N_2S_2 \bullet 1H_2O$: C 64.53; H 4.84; N 3.20; S 7.33; determined: C 58.82; H 4.60; N 3.29; S 7.12.

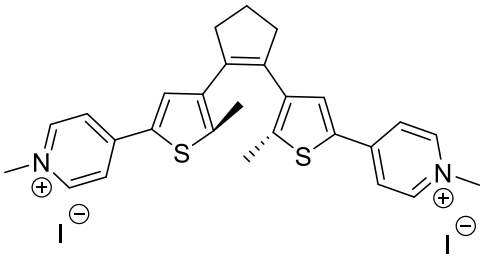

4,4'-(cyclopent-1-ene-1,2-diylbis(5-methylthiophene-4,2-diyl))bis(1-methylpyridin-1-ium) iodide (PF20): on one neck-flask under nitrogen atmosphere. **(4)** (0.378 g, 0.912 mmol) was dissolved with DCM. In iced bath, was added to the solution Iodomethane (0.5 g, 3 mmol). The mixture was stirred at room temperature, until the complete consumption of the starting material. Then the solvent was removed under vacuum, and the crude was washed with cold DCM to obtain a green solid in 83% (0.562 g).

^{1}H NMR (400 MHz, D_2O) δ (ppm) = 8.43 (d, *J* = 6.9 Hz, 4H), 7.90 (d, *J* = 7.0 Hz, 4H), 7.77 (s, 2H), 4.15 (s, 6H), 2.81 (t, *J* = 7.5 Hz, 4H), 2.13 – 1.99 (m, 2H), 1.98 (s, 6H).

EA: Calculated for $C_{27}H_{28}I_2N_2S_2 \cdot 1.5H_2O$: C 44.70; H 4.31; N 3.86; S 8.84; determined: C 44.78; H 4.36; N 3.81; S 8.61

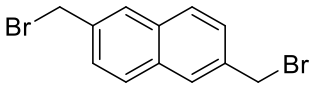

2,6-Bis(bromomethyl)naphthalene (6): N-bromosuccinimide (NBS) (0.5 g, 8.79 mmol) and 2,2'-azobis(isobutyronitrile) (AIBN) (0.03 mg, 0.2 mmol) were added to a solution of 2,6-dimethyl naphthalene (0.3 mg, 1.92 mmol) dissolved in 40 mL of CCl_4 at room temperature. The mixture was refluxed under N_2 until the consumption of the starting material. The mixture was cooldown at room temperature and filtered. The filtrate was dried over Na_2SO_4., concentrated, and the residue was purified by silica gel column chromatography with dichloromethane to give (6) as colourless needles (0.485 g) with an 81% yield.

^{1}H NMR (400 MHz, $CDCl_3$) δ (ppm) = 7.96 – 7.70 (m, *J* = 8.4 Hz, 4H), 7.52 (d, *J* = 8.7 Hz, 2H), 4.66 (s, 4H).

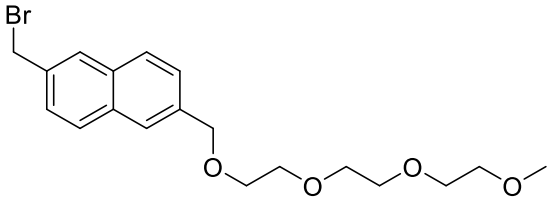

5-bromomethyl-1-(4-methoxy ethoxy) naphthalene (7): To a suspension of NaH (60%, 0.002 g,0.046 mmol) in THF (10 mL) cooled to ice bath temperature was added a solution of Triethylene glycol monomethyl ether (0.5 mL, 0.046 mmol). The mixture was stirred for 30 minutes at room temperature. Then **(6)** (0.05 g; 0.180 mmol) was slowly added. The reaction mixture was refluxed until TLC revealed completion of the reaction. After cooling the reaction mixture to ice bath temperature, excess NaH was quenched by adding sat. aq NH_4Cl solution. The two layers were separated, and the aqueous layer was extracted with EtOAc. The combined organic phases were dried over anhydrous Na_2SO_4, and the solvent was evaporated under reduced pressure to obtain a crude reaction mass. (not purified)

4.2 MATERIALS AND REAGENTS

Solvent and Reagents for synthesis

Benzene (Merck), methanol (Sigma-Aldrich), tetrahydrofuran (THF) (Scharlau), diethyl ether (LabChem), hexane (LabChem), ethyl acetate (LabChem), dichloromethane (LabChem), Acetic Acid (), sodium hydroxide (Eka), sodium sulfate anhydrous (Carbo Erba), Potassium carbonate (K_2CO_3, Riedel-de Haen). 2-Methyltiophene (Alfa Aesar, 98 %), *N*-chlorosuccinimide (Aldrich, 98 %), Glutaryl Chloride (Aldrich, 97 %), diphenylacetic acid (Aldrich, 99 %), Aluminium Chloride ($AlCl_3$, Sigma Aldrich, 98%), carbon disulfide (Aldrich, >99.9 %), Zn dust (≥99 %), Titanium Tetrachloride (Aldrich, 98%), n-butyl lithium (pentane solution, Aldrich), hydrochloric acid (Sigma-Aldrich),

4.3 METHODOLOGIES

NMR Spectroscopy

NMR spectra were done on a Bruker AMX 400 instrument operating at 400.13 MHz (^{1}H), 100.61 MHz (^{13}C). The NMR spectrometers are part of The National NMR Facility.

Elemental analysis

For this technique was performed on Thermofinnigan Flas EA serie 1112.

UV-Visible Spectroscopy

UV-Visible spectroscopy was done using Varian Cary 100 Bio spectrophotometer at room temperature.

Fluorescence Spectroscopy

Fluorescence measurements were made in a SPEX Fluorolog F111 at room temperature. Quartz cells with an optical path of 1cm were used.

Photochemical studies

Photo-excitation in continuous irradiation experiments was carried out with a Xe/Hg lamp (200W) using a cut-off or a bandpass filter. The photochromic solution was stirred with a magnetic bar in a 1 cM-2 x 1 cM-2 quartz and PMMA cell.

Open-isomer was converted to Closed-isomer, irradiating a sample with a bandpass filter (365 nm) followed by UV-Vis spectroscopy, to ensure the photostationary state of each sample.

Spectrophotometric titration

In a cell containing a solution of PFn was added a mixture of CBn with PFn (The titrant cell contains PFn (same concentration as the titrated cell) in order to simplify the calculations) and UV-Vis spectroscopy was made in each step. The conditions of each experiment are mentioned above.

Mathematical model for the determination of binding constants

The aim of each binding scenario is to reach an equation that relates the measured signal to the total concentration of the host and guest through the desired values of K. These equations are derivatives from the equilibrium, mass balance and signal-to-concentration relationship equations. Both used binding models and the used equation are explained above.[77]

1:1 (Host-Guest) Binding Model

In this model is assumed that both host (H) and guest (G) have only one binding site, the equilibrium equation, the desired binding constant (K) are expressed in Eq. (6 and 7)

$$H + G \leftrightarrows HG \quad K_{11} \qquad (6)$$

$$K_{11} = \frac{[HG]}{[H][G]} \qquad (7)$$

$$[HG] = K_{11}[H][G] \qquad (8)$$

Mass balance of each compound in solution is express in eq. (9 and 10)

$$[G]_0 = [G] + [HG] \qquad (9)$$

$$[H]_0 = [H] + [HG] \qquad (10)$$

Then the equation system is derived an equation express only by one unknown concentration ([G])

$$[H]_0 = [H] + K_{11}[H][G] \qquad (11)$$

$$\frac{[H]_0}{1+K_{11}[G]} = [H] \qquad (12)$$

$$[G]_0 = [G] + K_{11}[H][G] \qquad (13)$$

$$[G]_0 = [G] + K_{11}\left(\frac{[H]_0}{1+K_{11}[G]}\right)[G] \qquad (14)$$

The demonstration of eq (14) yield a quadratic equation (15)

$$K_{11}[G]^2 + (1 + K_{11}[H]_0 - K_{11}[G]_0)[G] - [G]_0 = 0 \qquad (15)$$

And now [G] can be determined using a quadratic equation (16)

$$[G] = \frac{-(1+K_{11}[H]_0-K_{11}[G]_0)+\sqrt{(1+K_{11}[H]_0-K_{11}[G]_0)^2+4K_{11}[G]_0}}{2K_{11}} \qquad (16)$$

Now is possible to determine the concentration of each component in the solution, using for this effect equation (8,12 and 16) Equation (17) was used to fit the data and this way was possible to determined K_{11}.

$$Abs^{cal} = \varepsilon^{G}[G] + \varepsilon^{HG}[HG] \qquad (17)$$

2:1 Binding Model

In this model is assumed that guest have two binding sites and Host have only one binding site, the equilibrium equation, the desired binding constant (K) are expressed in Eq. (18-21)

$$H + G \leftrightarrows HG \quad K_{11} \qquad (18)$$

$$HG + H \leftrightarrows H_2G \quad K_{21} \qquad (19)$$

$$K_{11} = \frac{[HG]}{[H][G]} \qquad (20)$$

$$K_{21} = \frac{[H_2G]}{[H][HG]} \qquad (21)$$

$$[HG] = K_{11}[H][G] \qquad (22)$$

$$[H_2G] = K_{21}[H][HG] \qquad (23)$$

Mass balance of each compound in solution is express in eq. (24 and 25)

$$[G]_0 = [G] + [HG] + [H_2G] \qquad (24)$$

$$[H]_0 = [H] + [HG] + 2[H_2G] \qquad (25)$$

Then, the mass balance and equilibrium equations can be combined to reach one equation with one unknown equilibrium concentration ([H]), as in the previous model.

$$[G]_0 = [G] + K_{11}[H][G] + K_{11}K_{21}[G][H]^2 \qquad (26)$$

$$[G] = \frac{[G]_0}{1+K_{11}[H]+K_{11}K_{21}[H]^2} \qquad (27)$$

$$[H]_0 = [H] + K_{11}[H][G] + 2K_{11}K_{21}[G][H]^2 \qquad (28)$$

$$[H]_0 = [H] + K_{11}\left(\frac{[G]_0}{1+K_{11}[H]+K_{11}K_{21}[H]^2}\right)[H] + 2K_{11}K_{21}\left(\frac{[G]_0}{1+K_{11}[H]+K_{11}K_{21}[H]^2}\right)[H]^2 \qquad (29)$$

$$[H]_0 = [H] + \left(\frac{K_{11}[H]+2K_{11}K_{21}[H]^2}{1+K_{11}[H]+K_{11}K_{21}[H]^2}\right)[G]_0 \qquad (30)$$

Rearranging the equation (30) results in a cubic equation for [H], equation (31)

$$K_{11}K_{21}[H]^3 + (K_{11} + 2K_{11}K_{21}[G]_0 - K_{11}K_{21}[H]_0)[H]^2 + (1 + K_{11}[H]_0 - K_{11}[G]_0)[H] - [G]_0 = 0 \qquad (31)$$

To solve the cubic equation, Newton's method (equation 32) was applied to iteratively determine the numeric solution of [H].

$$x_{n+1} = x_n - \left(\frac{f(x_n)}{f'(x_n)}\right) \qquad (32)$$

Now is possible to determine the concentration of each component in the solution, using for this effect equations (22,23,27 and 31) Equation (33) was used to fit the UV-Vis data and equation (34) was used to fit the NMR data and this way was possible to determined K_{11} and K_{21}.

$$Abs^{cal} = \varepsilon^G[G] + \varepsilon^{HG}[HG] + \varepsilon^{H_2G}[H_2G] \qquad (33)$$

$$\delta^{cal} = x^G\delta^G + x^{HG}\delta^{HG} + x^{H_2G}\delta^{H_2G} \qquad (34)$$

5 REFERENCES

(1) Bouas-Laurent, H.; Dürr, H. Organic Photochromism (IUPAC Technical Report). *Pure Appl. Chem.* **2001**, *73* (4), 639–665.

(2) Hirshberg, Y. Photochromie Dans La Serie de La Bianthrone. *Compt. Rend.* **1950**, *231*, 903–904.

(3) Pardo, R.; Zayat, M.; Levy, D. Photochromic Organic–inorganic Hybrid Materials. *Chem. Soc. Rev.* **2011**, *40* (2), 672–687.

(4) Rie, B. M. I. Review Photochromism of Diarylethene Molecules and Crystals. *Proc. Jpn. Acad.* **2010**, *86*, 472–483.

(5) Irie, M.; Fukaminato, T.; Matsuda, K.; Kobatake, S. Photochromism of Diarylethene Molecules and Crystals: Memories, Switches, and Actuators. *Chem. Rev.* **2014**, *114* (24), 12174–12277.

(6) Tian, H.; Zhang, J. *Photochromic Materials: Preparation, Properties and Applications*; Tian, H., Zhang, J., Eds.; Wiley-VCH Verlag GmbH & Co. KGaA: Weinheim, Germany, 2016.

(7) Irie, M.; Fukaminato, T.; Matsuda, K.; Kobatake, S. Photochromism of Diarylethene Molecules and Crystals: Memories, Switches, and Actuators. *Chem. Rev.* **2014**, *114* (24), 12174–12277.

(8) Browne, W. R.; Feringa, B. L. Making Molecular Machines Work. *Nat. Nanotechnol.* **2006**, *1* (1), 25–35.

(9) Tian, H.; Yang, S. Recent Progresses on Diarylethene Based Photochromic Switches. *Chem. Soc. Rev.* **2004**, *33* (2), 85–97.

(10) Irie, M. Diarylethenes for Memories and Switches. *Chem. Rev.* **2000**, *100* (5), 1685–1716.

(11) Nakamura, S.; Irie, M. Thermally Irreversible Photochromic Systems. A Theoretical Study. *J. Org. Chem.* **1988**, *53* (Ic), 6136–6138.

(12) Sumi, T.; Takagi, Y.; Yagi, A.; Morimoto, M.; Irie, M. Photoirradiation Wavelength Dependence of Cycloreversion Quantum Yields of Diarylethenes. *Chem. Commun.* **2014**, *50*, 3928–3930.

(13) Favaro, G.; Mazzucato, U.; Ortica, F.; Smimmo, P. Thermal Reversibility and Bistability in Photochromic Diarylethenes. *Inorganica Chim. Acta* **2007**, *360* (3), 995–999.

(14) Herder, M. Improving the Design of Diarylethene Photoswitches and Their Exploitation as Remote-Controlled Building Blocks, Humboldt-Universität zu Berlin, Mathematisch-Naturwissenschaftliche Fakultät, 2015.

(15) Irie, M.; Sayo, K. Solvent Effects on the Photochromic Reactions of Diarylethene Derivatives. *J. Phys. Chem.* **1992**, *96*, 7671–7674.

(16) Irie, M.; Mohri, M. Thermally Irreversible Photochromic Systems. Reversible Photocyclization of Diarylethene Derivatives. *J. Org. Chem.* **1988**, *53* (4), 803–808.

(17) Hanazawa, M.; Sumiya, R.; Horikawa, Y.; Irie, M. Thermally Irreversible Photochromic Systems. Reversible Photocyclization of 1,2-Bis (2-Methylbenzo[b]thiophen-3-Yl)perfluorocyclocoalkene Derivatives. *J. Chem. Soc. Chem. Commun.* **1992**, *0* (3), 206–207.

(18) Lucas, L. N.; Jong, J. J. D. de; Esch, J. H. van; Kellogg, R. M.; Feringa, B. L. Syntheses of Dithienylcyclopentene Optical Molecular Switches. *European J. Org. Chem.* **2003**, *2003* (1), 155–166.

(19) Nakashima, T.; Atsumi, K.; Kawai, S.; Nakagawa, T.; Hasegawa, Y.; Kawai, T. Photochromism of Thiazole-Containing Triangle Terarylenes. *European J. Org. Chem.* **2007**, *2007* (19), 3212–3218.

(20) Fukumoto, S.; Nakashima, T.; Kawai, T. Photon-Quantitative Reaction of a Dithiazolylarylene in Solution. *Angew. Chemie Int. Ed.* **2011**, *50* (7), 1565–1568.

(21) Muszkat, K. A.; Fischer, E. Structure, Spectra, Photochemistry, and Thermal Reactions of the 4a,4b-Dihydrophenanthrenes. *J. Chem. Soc. B Phys. Org.* **1967**, *0* (0), 662–678.

(22) Uchida, K.; Tsuchida, E.; Aoi, Y.; Nakamura, S.; Irie, M. Substitution Effect on the Coloration Quantum Yield of a Photochromic Bisbenzothienylethene. *Chem. Lett.* **1999**, *28* (1), 63–64.

(23) Kobatake, S.; Irie, M. Synthesis and Photochromism of Diarylethenes with Isopropyl Groups at the Reactive Carbons and Long π-Conjugated Heteroaryl Groups. *Chem. Lett.* **2003**, *32* (11), 1078–1079.

(24) Takami, S.; Kawai, T.; Irie, M. Photochromism of Dithiazolylethenes Having Methoxy Groups at the Reaction Centers. *European J. Org. Chem.* **2002**, *2002* (22), 3796–3800.

(25) Higashiguchi, K.; Matsuda, K.; Asano, Y.; Murakami, A.; Nakamura, S.; Irie, M. Photochromism of Dithienylethenes Containing Fluorinated Thiophene Rings. *European J. Org. Chem.* **2005**, *2005* (1), 91–97.

(26) Morimitsu, K.; Kobatake, S.; Irie, M. Control of Cycloreversion Quantum Yields of Diarylethenes by Introduction of Substituents at the Reactive Carbons. *Mol. Cryst. Liq. Cryst.* **2005**, *431* (1), 451–454.

(27) Bens, A. T.; Frewert, D.; Kodatis, K.; Kryschi, C.; Martin, H.-D.; Trommsdorff, H. P. Coupling of Chromophores: Carotenoids and Photoactive Diarylethenes – Photoreactivity versus Radiationless Deactivation. *European J. Org. Chem.* **1998**, *1998* (11), 2333–2338.

(28) Lehn, J.-M. Supramolecular Chemistry—Scope and Perspectives Molecules, Supermolecules, and Molecular Devices(Nobel Lecture). *Angew. Chemie Int. Ed. English* **1988**, *27* (1), 89–112.

(29) Grote, Z.; Scopelliti, R.; Severin, K. Adaptive Behavior of Dynamic Combinatorial Libraries Generated by Assembly of Different Building Blocks. *Angew. Chemie Int. Ed.* **2003**, *42* (32), 3821–3825.

(30) Aida, T.; Meijer, E. W.; Stupp, S. I. Functional Supramolecular Polymers. *Science* **2012**, *335* (6070), 813–817.

(31) Grote, Z.; Scopelliti, R.; Severin, K. Adaptive Behavior of Dynamic Combinatorial Libraries Generated by Assembly of Different Building Blocks. *Angew. Chemie - Int. Ed.* **2003**, *42* (32), 3821–3825.

(32) Yao, X.; Li, T.; Wang, J.; Ma, X.; Tian, H. Recent Progress in Photoswitchable Supramolecular Self-Assembling Systems. *Adv. Opt. Mater.* **2016**, *4* (9), 1322–1349.

(33) Zhang, J.; Ma, P. X. Cyclodextrin-Based Supramolecular Systems for Drug Delivery: Recent Progress and Future Perspective. *Adv. Drug Deliv. Rev.* **2013**, *65* (9), 1215–1233.

(34) Wang, Y.; Xu, H.; Zhang, X. Tuning the Amphiphilicity of Building Blocks: Controlled Self-Assembly and Disassembly for Functional Supramolecular Materials. *Adv. Mater.* **2009**, *21* (28), 2849–2864.

(35) Yang, H.; Yuan, B.; Zhang, X.; Scherman, O. A. Supramolecular Chemistry at Interfaces: Host–Guest Interactions for Fabricating Multifunctional Biointerfaces. *Acc. Chem. Res.* **2014**, *47* (7), 2106–2115.

(36) Freeman, W. A.; Mock, W. L.; Shih, N. Y. Cucurbituril. *J. Am. Chem. Soc.* **1981**, *103* (24), 7367–7368.

(37) Mock, W. L.; Shih, N. Y. Host-Guest Binding Capacity of Cucurbituril. *J. Org. Chem.* **1983**, *48* (20), 3618–3619.

(38) Assaf, K. I.; Nau, W. M. Cucurbiturils: From Synthesis to High-Affinity Binding and Catalysis. *Chem. Soc. Rev.* **2015**, *44* (2), 394–418.

(39) Liu, Y.; Huang, Z.; Tan, X.; Wang, Z.; Zhang, X.; Online, V. A.; Liu, Y.; Huang, Z.; Tan, X.; Wang, Z.; et al. Cucurbit[8]uril-Based Supramolecular Polymers: Promoting Supramolecular Polymerization by Metal-Coordination. *Chem Commun* **2013**, *49* (51), 5766–5768.

(40) Nally, R.; Isaacs, L. Toward Supramolecular Polymers Incorporating Double Cavity Cucurbituril Hosts. *Tetrahedron* **2009**, *65* (35), 7249–7258.

(41) Nau, W. M.; Florea, M.; Assaf, K. I. Deep inside Cucurbiturils: Physical Properties and Volumes of Their Inner Cavity Determine the Hydrophobic Driving Force for Host-Guest Complexation. *Isr. J. Chem.* **2011**, *51* (5–6), 559–577.

(42) Barrow, S. J.; Kasera, S.; Rowland, M. J.; del Barrio, J.; Scherman, O. A. Cucurbituril-Based Molecular Recognition. *Chem. Rev.* **2015**, *115* (22), 12320–12406.

(43) Tian, F.; Jiao, D.; Biedermann, F.; Scherman, O. A. Orthogonal Switching of a Single Supramolecular

Complex. *Nat. Commun.* **2012**, *3*, 1207.

(44) Ravve, A. *Principles of Polymer Chemistry*; Springer New York: New York, NY, 2012.

(45) Jenkins, A. D.; Kratochvíl, P.; Stepto, R. F. T.; Suter, U. W. Glossary of Basic Terms in Polymer Science (IUPAC Recommendations 1996). *Pure Appl. Chem.* **1996**, *68* (12), 2287–2311.

(46) Wang, S.; Li, X.; Chen, B.; Luo, Q.; Tian, H. Photochromic Copolymers Containing Bisthienylethene Units. *Macromol. Chem. Phys.* **2004**, *205* (11), 1497–1507.

(47) Jeong, Y.; Park, D. G.; Kim, E.; Yang, S. I.; Ahn, K.-H. Polymerization of a Photochromic Diarylethene by Friedel−Crafts Alkylation. *Macromolecules* **2006**, *39* (9), 3106–3109.

(48) Stellacci, F.; Bertarelli, C.; Toscano, F.; Gallazzi, M. C.; Zotti, G.; Zerbi, G. High Quantum Yield Diarylethene-Backbone Photochromic Polymer. *Adv. Mater.* **1999**, *11* (4), 292–295.

(49) Becker, D.; Konnertz, N.; Böhning, M.; Schmidt, J.; Thomas, A. Light-Switchable Polymers of Intrinsic Microporosity. *Chem. Mater.* **2016**, *28* (23), 8523–8529.

(50) Cao, L.; Wang, Z.; Zong, S.; Zhang, S.; Zhang, F.; Jin, G. Volume Holographic Polymer of Photochromic Diarylethene for Updatable Three-Dimensional Display. *J. Polym. Sci. Part B Polym. Phys.* **2016**, *54* (20), 2050–2058.

(51) Becker, D.; Konnertz, N.; Böhning, M.; Schmidt, J.; Thomas, A. Light-Switchable Polymers of Intrinsic Microporosity. *Chem. Mater.* **2016**, *28* (23), 8523–8529.

(52) Yan, X.; Wang, F.; Zheng, B.; Huang, F. Stimuli-Responsive Supramolecular Polymeric Materials. *Chem. Soc. Rev.* **2012**, *41* (18), 6042–6065.

(53) Brunsveld, L.; Folmer, B. J. B.; Meijer, E. W.; Sijbesma, R. P. Supramolecular Polymers. *Chem. Rev.* **2001**, *101* (12), 4071–4098.

(54) De Greef, T. F. A.; Smulders, M. M. J.; Wolffs, M.; Schenning, A. P. H. J.; Sijbesma, R. P.; Meijer, E. W. Supramolecular Polymerization. *Chem. Rev.* **2009**, *109* (11), 5687–5754.

(55) Avakyan, N.; Greschner, A. A.; Aldaye, F.; Serpell, C. J.; Toader, V.; Petitjean, A.; Sleiman, H. F. Reprogramming the Assembly of Unmodified DNA with a Small Molecule. *Nat. Chem.* **2016**, *8* (4), 368–376.

(56) Liu, Y.; Wang, Z.; Zhang, X. Characterization of Supramolecular Polymers. *Chem. Soc. Rev.* **2012**, *41* (18), 5922–5932.

(57) Liu, Y.; Yu, Y.; Gao, J.; Wang, Z.; Zhang, X. Water-Soluble Supramolecular Polymerization Driven by Multiple Host-Stabilized Charge-Transfer Interactions. *Angew. Chemie Int. Ed.* **2010**, *49* (37), 6576–6579.

(58) Pimenta, L. S.; Gusevskaya, E. V.; Alberto, E. E. Intermolecular Halogenation/Esterification of Alkenes with N -Halosuccinimide and Acetic Acid Catalyzed by 1,4-Diazabicyclo[2.2.2]octane. *Adv. Synth. Catal.* **2017**, *359* (13), 2297–2303.

(59) Davlieva, M. G.; Lindeman, S. V.; Neretin, I. S.; Kochi, J. K. Isolation, X-Ray Structures, and Electronic Spectra of Reactive Intermediates in Friedel−Crafts Acylations †. *J. Org. Chem.* **2005**, *70* (10), 4013–4021.

(60) Whalley, P. The Comparison of Friedel-Crafts Alkylation and Acylation as a Means to Synthesise Alkyl Xylenes. *Plymouth Student Sci.* **2016**, *9* (1), 252–296.

(61) McMurry, J. E.; Fleming, M. P. New Method for the Reductive Coupling of Carbonyls to Olefins. Synthesis of .beta.-Carotene. *J. Am. Chem. Soc.* **1974**, *96* (14), 4708–4709.

(62) Takeda, T.; Tsubouchi, A. The McMurry Coupling and Related Reactions. In *Organic Reactions*; John Wiley & Sons, Inc.: Hoboken, NJ, USA, 2013; Vol. 82, pp 1–470.

(63) Fürstner, A.; Bogdanović, B. New Developments in the Chemistry of Low-Valent Titanium. *Angew. Chemie Int. Ed. English* **1996**, *35* (21), 2442–2469.

(64) Mukaiyama, T.; Sato, T.; Hanna, J. REDUCTIVE COUPLING OF CARBONYL COMPOUNDS TO

PINACOLS AND OLEFINS BY USING TiCl 4 AND Zn. *Chem. Lett.* **1973**, *2* (10), 1041–1044.

(65) Miyaura, N.; Yamada, K.; Suzuki, A. A New Stereospecific Cross-Coupling by the Palladium-Catalyzed Reaction of 1-Alkenylboranes with 1-Alkenyl or 1-Alkynyl Halides. *Tetrahedron Lett.* **1979**, *20* (36), 3437–3440.

(66) Miyaura, N.; Suzuki, A. Palladium-Catalyzed Cross-Coupling Reactions of Organoboron Compounds. *Chem. Rev.* **1995**, *95* (7), 2457–2483.

(67) García-Melchor, M.; Braga, A. A. C.; Lledós, A.; Ujaque, G.; Maseras, F. Computational Perspective on Pd-Catalyzed C–C Cross-Coupling Reaction Mechanisms. *Acc. Chem. Res.* **2013**, *46* (11), 2626–2634.

(68) Amatore, C.; Jutand, A.; Le Duc, G. Kinetic Data for the Transmetalation/Reductive Elimination in Palladium-Catalyzed Suzuki-Miyaura Reactions: Unexpected Triple Role of Hydroxide Ions Used as Base. *Chem. - A Eur. J.* **2011**, *17* (8), 2492–2503.

(69) Wang, L.; Zhang, Y.; Liu, L.; Wang, Y. Palladium-Catalyzed Homocoupling and Cross-Coupling Reactions of Aryl Halides in Poly(ethylene Glycol). *J. Org. Chem.* **2006**, *71* (3), 1284–1287.

(70) Mukhopadhyay, S.; Rothenberg, G.; Gitis, D.; Sasson, Y. On the Mechanism of Palladium-Catalyzed Coupling of Haloaryls to Biaryls in Water with Zinc. *Org. Lett.* **2000**, *2* (2), 211–214.

(71) Shezad, N.; Clifford, A. A.; Rayner, C. M. Pd-Catalysed Coupling Reactions in Supercritical Carbon Dioxide and under Solventless Conditions. *Green Chem.* **2002**, *4* (1), 64–67.

(72) Rekharsky, M. V.; Inoue, Y. Thermodynamics of Cucurbituril Complexation in Aqueous Solutions. *Netsu Sokutei* **2007**, *34* (5), 232–243.

(73) Liu, G.; Zhang, Y.-M.; Wang, C.; Liu, Y. Dual Visible Light-Triggered Photoswitch of a Diarylethene Supramolecular Assembly with Cucurbit[8]uril. *Chem. - A Eur. J.* **2017**.

(74) Mendes, D. C.; Ramamurthy, V.; Da Silva, J. P. Identification of Guest–Host Inclusion Complexes in the Gas Phase by Electrospray Ionization–Mass Spectrometry. *J. Chem. Educ.* **2015**, *92* (6), 1091–1094.

(75) Da Silva, J. P.; Jayaraj, N.; Jockusch, S.; Turro, N. J.; Ramamurthy, V. Aggregates of Cucurbituril Complexes in the Gas Phase. *Org. Lett.* **2011**, *13* (9), 2410–2413.

(76) Montes-Navajas, P.; Corma, A.; Garcia, H. Complexation and Fluorescence of Tricyclic Basic Dyes Encapsulated in Cucurbiturils. *ChemPhysChem* **2008**, *9* (5), 713–720.

(77) Hargrove, A. E.; Zhong, Z.; Sessler, J. L.; Anslyn, E. V. Algorithms for the Determination of Binding Constants and Enantiomeric Excess in Complex Host : Guest Equilibria Using Optical Measurements. *New J. Chem.* **2010**, *34* (2), 348–354.

6 APPENDIX

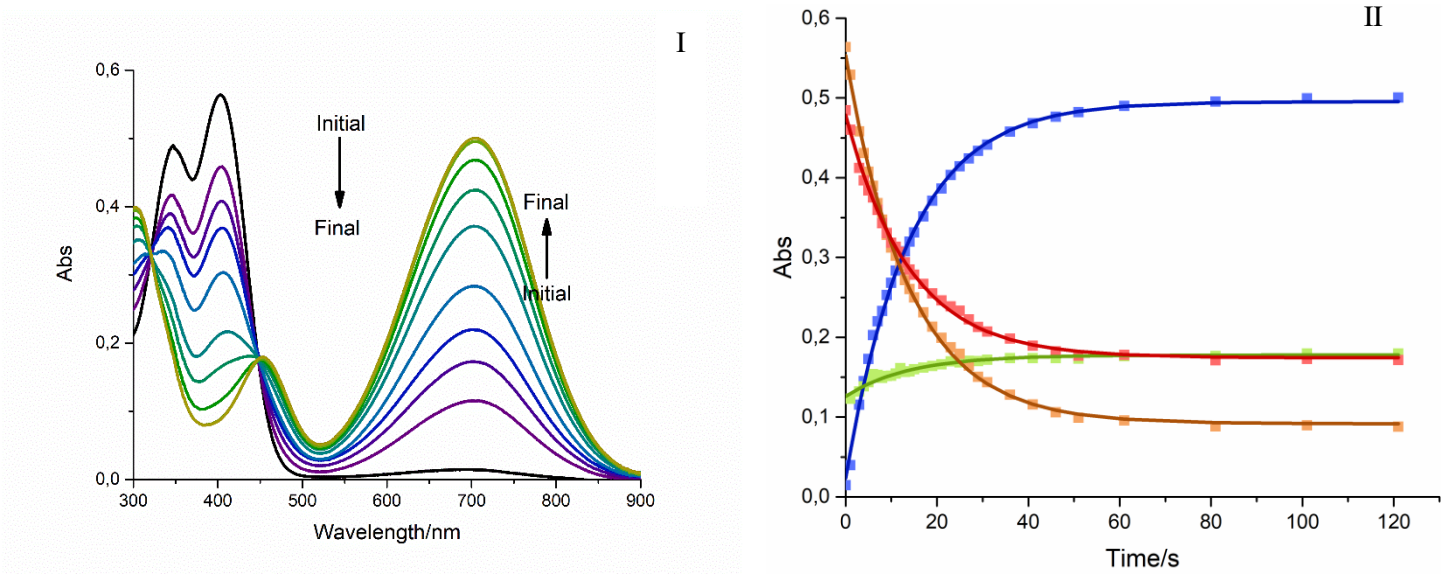

Figure 6.1 (I) Spectral variation of PF20.CB7 upon photoirradiation in water; (II) Experimental data for cyclization reaction (Blue) 706 nm; (red) 347 nm; (Orange) 404 nm; (Green) 453 nm. Solid lines represent the best least squares fit to equation (5); conditions: [PF20]= $2x10^{-5}$ M; [CB7]= $5x10^{-3}$ M; T=20ºC; λirr=365 nm.

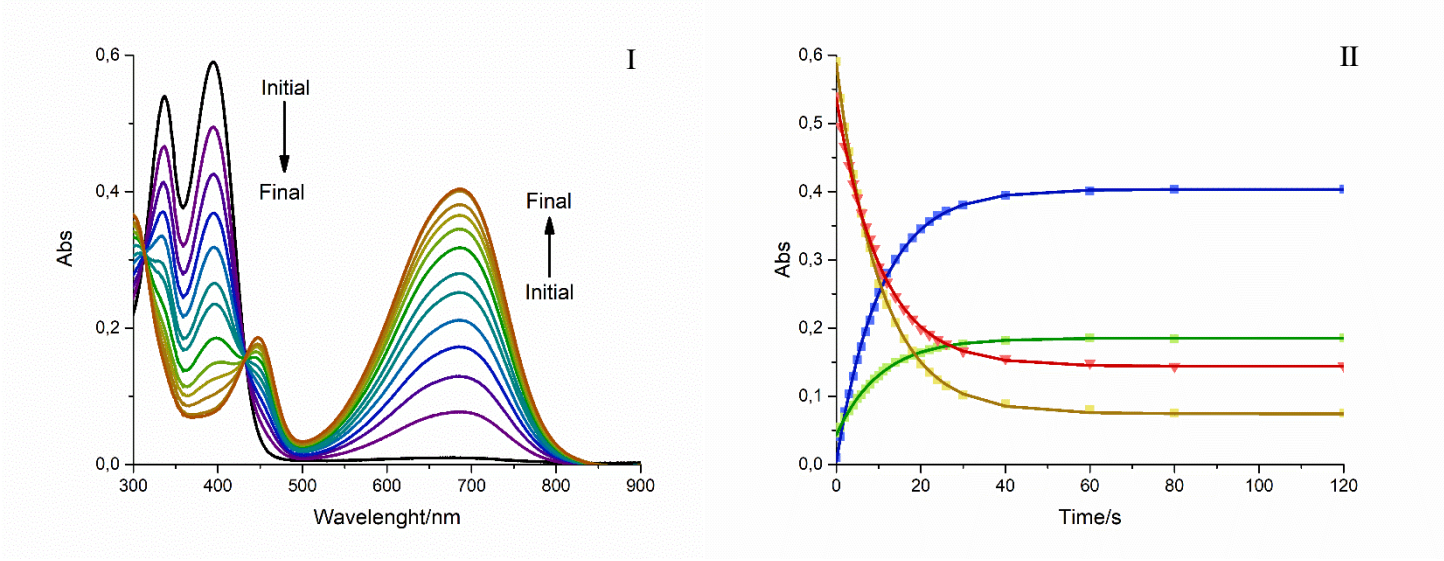

Figure 6.2 (I) Spectral variation of PF20.CB8 upon photoirradiation in water; (II) Experimental data for cyclization reaction (Blue) 690 nm; (red) 336 nm; (Yellow) 398 nm; (Green) 452 nm. Solid lines represent the best least squares fit to equation (5).; conditions: [PF20]= $2x10^{-5}$ M; [CB8]= $0.1x10^{-3}$ M; T=20ºC; λirr=365 nm.

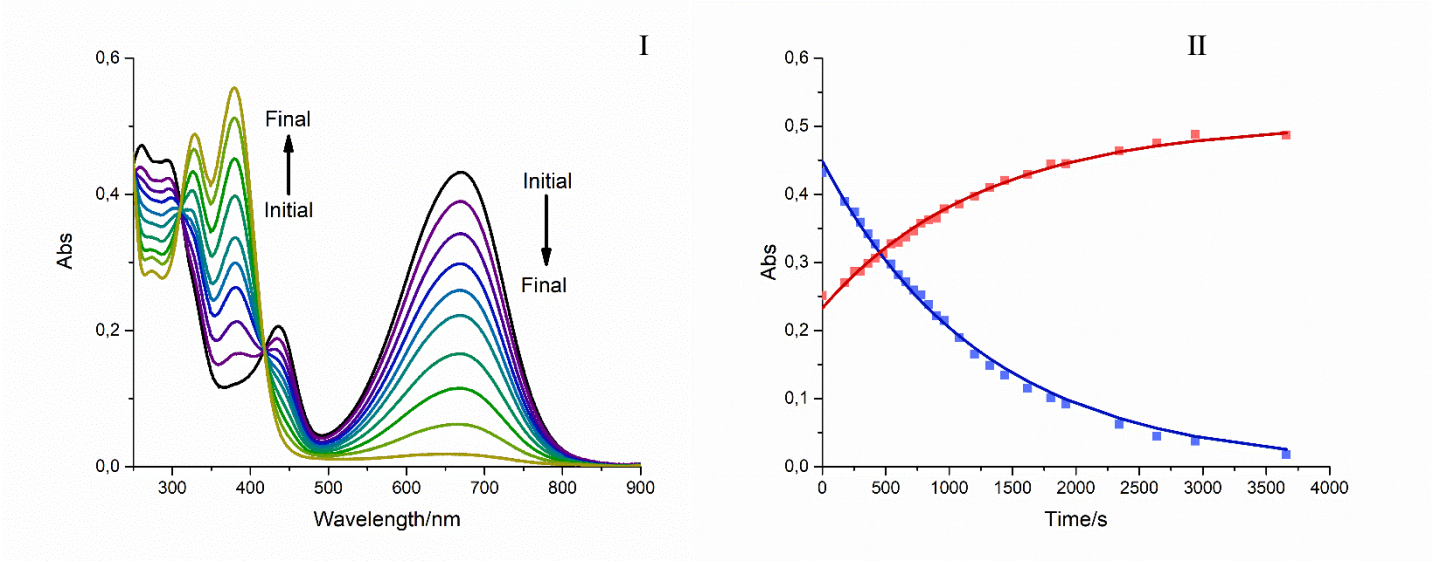

Figure 6.3 (I) Spectral variation of PF20 upon photoirradiation in water; (II) Experimental data for cycloreversion reaction (Blue) 690 nm; (red) 336 nm. Solid lines represent the best least squares fit to equation (5).; conditions: [PF20]= $2x10^{-5}$ M; T=20ºC; λirr=550 nm.

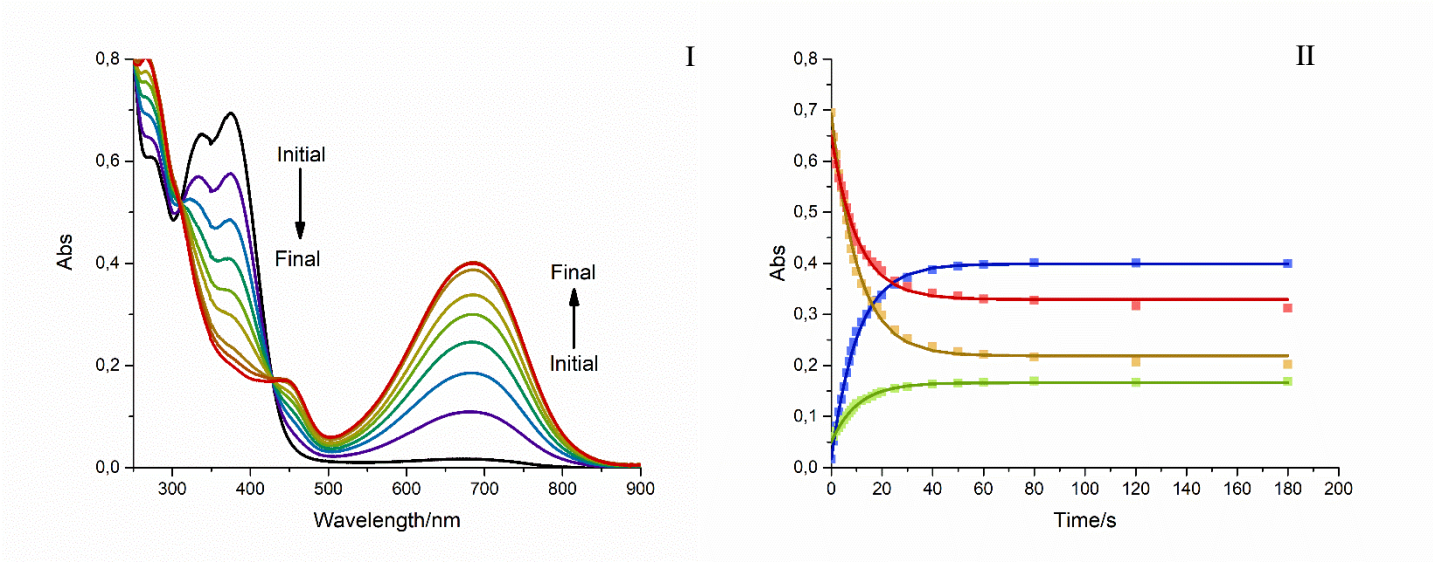

Figure 6.4 (I) Spectral variation of PF7.CB8 upon photoirradiation in water; (II) Experimental data for cyclization reaction (Blue) 686 nm; (red) 338 nm ; (yellow) 375 nm ; (Green) 450 nm. Solid lines represent the best least squares fit to equation (5).; conditions: [PF7]= $2.5x10^{-5}$ M; [CB8]= $0.1x10^{-3}$ M T=20ºC; λirr=365 nm.

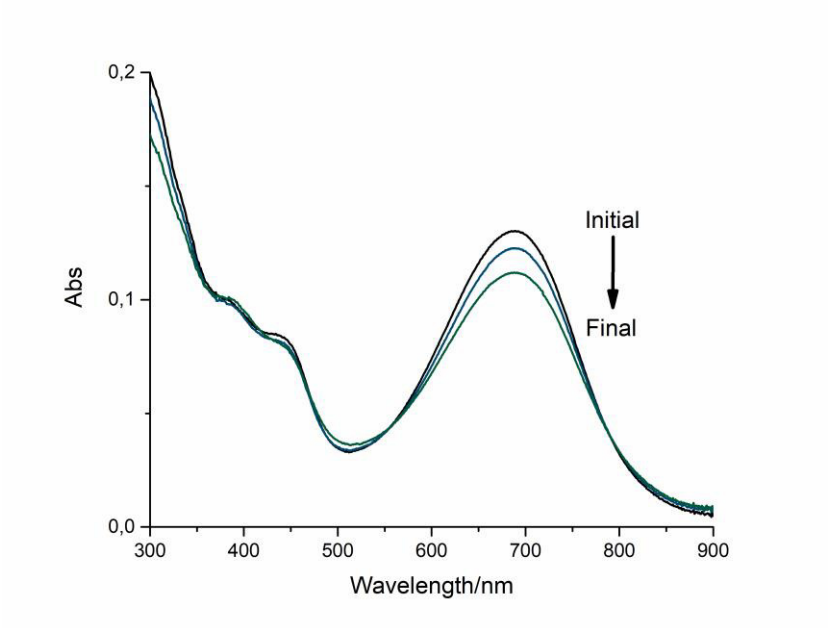

Figure 6.5 Spectral variation of PF7 upon photoirradiation in water. conditions: [PF7]= $2.5x10^{-5}$ M; T=20ºC; λirr=550 nm.

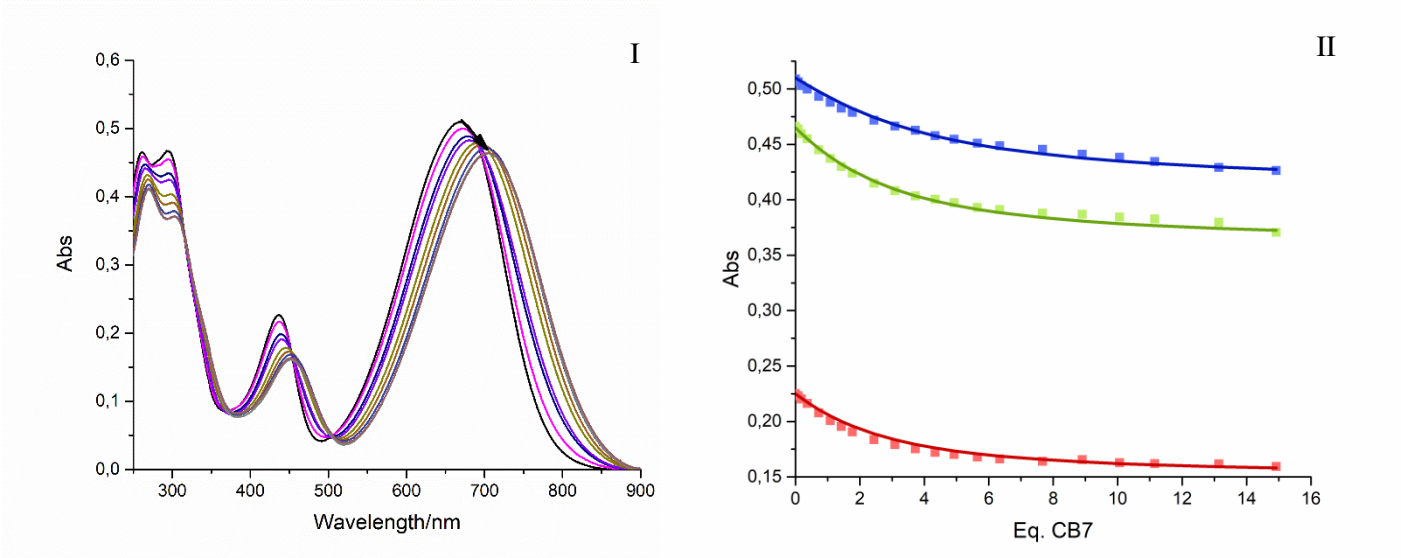

Figure 6.6 *(I)* UV-Vis titration of PF20 (closed form) with CB7. (II) Plot of experimental data (points); (Blue) 671 nm; (Green) 295 nm; (Red) 438 nm. (lines) best least squares fit of the data to a 1:1 association model. Conditions: [PF20] = $2x10^{-6}$ M.

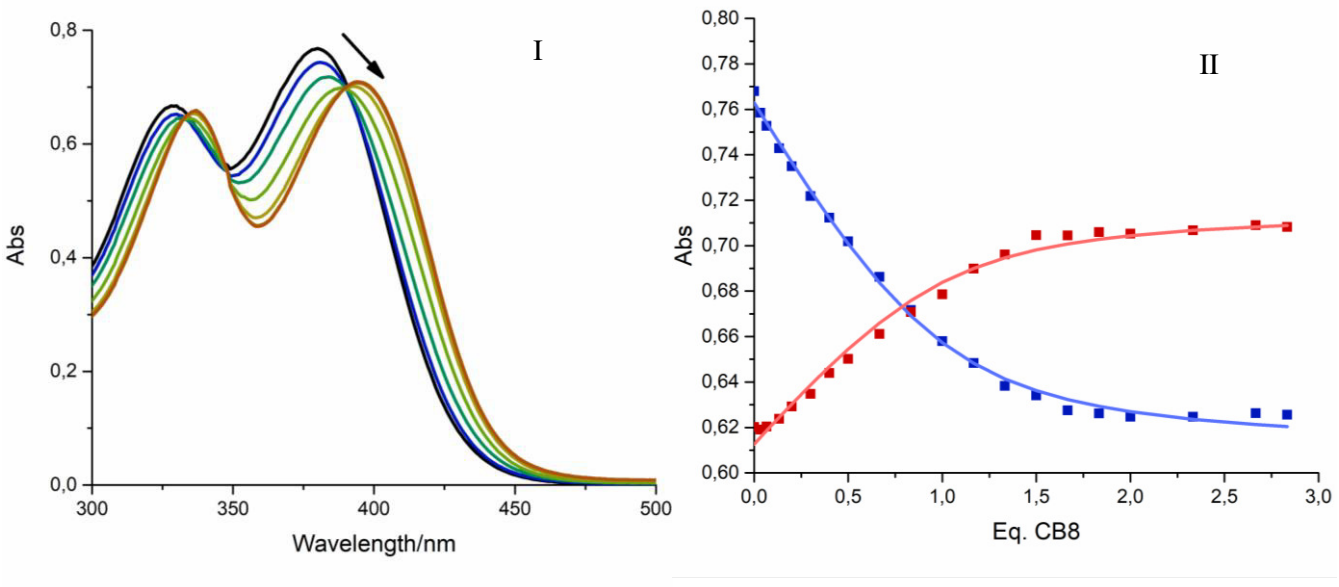

Figure 6.7 *(I)* UV-Vis titration of PF20 (open form) with CB8. (II) Plot of experimental data (points); (Blue) 380 nm; (Red) 396 nm; (lines) best least squares fit of the data to a 1:1 association model. Conditions: [PF20]= $2x10^{-6}$ M

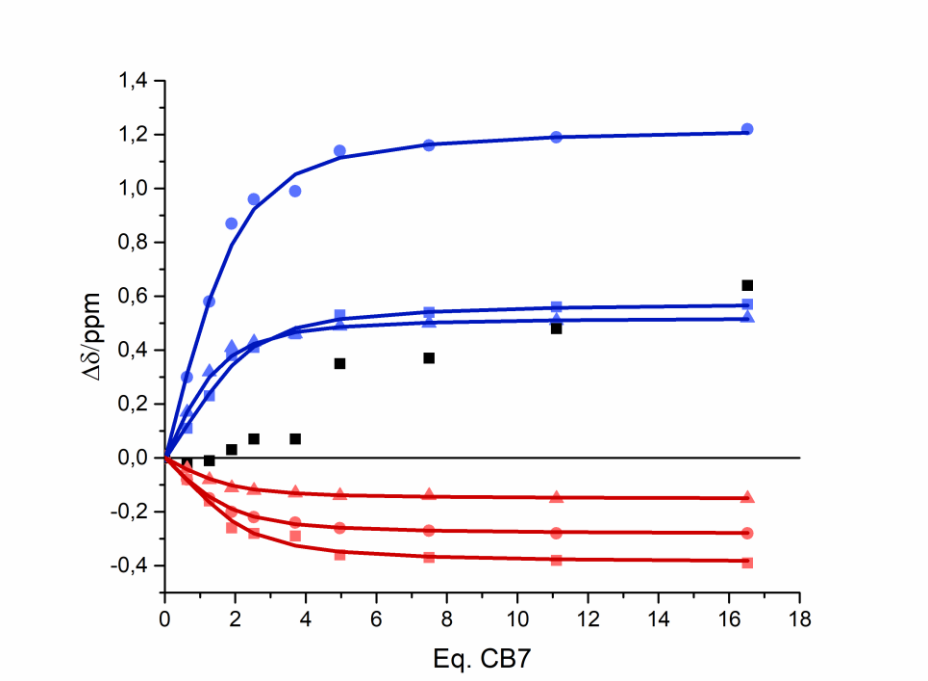

Figure 6.8 Plot of the chemical shift of PF20 (Open isomer) titration with CB7. Solid lines correspond to the best fitting of the experimental data.

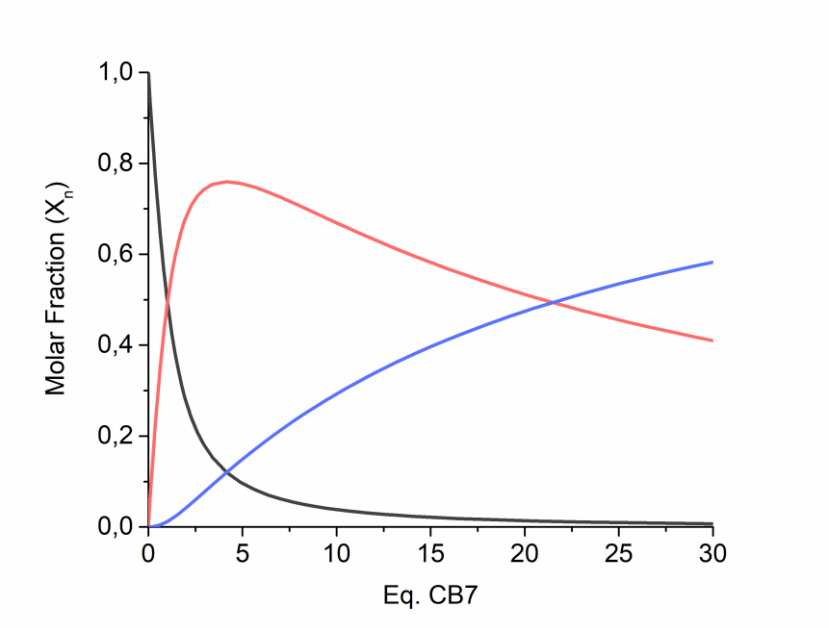

Figure 6.9 Molar fraction of PF20 (open) with CB7. (Black line) PF20; (Red line) [11]; (Blue line) [21]

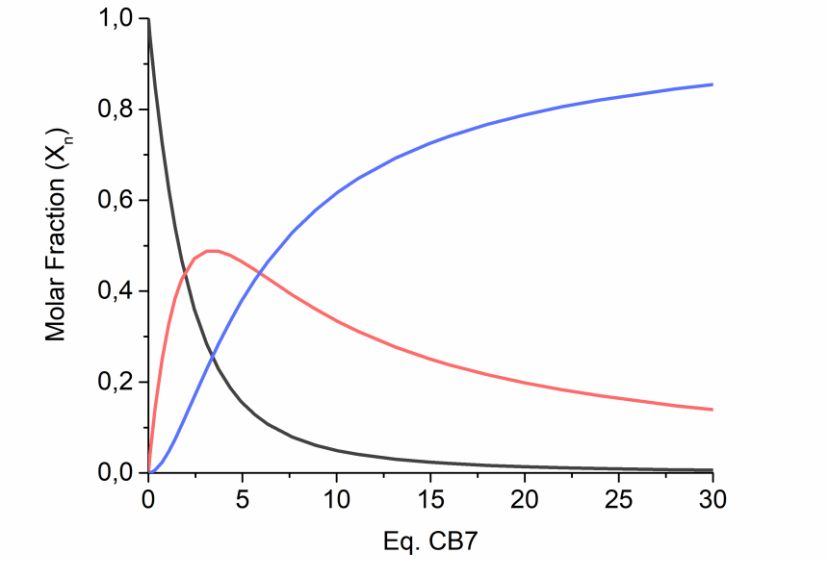

Figure 6.10 Molar fraction of PF20 (closed): CB7. (Black line) PF20; (Red line) [11]; (Blue line) [21]

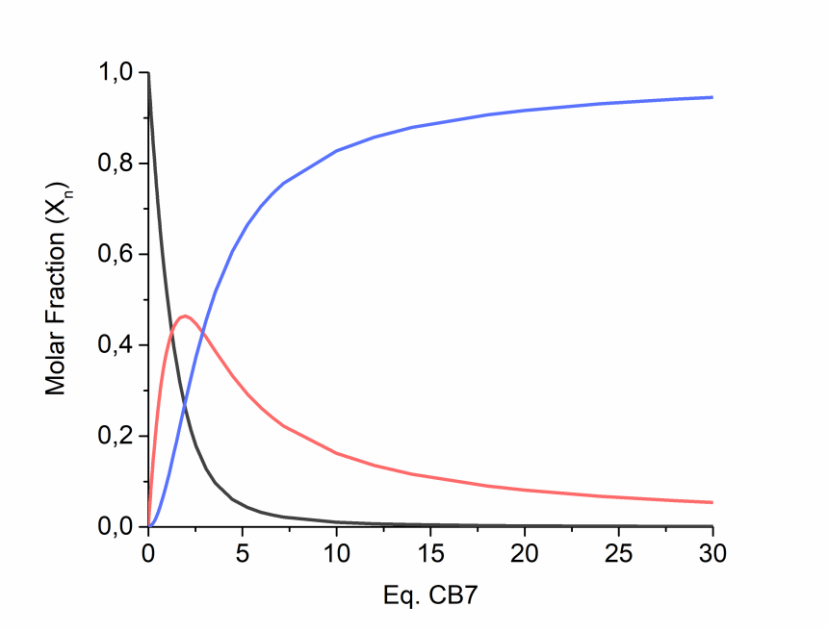

Figure 6.11 Molar fraction of PF7 (Open): CB7. (Black line) PF7; (Red line) [11]; (Blue line) [21]

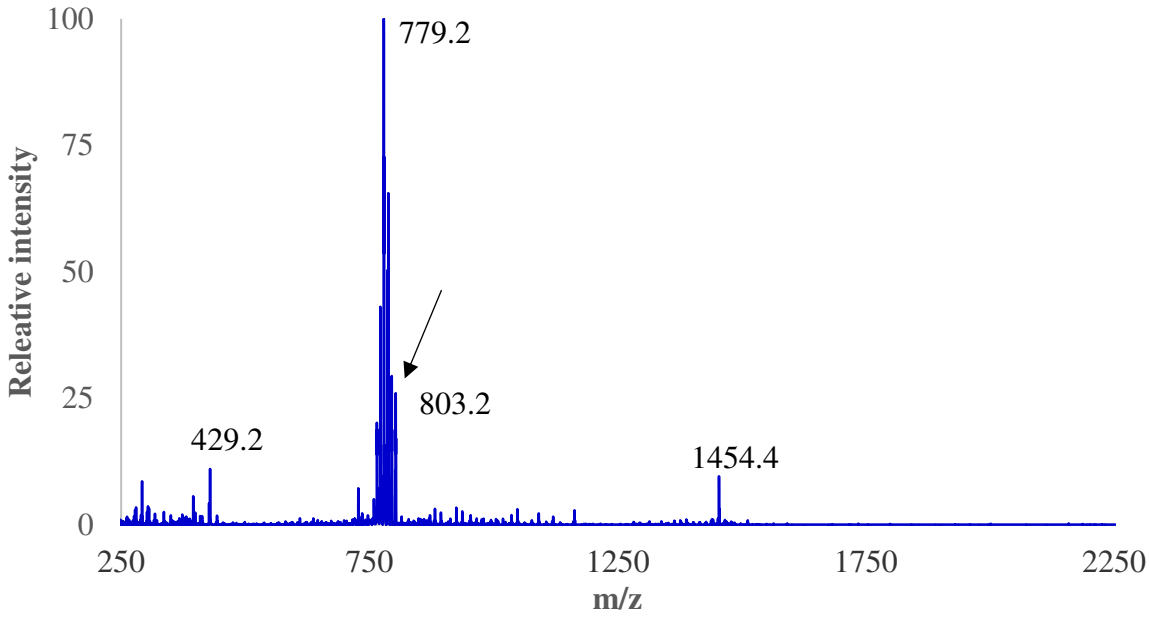

Figure 6.12 ESI-MS-MS spectra of m/z 803 of PF20 with CB7. [PF20] = 50µM; [CB7] = 50µM

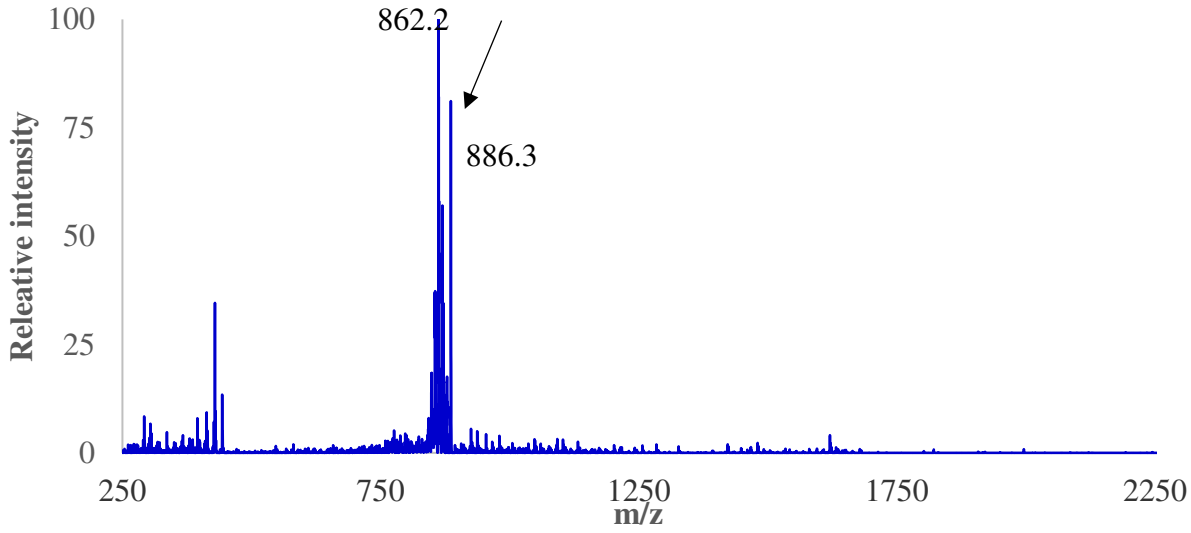

Figure 6.13 ESI-MS-MS spectra of m/z 886 of PF20 with CB8. [PF20] = 50µM; [CB8] = 100µM

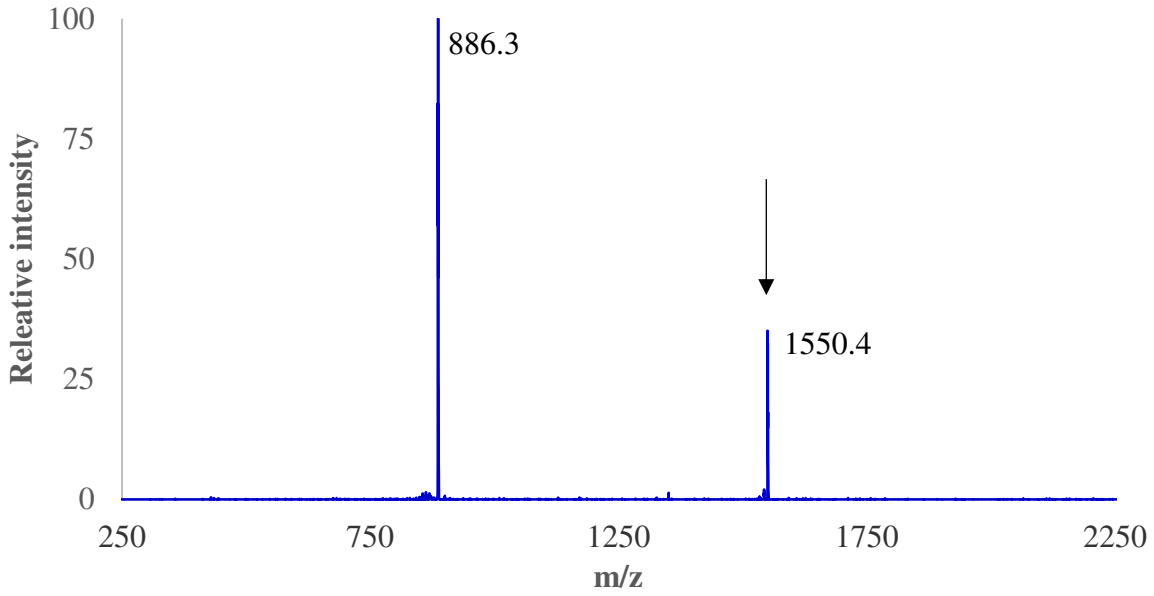

Figure 6.14 ESI-MS-MS spectra of m/z 1550 of PF20 with CB8. [PF20] = 50µM; [CB8] = 100µM

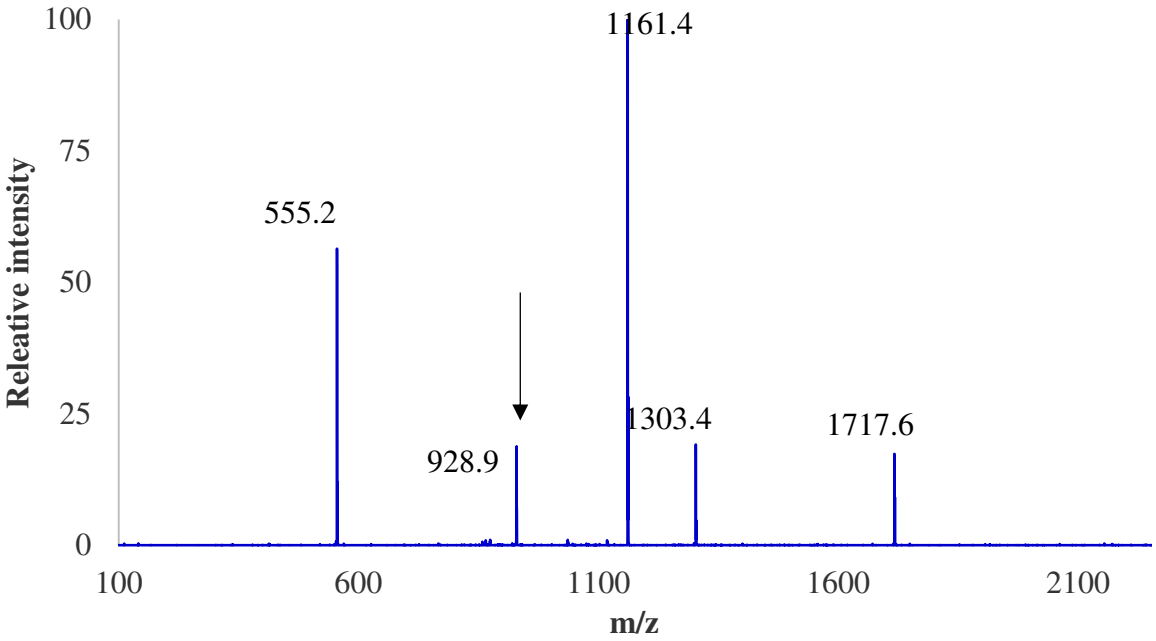

Figure 6.15 ESI-MS-MS spectra of m/z 928 of PF7 with CB7. [PF7] = 50µM; [CB7] = 100µM

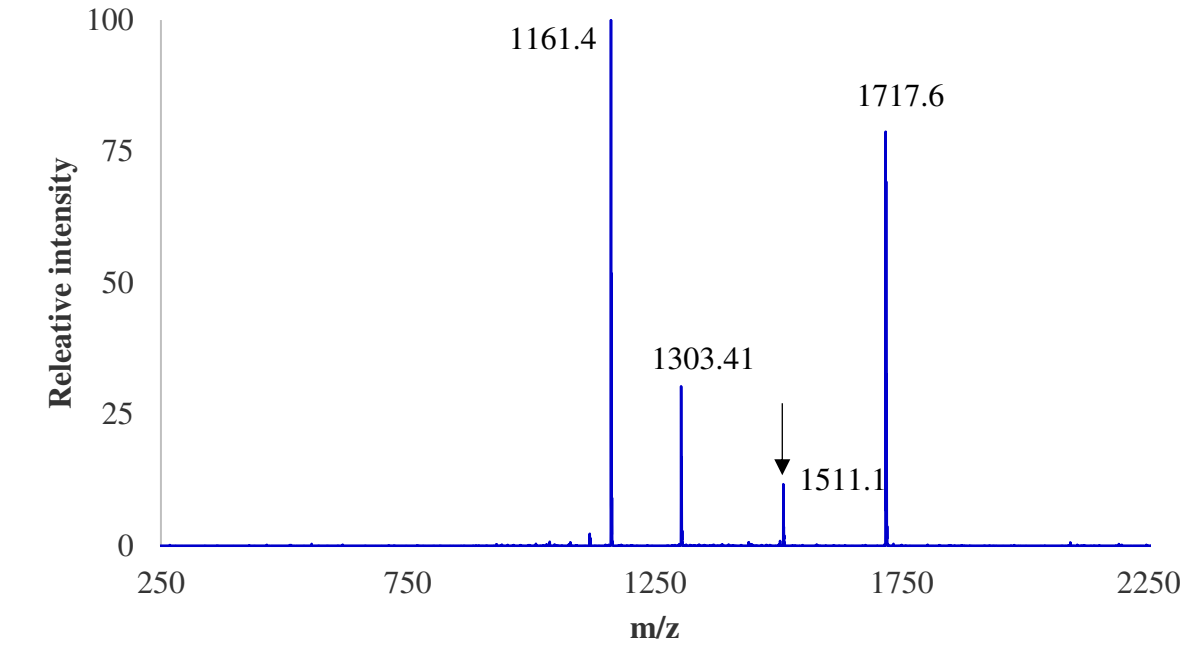

Figure 6.16 ESI-MS-MS spectra of m/z 1511 of PF7 with CB7. [PF7] = 50µM; [CB7] = 25µM

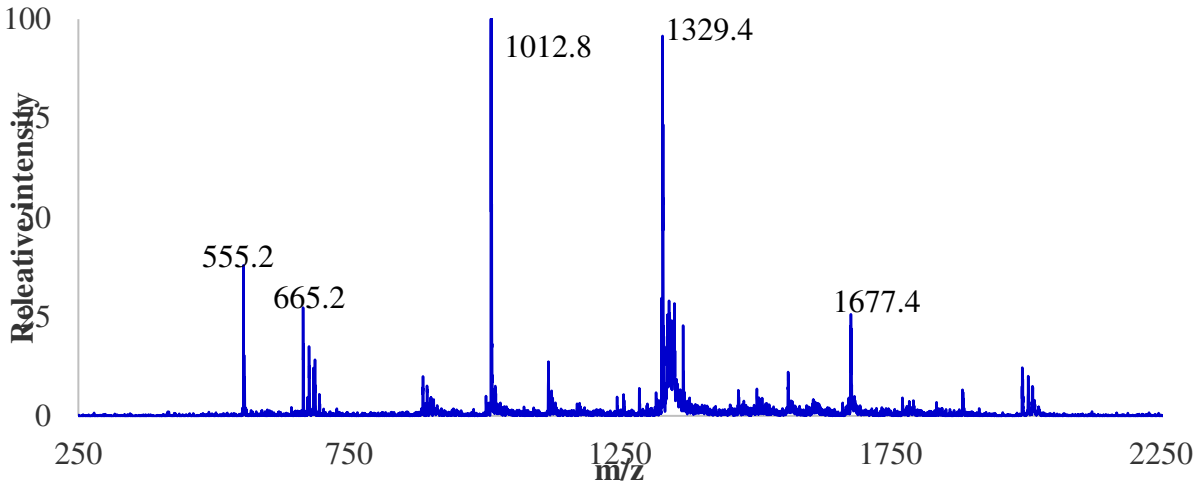

Figure 6.17 Full ESI-MS spectra of PF7 with CB8. [PF7] = 50µM; [CB8] = 25µM

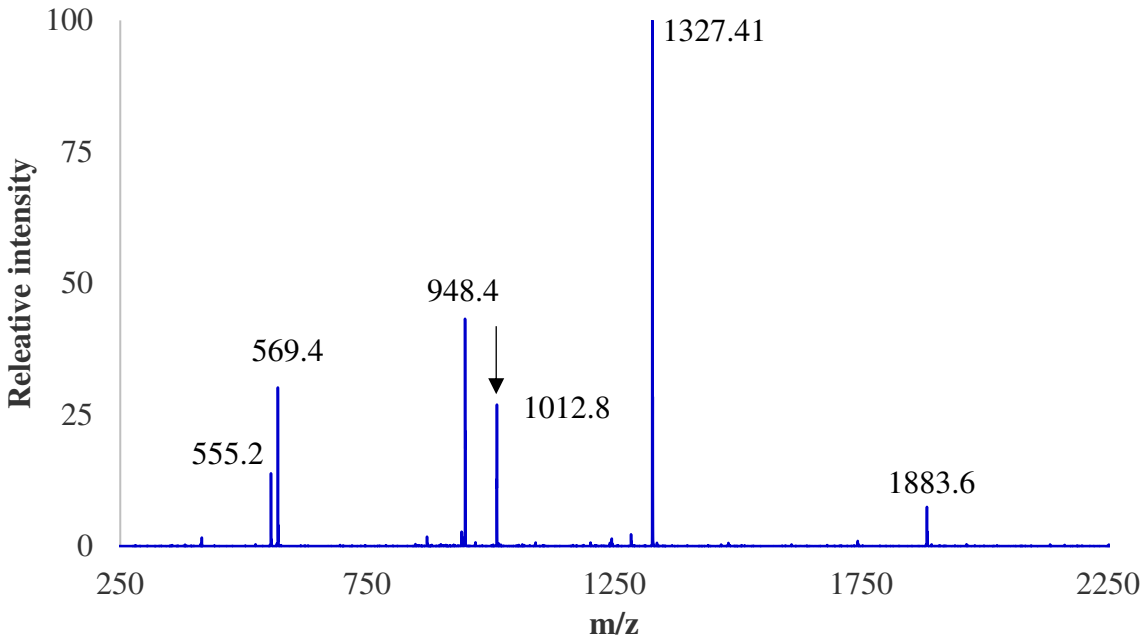

Figure 6.18 ESI-MS-MS spectra of m/z 1012 of PF7 with CB8. [PF7] = 50µM; [CB8] = 25µM

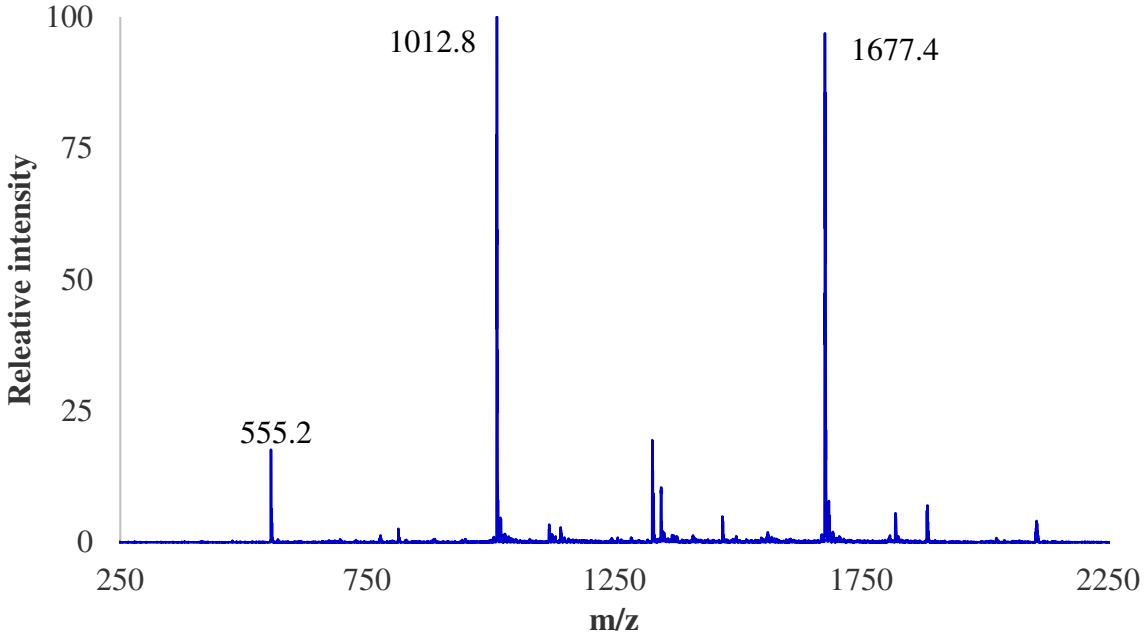

Figure 6.19 ESI-MS spectra under not soft conditions of PF7 with CB8. [PF7] = 50µM; [CB8] = 100µM

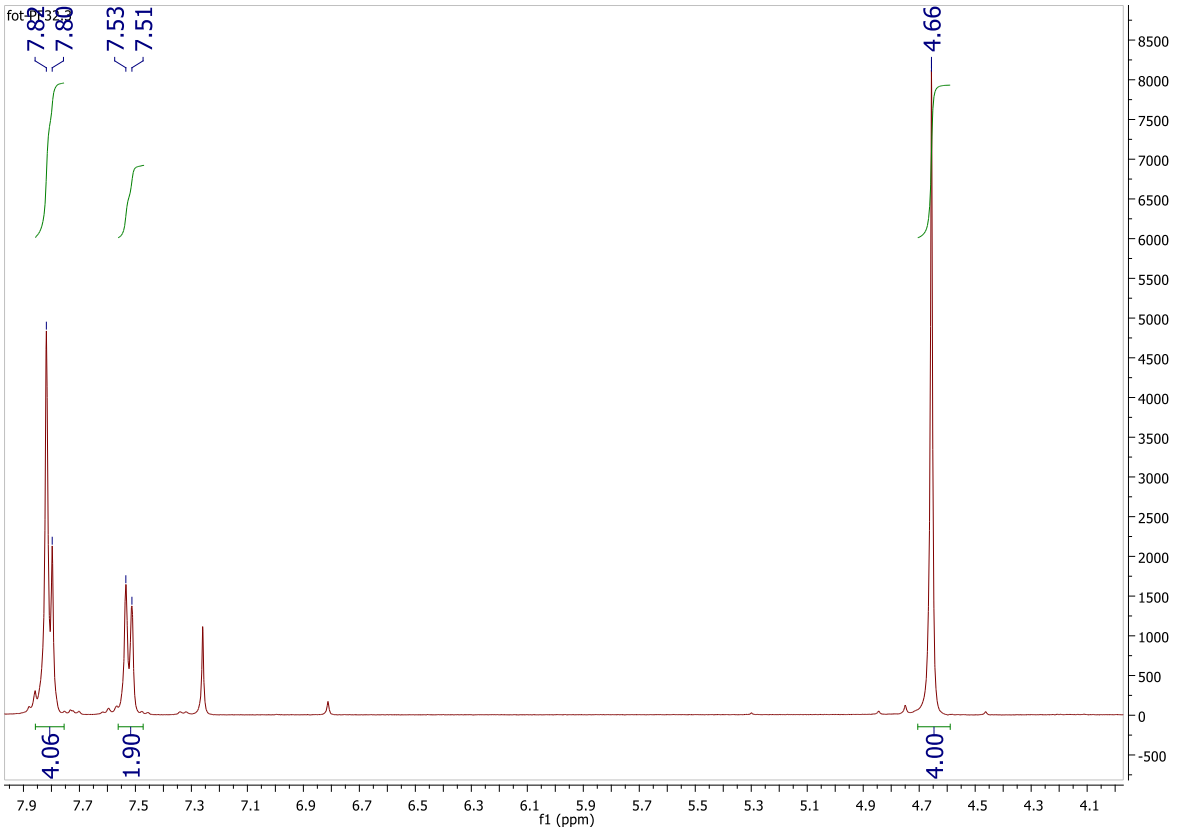

Figure 6.20 ^{1}H NMR spectra of (1) in $CDCl_3$

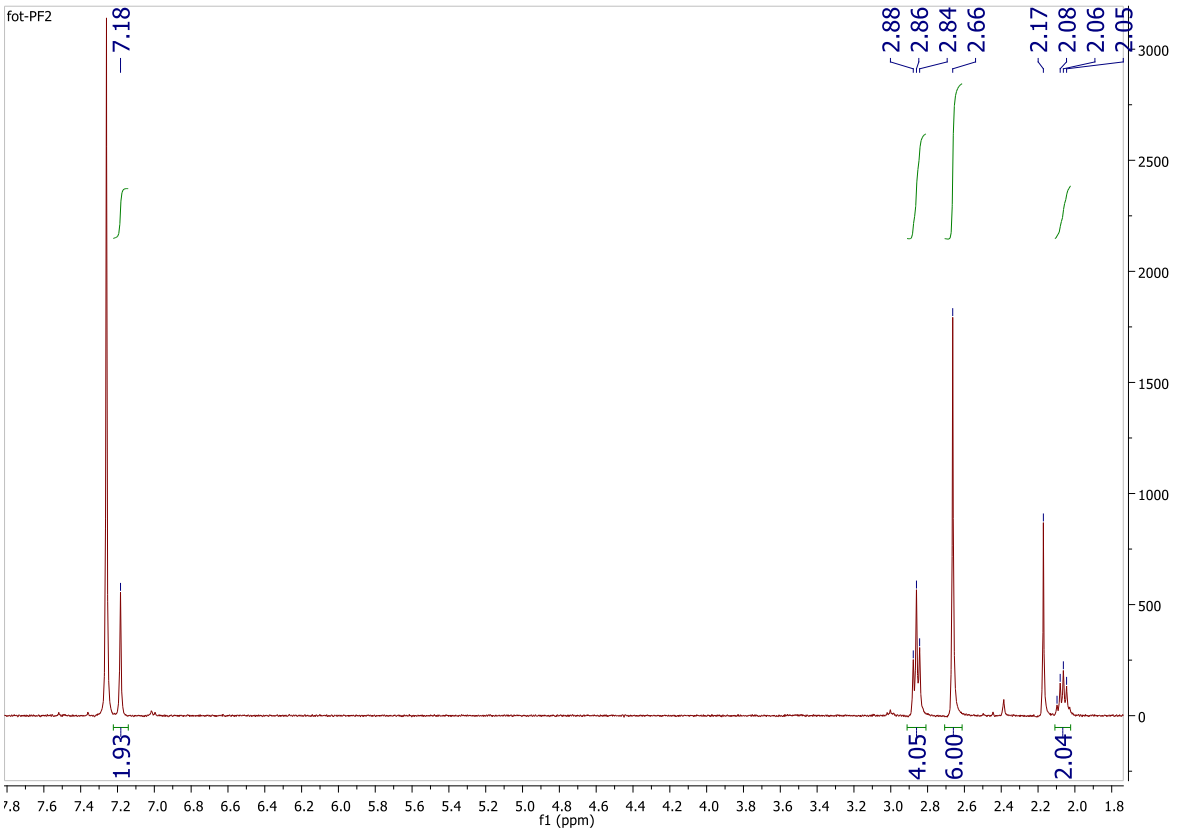

Figure 6.21 ^{1}H NMR spectra of (2) in $CDCl_3$

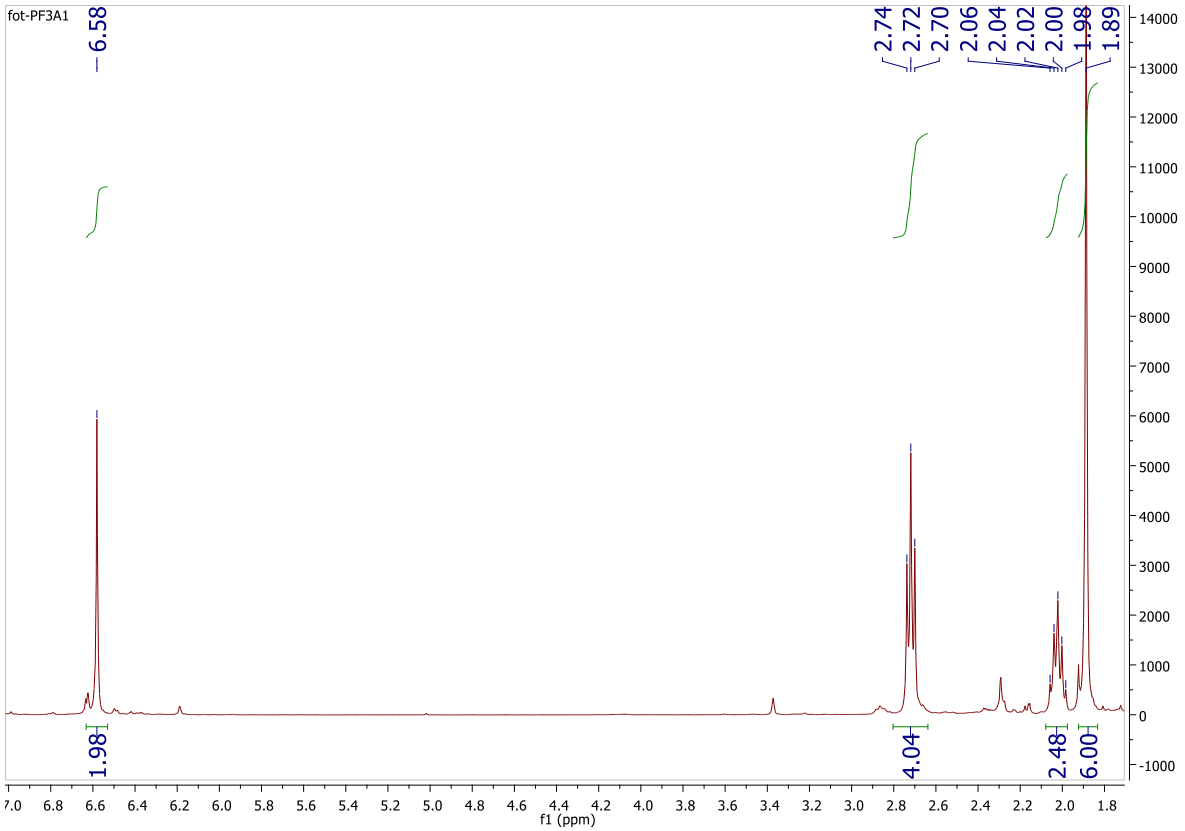

Figure 6.22 ^{1}H NMR spectra of (3) in $CDCl_3$

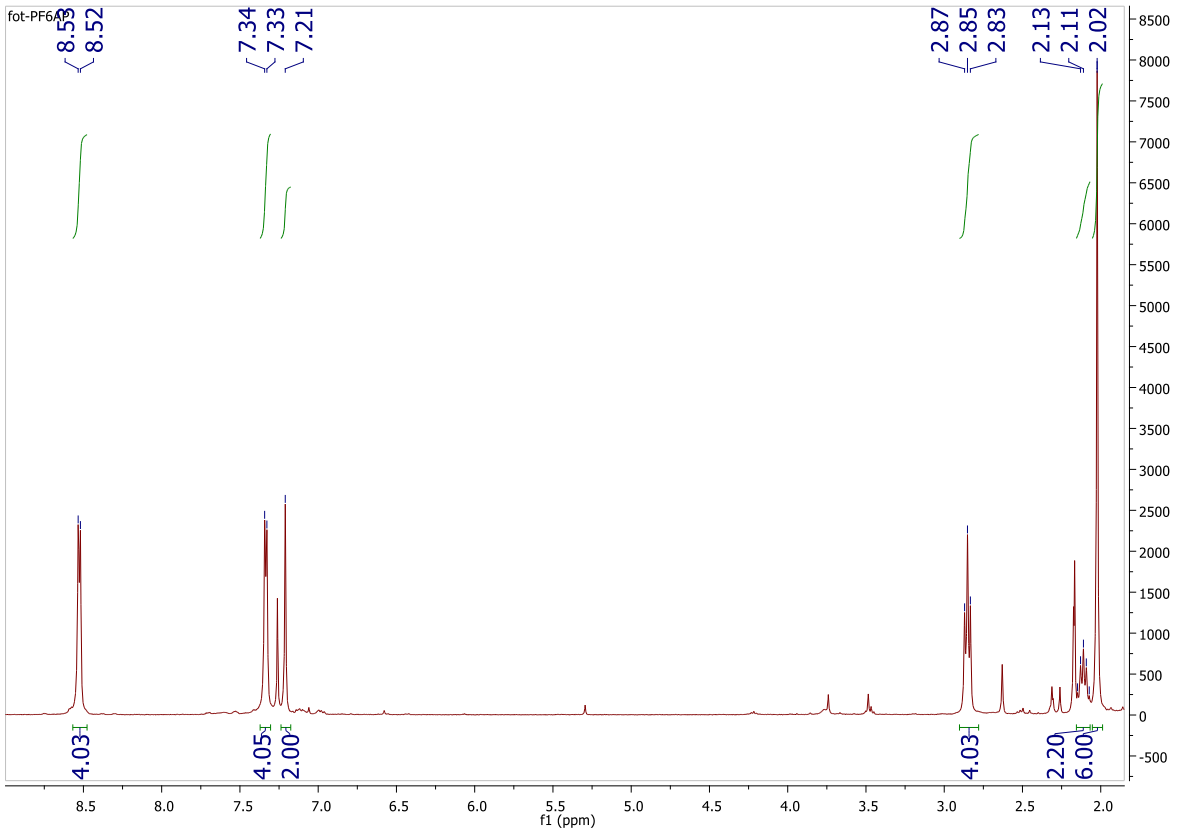

Figure 6.23 ^{1}H NMR spectra of (4) in $CDCl_3$

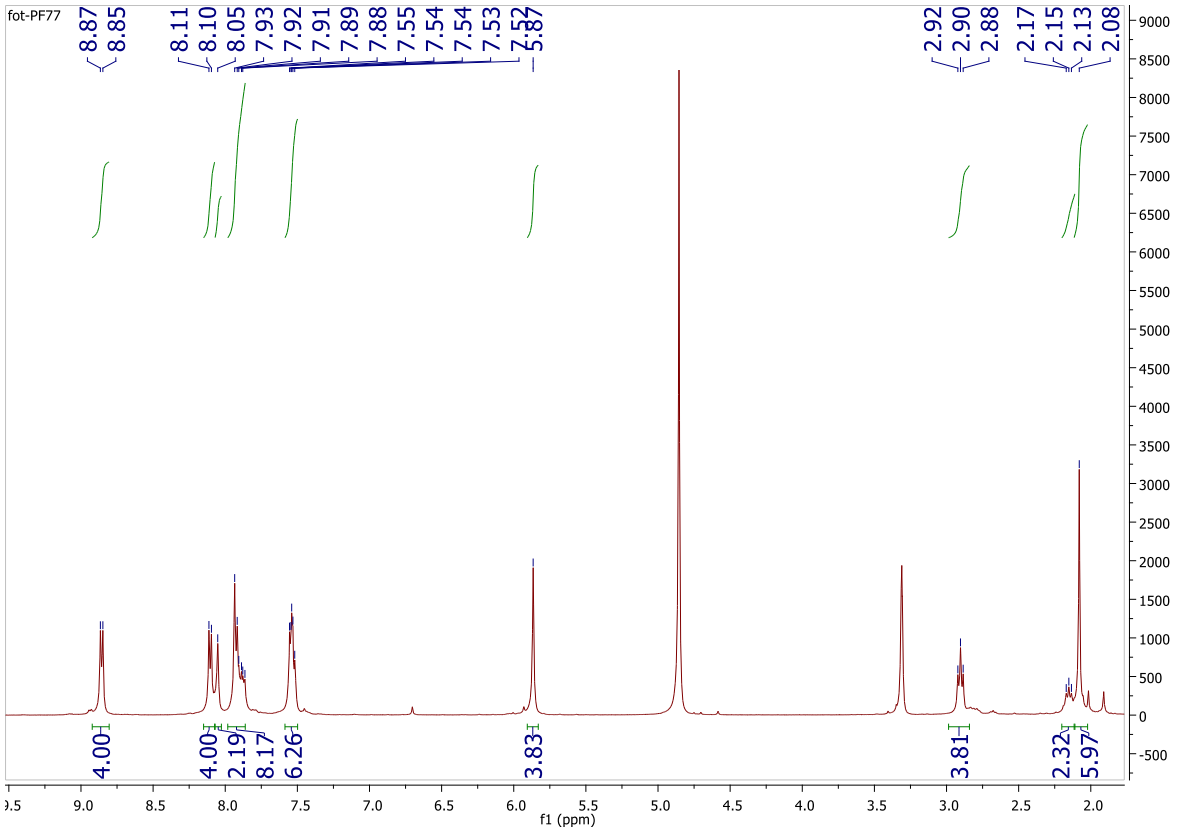

Figure 6.24 ^{1}H NMR spectra of (PF7) in MeOD.

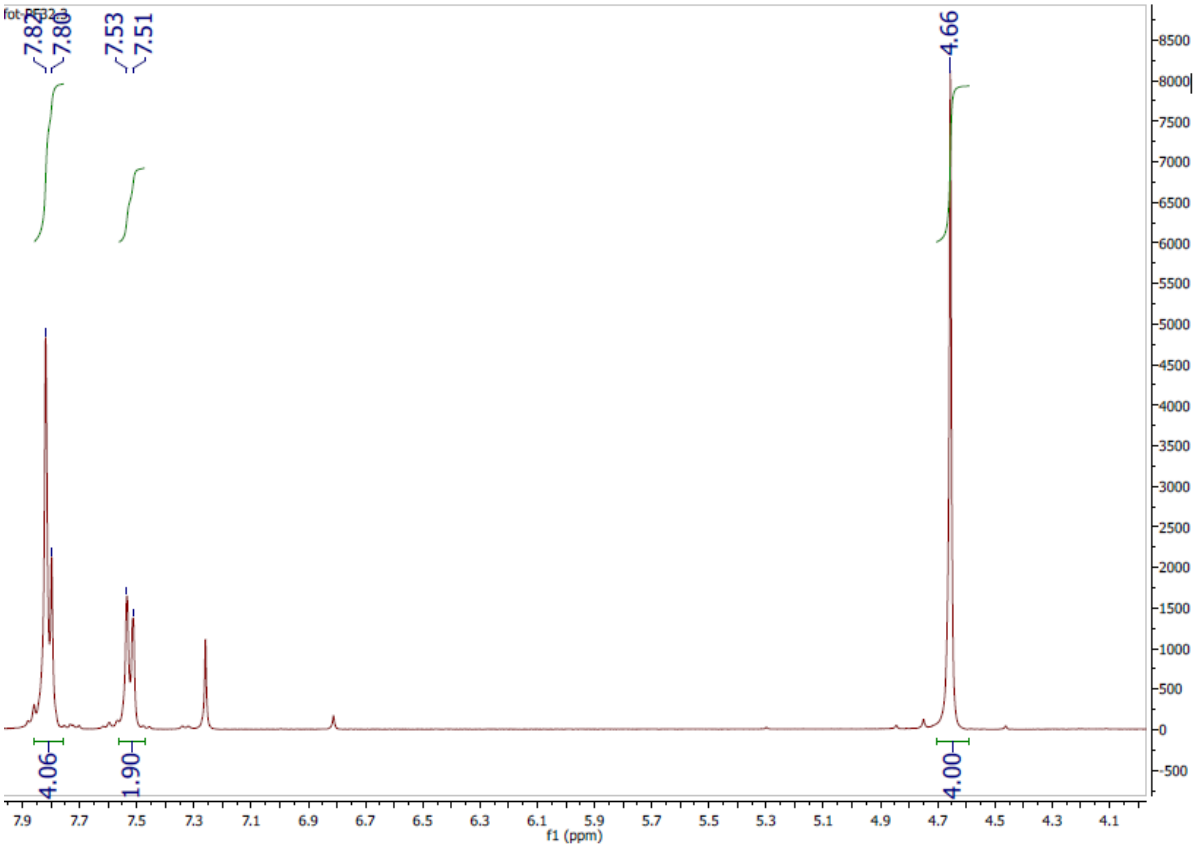

Figure 6.25 ^{1}H NMR spectra of (6) in $CDCl_3$

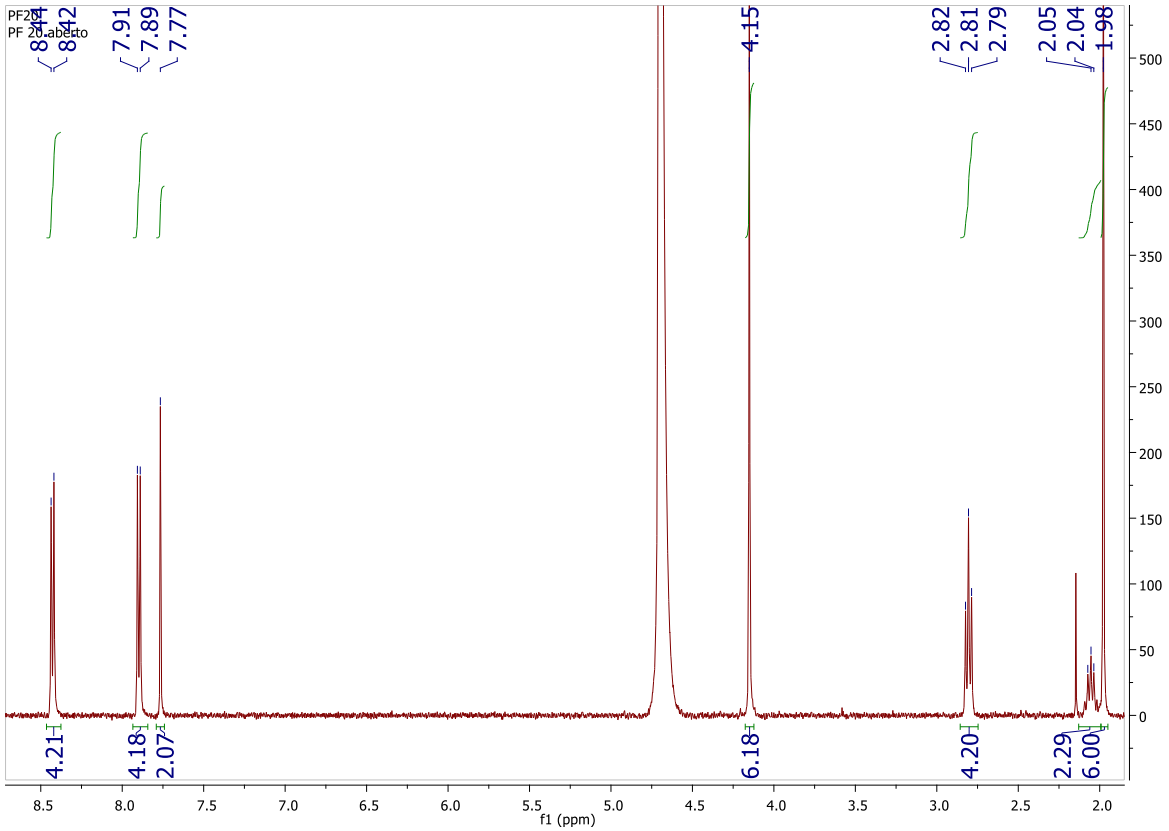

Figure 6.26 ^{1}H NMR spectra of (PF20) in D_2O

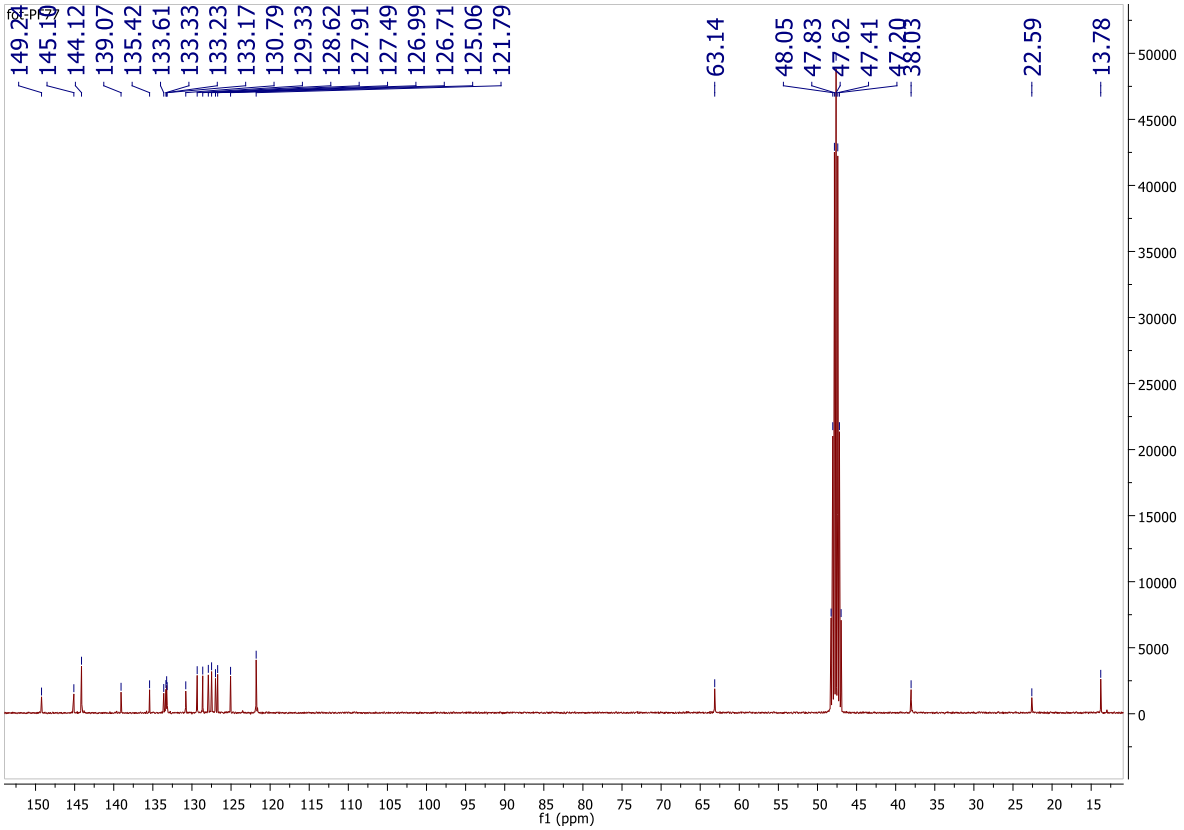

Figure 6.27 ^{13}C NMR spectra of (PF20) in CD_3OD

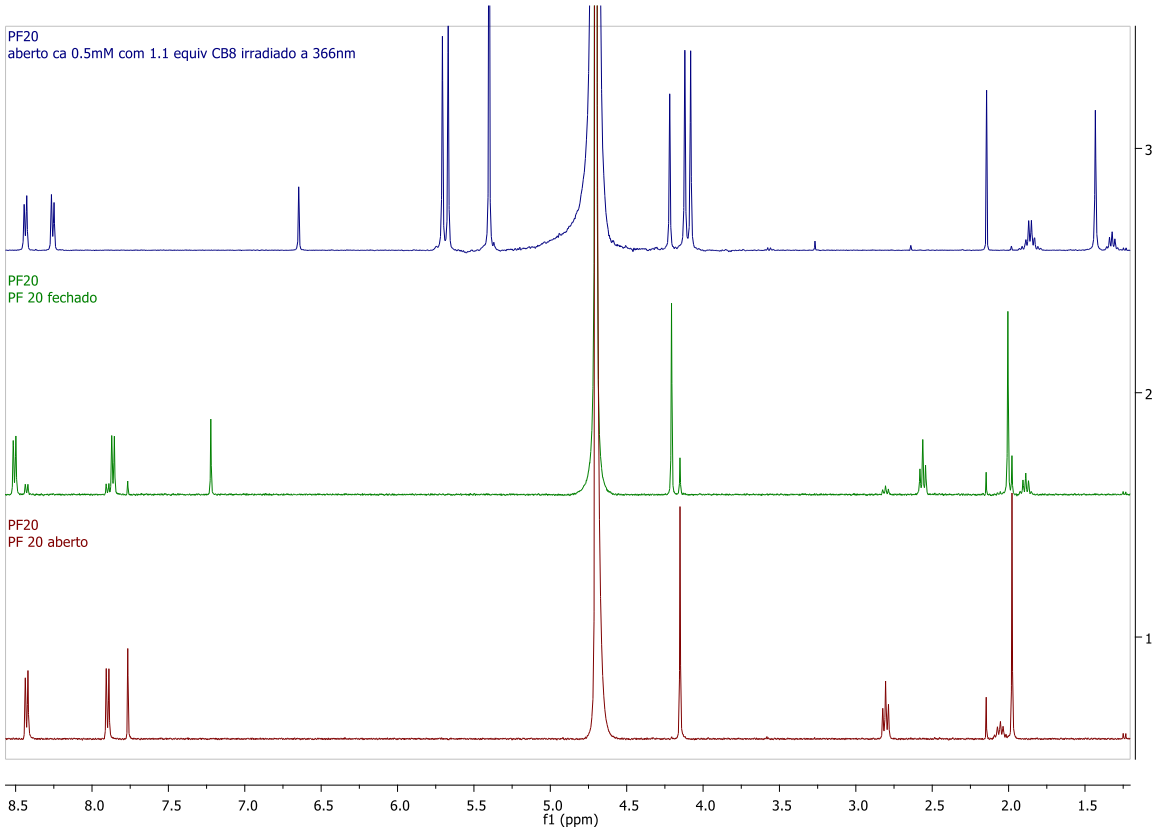

Figure 6.28 ^{1}H NMR spectra of PF20 (red) open; (green) PSS; (blue) PSS with CB8 irradiated at 365 nm

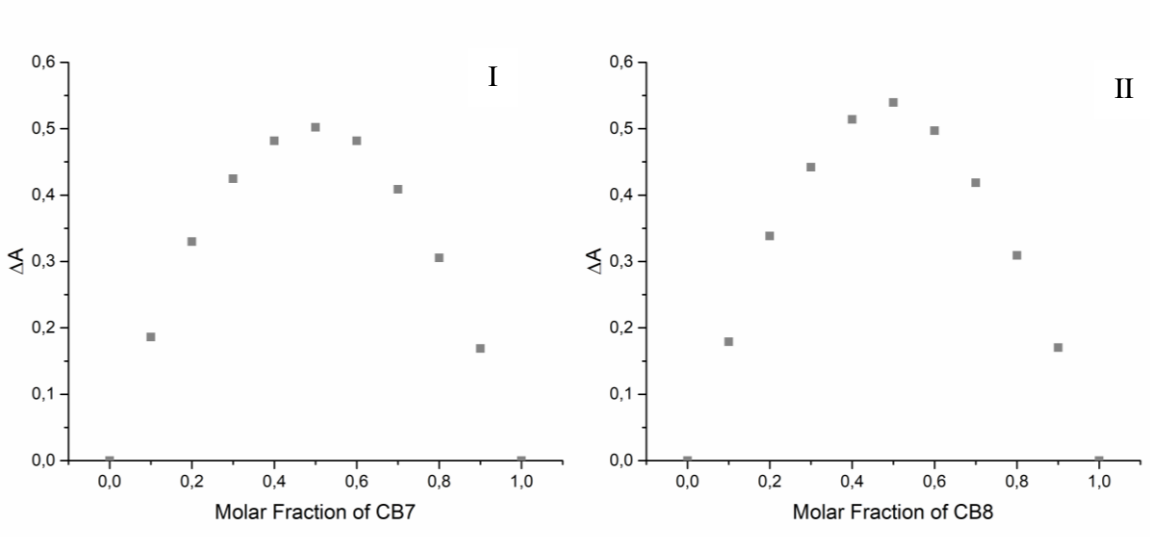

Figure 6.29 Job Plot's od the interaction between PF20 (open isomer) with CB7 (I) and CB8 (II), followed at 381 nm. [total] = 6.3×10^{-5}.

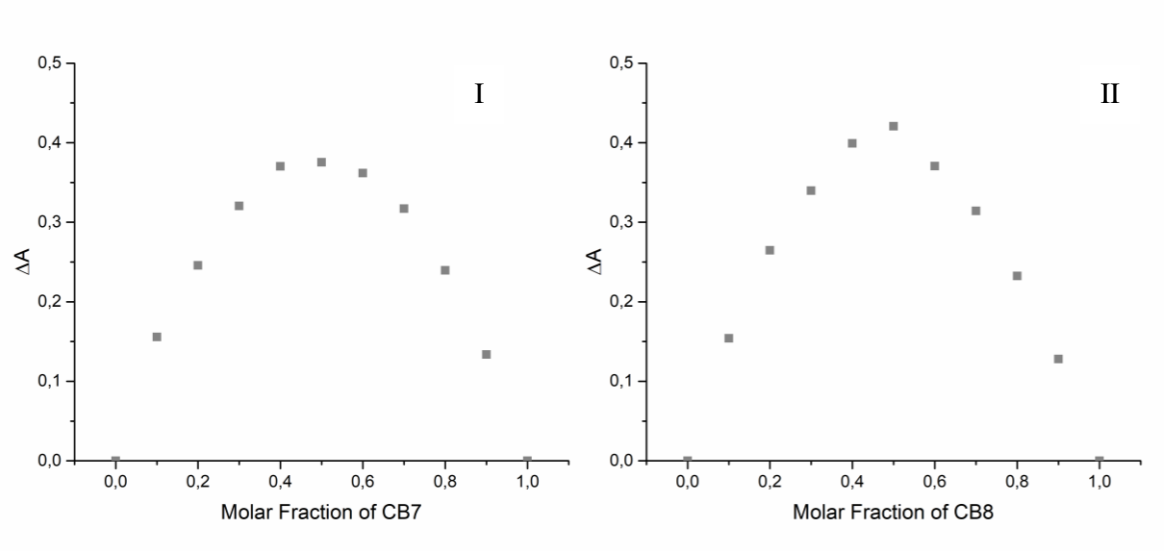

Figure 6.30 Job Plot's od the interaction between PF20 (closed isomer) with CB7 (I) and CB8 (II), followed at 678 nm. [total] = 6.3×10^{-5} M

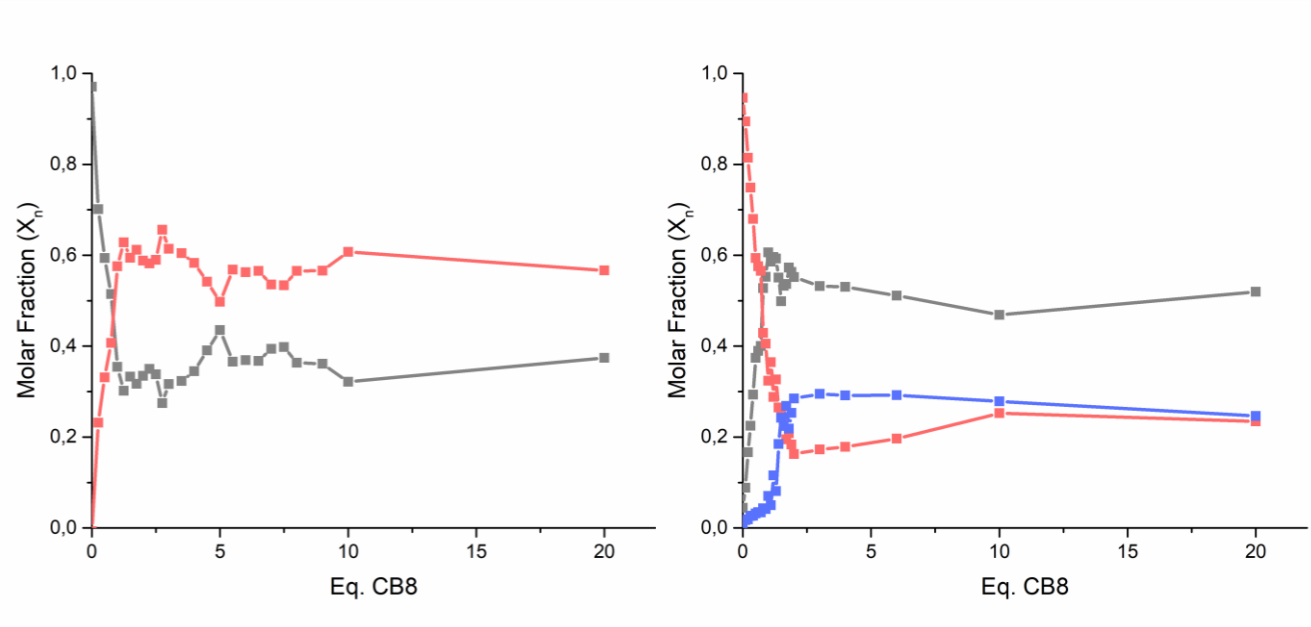

Figure 6.31 Molar Fraction versus Equiv. of CB7 for (I) PF20 and (II) PF7 determined by Lifetime titration results. (Black) Guest; (RED) [11]; (Blue) [12]; Conditions: [guest] = 5×10^{-6} M; λ_{ex} 373 nm.

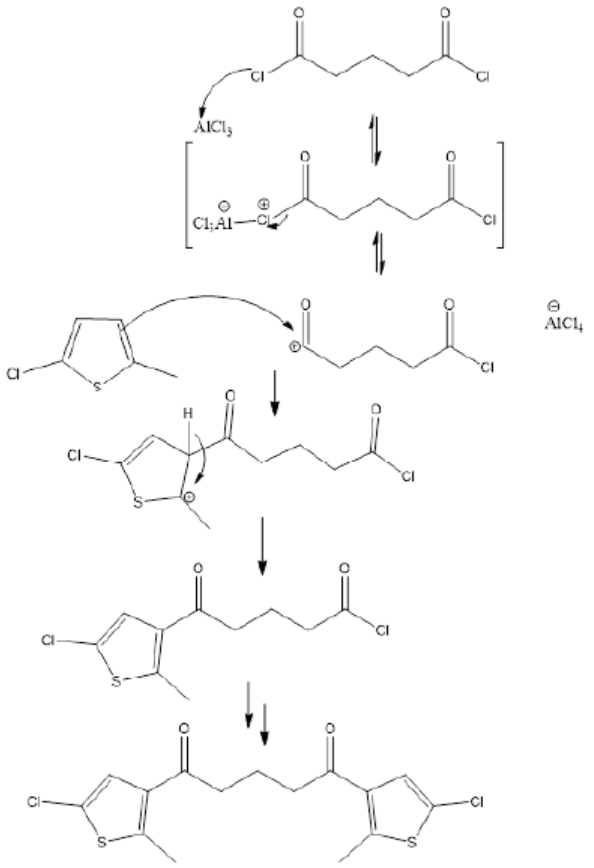

Figure 6.32 Mechanism of reaction (II, Friedel-Craft Acylation).

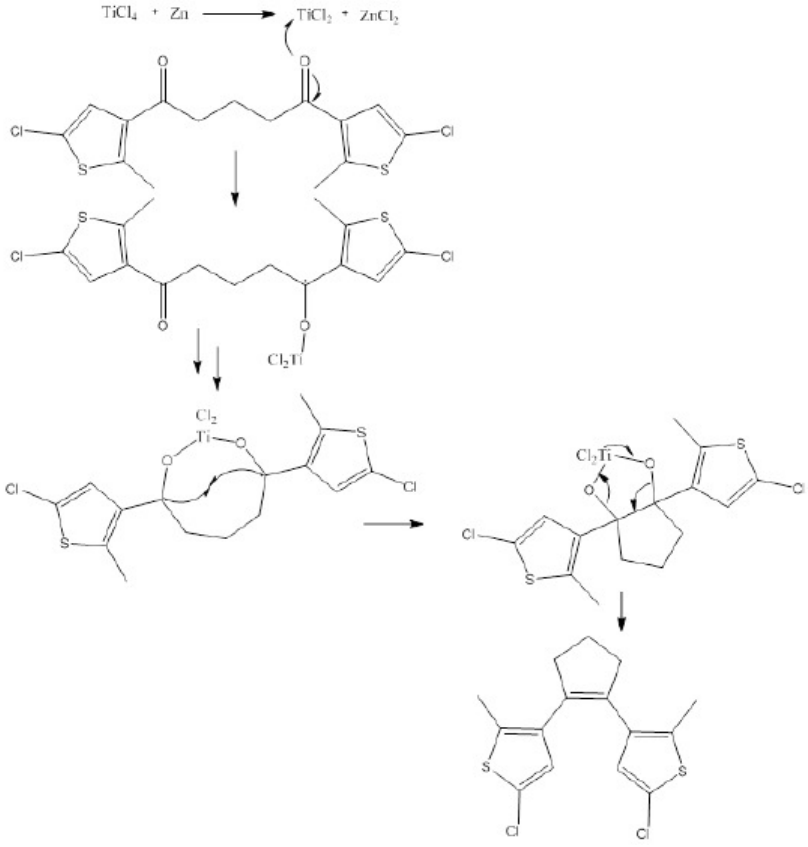

Figure 6.33 Mechanism of reaction (III, McMurry Cyclization)

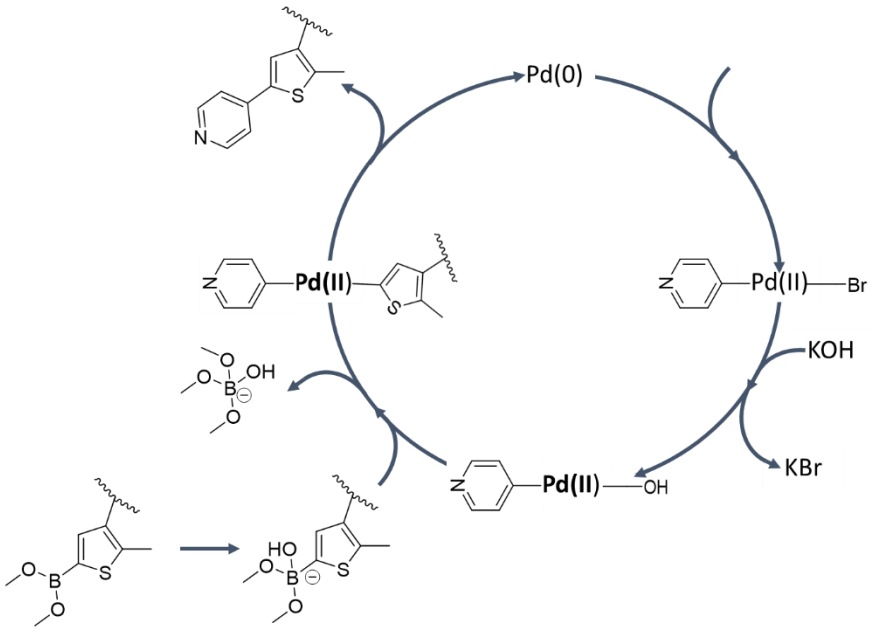

Figure 6.34 Cyclic mechanism of reaction (IV, Suzuki Coupling)